Identification and functional investigation of novel disease genes of a susceptibility locus for type 2 diabetes mellitus

Inaugural-Dissertation

Zur Erlangung des Doktorgrades
der Mathematisch-Naturwissenschaftlichen Fakultät
der Heinrich-Heine-Universität Düsseldorf

vorgelegt von

Sarah Annemarie Görigk
aus Moers

Düsseldorf, Juli 2023

Summary

The development of type 2 diabetes mellitus (T2D) due to genetic predisposition is a complex field in metabolic research. In the past, genome-wide linkage analyses of mouse inbred strains have identified almost 200 quantitative trait loci (QTL) for diabetes-related traits. However, identification of the causal gene variants remains challenging and many of them account for only a small percentage of the total heritability. To enhance the efficiency of gene discovery, a collective diabetes cross project was initiated which combined different crossbreeding approaches of inbred mouse strains that vary in their T2D susceptibilities. Among other loci, a novel QTL was previously identified on chromosome 4 (*Nbg4; NZO blood glucose on chromosome 4*) within a backcross of obese and T2D-prone New Zealand Obese (NZO) and lean, diabetes-resistant 129P2/OlaHsd (Ola) mice. Initial investigations revealed major linkage of this locus with blood glucose levels (LOD 7.1) where heterozygous NZO/Ola-allele carriers displayed strikingly elevated blood glucose levels compared to NZO/NZO-allele carriers. The aim of the present study was to investigate the metabolic features of the *Nbg4* locus to filter for causal gene variants. Phenotypical characterization of congenic mice confirmed the diabetogenic effect in mice carrying the proximal region of *Nbg4* (*Nbg4p*; 40-77 Mb), thereby reducing the critical fragment to a size of 37 Mb. As expected, homozygous Ola-allele carriers of *Nbg4p* (*Nbg4p*$^{O/O}$) showed a strikingly elevated diabetes prevalence, presumably due to reduced whole-body glucose tolerance. Moreover, investigations of the adipose tissue revealed an early-onset insulin resistance phenotype in *Nbg4p*$^{O/O}$ mice, which was characterized by significantly reduced fat tissue-specific glucose uptake and endogenous GLUT4 protein abundance. Furthermore, *Nbg4p*$^{O/O}$ mice displayed an increase in hepatic glucose production, indicating that *Nbg4p* regulates insulin sensitivity in both, adipose tissue and the liver. Finally, a combination of haplotype and gene expression analyses was used to select potential candidate genes that may contribute to the diabetogenic effects of *Nbg4p*. As a second aim of this study, novel candidate genes, which were identified within two independent approaches of the collective diabetes cross project, were investigated for their potential impact on T2D development. With this, a potential causal relationship of the gene *Alad* with *Nbg4p* was confirmed by its impact on glucose uptake in adipocytes. Moreover, a potential contribution of the gene *Nudt19* on *Nbg7*, another blood glucose QTL, was confirmed in cultured liver cells by its regulation of the hepatic lipid metabolism. Future studies will focus on the detailed mechanisms by which these genes contribute to hyperglycemia and the development of T2D.

Zusammenfassung

Die Entstehung des Typ 2 Diabetes mellitus (T2D) durch genetische Prädisposition ist ein komplexer Bereich in der Erforschung von Stoffwechselerkrankungen. Genomweite Assoziationsstudien in Maus-Inzuchtstämmen haben bereits um die 200 diabetes-assoziierte Kopplungen (*Quantitative Trait Loci; QTL*) ermittelt. Dennoch stellt die Identifizierung der zugrundeliegenden Risikogene eine herausfordernde Aufgabe dar, da viele dieser Gene nur einen kleinen Teil der Heritabilität ausmachen. Um die Effizienz zur Ermittlung von solchen Risikogenen zu steigern, wurde das *Collective Diabetes Cross* Projekt eingeführt, welches verschiedene Kreuzungsansätze mit Mäusen unterschiedlicher Diabetes-Suszeptibilität kombiniert. Im Rahmen dieser Studie wurde unter anderem ein neuer QTL auf Chromosom 4 (*Nbg4; NZO blood glucose on chromosome 4*) in einer Kreuzung aus diabetesanfälligen *New Zealand Obese* (NZO) und schlanken, diabetesresistenten 129P2/OlaHsd (Ola) Mäusen (N2(NZOxOla)) identifiziert (LOD 7,1). Erste Untersuchungen zeigten eine wesentliche Assoziation des Lokus mit Blutglukose, welche verglichen mit homozygoten NZO/NZO Tieren deutlich erhöht in heterozygoten NZO/Ola Allelträgern auftrat. Ziel dieser Arbeit war es die metabolischen Eigenschaften des *Nbg4* Lokus und die zugrundeliegenden Genvarianten zu untersuchen. Die phänotypische Charakterisierung von kongenen Mäusen validierte den diabetogenen Effekt in Mäusen welche einen proximalen Sublokus von *Nbg4* (*Nbg4p*; 40-77 Mb) trugen, sodass die kritische Region auf 37 Mb begrenzt werden konnte. Wie erwartet zeigten homozygote Ola-Allelträger (*Nbg4p*$^{O/O}$) eine wesentlich höhere Diabetesprävalenz, welche vermutlich durch die Einschränkung der ganzheitlichen Glukosetoleranz hervorgeht. Untersuchungen des Fettgewebes offenbarten eine früh einsetzende Insulinresistenz in *Nbg4p*$^{O/O}$ Mäusen, welche einhergehend mit reduzierter Glukoseaufnahme und geringer GLUT4 Proteinexpression erklärt werden können. Weiterhin wurde in *Nbg4p*$^{O/O}$ Mäusen eine Erhöhung in der hepatischen Glukoseproduktion beobachtet was darauf hinweisen lässt, dass *Nbg4p* die Insulinsensitivität sowohl im Fettgewebe als auch in der Leber reguliert. Schließlich wurden Haplotypen- und Genexpressionsanalysen kombiniert um potentielle Risikogene für *Nbg4p* zu selektieren. Ein weiteres Ziel dieser Arbeit war die funktionale Untersuchung von ausgewählten Kandidatengenen zweier unabhängiger Kreuzungen des *Collective Diabetes Cross* Projektes. Dabei wurde ein potentieller Zusammenhang zwischen dem Gen *Alad* mit *Nbg4p* durch die Beeinträchtigung der Glukoseaufnahme in Adipozyten bestätigt. Ebenso konnte ein potentieller Beitrag von *Nudt19* auf *Nbg7,* ein weiterer Blutglukose QTL*,* durch die Regulation des hepatischen Lipidstoffwechsels nachgewiesen werden. Zukünftige Analysen

sollen einen Fokus auf die zugrundeliegenden Mechanismen legen um einen möglichen Einfluss dieser Gene auf die Entstehung von Hyperglykämie und T2D zu erklären.

Table of contents

1. Introduction

1.1 *Diabetes mellitus* – A multifactorial disease

The 21st century depicts a time that is so different than ever before. With the introduction of the digital era in developed countries, jobs were less physically demanding and the import of foods from all over the world made a big change in our dietary. In addition, the severe restrictions during the novel pandemic, derived from the coronavirus in 2019 (COVID-19), changed not only our daily routine, but also contributed to main health problems.

Overweight and obesity are just few of the global health burdens with its continuously increasing numbers of affected people every year. Since 1975, the number of obese men has tripled worldwide. According to the Organisation for Economic Co-operation and Development (OECD) obesity rates will rise 5- to 10-fold until 2030[1]. Obesity often is accompanied with insulin resistance, a state of reduced efficiency of glucose uptake into peripheral insulin-sensitive tissues such as skeletal muscle, adipose tissue and liver. Consequently, a strong link with the development of *diabetes mellitus* has been discovered where insulin resistance represents the main cause of chronic hyperglycemia.

Diabetes is usually diagnosed by the determination of a highly increased blood glucose level. A fasting glucose concentration of 70 - 100 mg/dL (<5.6 mmol/L) is considered as normal while concentrations of 126 mg/dL (7 mmol/L) and higher is defined as diabetic [2]. The most known subtypes of diabetes are the type 1 diabetes (T1D) and type 2 diabetes (T2D), accounting for about 10 % and 90 % of all diabetes cases, respectively. While T1D is described as the result of the destruction of insulin-producing beta-cells caused by defects in the autoimmune response, the prevalence for T2D increases rather due to environmental and genetic changes [3]. With rising cases, diabetes has now entered the top 10 causes of death with an increase of 70 % since 2000 [4]. Further estimation of the global diabetes prevalence showed an increase of 112 million cases between 2017 and 2021 and it is predicted to rise for additional 106 million until 2030 which then accounts for a total number of 643 million affected people [3]. Thus, understanding the pathophysiology of T2D is essential for the development of future prevention and therapy strategies of the disease.

With a view of the aetiology of diabetes, it becomes clear that this metabolic disease is much more complex. Despite lifestyle and obesity there are also other causes like dyslipidemia, inflammation, as well as genetic and epigenetic factors that play a crucial role in the development of the different subtypes of diabetes [3]. Therefore, a lack of the detailed

understanding in the molecular function of diabetes aetiology makes it difficult to prevent a further increase of the prevalence and the severity of the disease. Unlike monogenic diabetes, which can be explained by a single gene mutation (e.g. maturity-onset diabetes of the youth; MODY) [5], T1D and T2D represent multifactorial subtypes of the disease. Despite the understanding that T1D mainly occurs as a result of defects in the body's own immune system caused by different genetic modifier, researchers now believe that additional virus infections such as the common flu or trauma experiences after pancreatic surgery can also trigger the onset of the disease [6]. However, most variables of different causes in the field of diabetes research have been identified for T2D. For example, environmental factors can include a sedentary lifestyle, poor dietary behavior, alcohol consumption, smoking, exposure to regular chemicals and air pollution [7]. On the other hand, also genetic predisposition displays a broad and complex field in T2D research. Depending on either population, family or twin-based studies, the range of T2D heritability varies a lot. Generally, if one parent is affected by T2D, there is a 40 % chance to develop T2D as well. If both parents suffer from T2D, the risk increases to 70 % [8-10]. Researcher in the field of diabetes are still aiming to identify the underlying genetic modifiers. Although a certain number of genes has been discovered to be involved in the onset and progression of T2D, it is more likely that T2D develops rather due to a combination of multiple gene variants that interact between each other and with environmental factors. Furthermore, it is known that these risk genes are not concentrated within one distinct region as it is the case in T1D, but rather scattered across the whole genome [11]. In conclusion, the aetiology of *diabetes mellitus* can provide important insights in the mechanistic pathways of the disease and therefore should be considered for future therapeutic interventions.

1.1.1 A new diabetes typology

So far, the current classification into T1D and T2D was based on the glycemic state, insulin availability, age and further defined clinical features that do not reflect the broad complexity that has been discovered in the recent years of diabetes research. Recent studies have now identified new subgroups of diabetes that display distinct patterns of the pathophysiology of the disease including the risk to develop known comorbidities. By this approach, diabetes can be subdivided into five groups: severe autoimmune diabetes (SAID), severe insulin-deficient diabetes (SIDD), severe insulin-resistant diabetes (SIRD), mild obesity-related diabetes (MOD) and mild age-related diabetes (MARD) [12]. Thereby, originally classified type 1 diabetes patients would belong to the SAID subgroup, whereas the other four subgroups are defined for

the more complex characteristics of type 2 diabetes. Although insulin deficiency is indicated as key feature of both SAID and SIDD, the latter is described with further complications leading to increased inflammation and retinopathy, as well as distinct expression patterns indicating rather determinants of type 2 diabetes [12, 13]. Increasing evidence suggest the association of the diabetes-related comorbidity of dysregulated hepatic lipid metabolism in the SIRD subgroup. Characteristics like insulin resistance, inflammation and a more frequently expression of a *Pnpla3* polymorphic variant increase the risk to develop non-alcoholic fatty liver disease (NAFLD) in this group [14, 15]. Furthermore, it has been shown that patients suffering from obesity- and age-related diabetes have a higher probability to be affected by a dysfunction in insulin secretion and impaired glucose tolerance by genetic predisposition of the *Tcf7l2* gene [12]. By proposing these novel subtypes of diabetes, the understanding of the heterogeneous mechanisms might help to increase the precision of diabetology.

1.2 Regulation of glucose homeostasis in health and disease

Maintenance of glucose homeostasis is the basis of a healthy metabolism as glucose represents the main fuel for almost every tissue. Therefore, regulation of blood glucose levels undergoes a stringent mechanism that is depending on different factors. Once glucose concentrations rise (e.g. after a meal), pancreatic beta-cells increase synthesis and secretion of insulin to promote glucose uptake into peripheral insulin-sensitive tissues (skeletal muscle, adipose tissue and liver). In liver and skeletal muscle, insulin facilitates the synthesis of glycogen and proteins, whereas lipids are promoted to be synthesized and stored in liver and adipose tissue. Furthermore, insulin also plays an important inhibiting role by preventing the degradation of glycogen and the excess synthesis of glucose in the liver, which all in all contributes to the whole-body glucose maintenance.

It is not uncommon that metabolic disorders such as obesity or diabetes undergo a metabolic switch from an anabolic to a catabolic state. Lack of insulin or insulin resistance leads to more catabolic events due to the increasing hyperglycaemic environment [16, 17]. As a consequence, lipolysis is activated in the adipose tissue and free fatty acids are released to the outer environment. Additionally, glycogenolysis is enhanced in the liver as well as gluconeogenesis, which together with the overall decreased glucose uptake causes a chronic state of hyperglycaemia, further leading to beta-cell failure and severe damage of other metabolic tissues. A summarized view of the signalling pathway with focus on insulin action and resistance will be described in the following section.
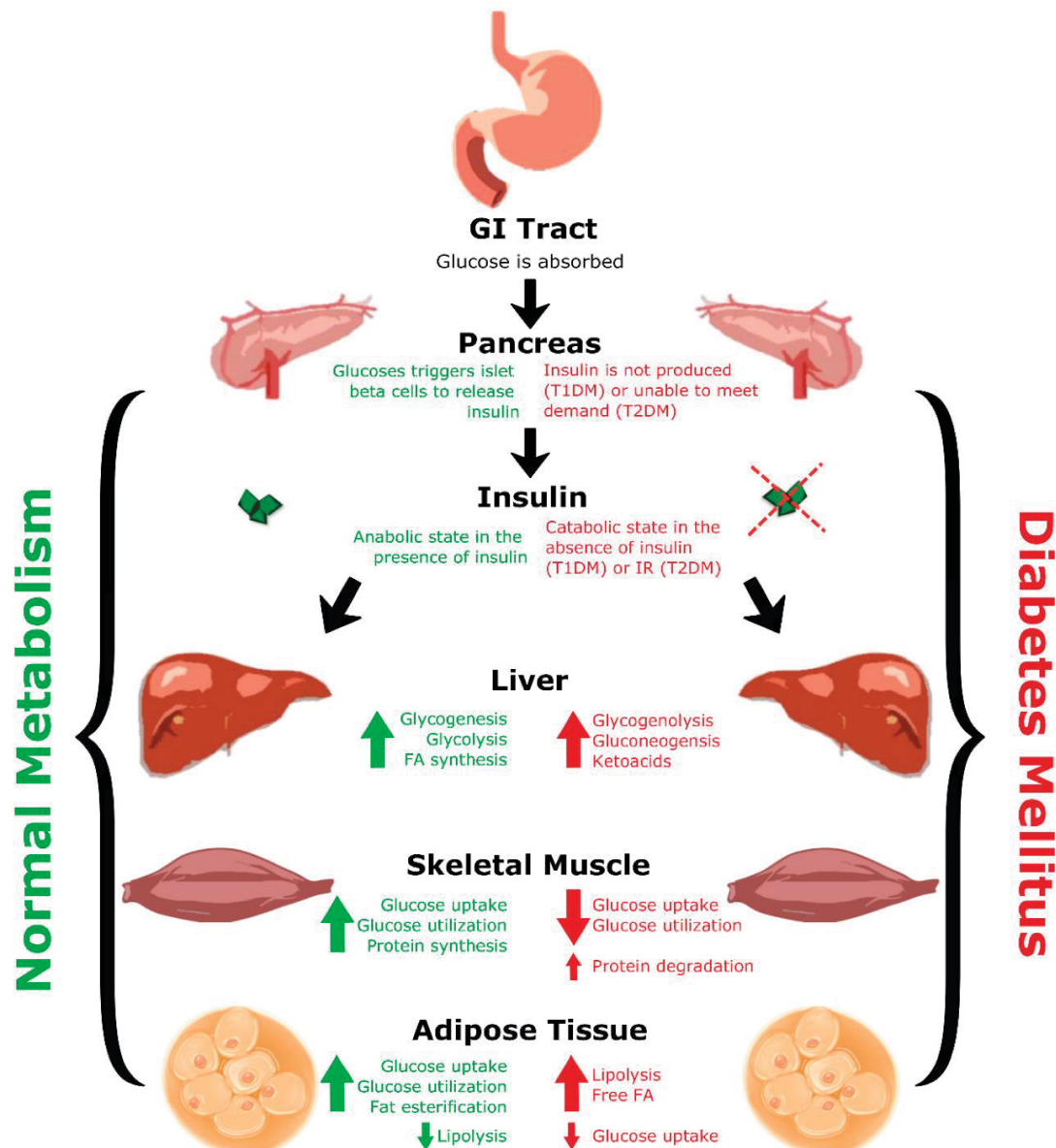
Fig. 1: Regulation of glucose homeostasis in health and disease. At a healthy state, digested glucose is absorbed into the bloodstream to induce insulin secretion by the pancreatic beta-cells. Insulin-responsive tissues help to maintain blood glucose levels by the uptake of excess glucose into skeletal muscle and adipose tissue and inhibition of gluconeogenesis in the liver. In an unbalanced metabolism, as in diabetic states, glucose remains in the circulation due to a decreased insulin sensitivity of the tissues, leading to a state called hyperglycaemia [18].

1.2.1 Insulin action and resistance

The effect of insulin action is of pleiotropic nature as it critically depends on the target tissue, the time course and the presence of other hormones. In general, the regulation of blood glucose levels is induced by binding of insulin to its receptor. Activation and subsequently phosphorylation of the insulin receptor enables phosphorylation of insulin receptor substrate (IRS) proteins, which further activates two major downstream signalling pathways. One of them is the phosphatidylinositol-3-kinase (PI3K) pathway, whereby the activation of protein kinase B (PKB or AKT) leads to a complex phosphorylation cascade of downstream effectors

with influence on several important cellular events, such as increased glucose metabolism, lipid or protein synthesis [19]. The second signalling pathway activated by IRS is that of the mitogen-activated protein kinase (MAPK) which, as indicated by its name, regulates mitogenic events like proliferation, differentiation and survival [20]. Consequently, a certain sensitivity towards insulin within the peripheral tissues is essential to ensure a proper regulation of cell growth, lipogenesis and glucose metabolism.

Skeletal muscle insulin sensitivity plays a major role for whole-body glucose homeostasis as it metabolizes the main fraction of circulating glucose. In this context, insulin stimulation promotes translocation of glucose transporter 4 (GLUT4) vesicles to the plasma membrane, which catalyses glucose transport into the cell. Once blood glucose concentrations are lowered and insulin levels decline, GLUT4 transporters are recycled back into their intracellular vesicles by endocytosis. Insulin resistance in skeletal muscle mainly evolves as a result of increased intracellular lipid metabolites that usually derive from elevated plasma concentrations of free fatty acids (FFA) [21, 22]. Thus, defects in glucose and FFA uptake into the skeletal muscle have been considered as the earliest symptoms in the development of T2D [23, 24]. Increasing amounts of intramyocellular triglycerides have further shown to decrease mitochondrial oxidative activity and ATP synthesis which strongly associate with insulin resistance and T2D [22].

In the liver, the most important function of insulin is the inhibition of hepatic glucose production. This can be achieved by the suppression of gluconeogenic enzymes, such as the phosphoenolpyruvate carboxylase (PEPCK) and the glucose-6-phosphatase (G6P), or by inactivation of glycogen synthase kinase-3 (GSK3) via the AKT signalling pathway [25, 26]. Furthermore, insulin mediates a metabolic switch in the hepatic lipid metabolism by the conversion of glucose to acetyl-Coenzyme A (CoA) during glycolysis. This step is essential for the *de novo* synthesis of hepatic lipids (DNL) to arrange a storage of triglycerides (TG) for times of high energy demand. Thereby, insulin induces the activation of lipogenic genes, such as the sterol-response-binding-protein-1c (SREBP-1c) and further mediates AKT-driven synthesis of very low-density lipoprotein (VLDLs), underscoring the close link between glucose and lipid metabolism[27]. Hepatic insulin resistance mainly leads to inadequate glucose uptake, storage and suppression of endogenous glucose production. Following severe hyperglycaemia often results in the development of hepatic steatosis or non-alcoholic fatty liver disease (NAFLD). Although hepatic insulin resistance is characterized by an impaired glucose tolerance and altered lipid metabolism, interestingly insulin-stimulated DNL is not always affected [28].

As an important energy storage and endocrine organ, the adipose tissue represents as well an essential insulin-responsive tissue. While lipolysis is effectively decreased by insulin resulting in reduced plasma fatty acid concentrations[29], most of the lipids derive from glucose oxidation or fatty acid synthesis, although glucose uptake into the adipose tissue accounts only for a small proportion (<10 %). In the form of triacylglycerols, other organs can further use these lipids as energy source after mobilization of the TGs as long-chain fatty acids through the bloodstream. In the insulin resistant state, both increased lipolysis and inhibited triacylglycerol uptake are the leading cause of elevated plasma fatty acid levels. Another result of insulin resistance in adipose tissue is the accumulation of ectopic fat in obese patients. While subcutaneous fat depots have a beneficial impact on the whole-body metabolism, expanding visceral fat has increasing evidence to contribute to T2D [30]. Especially in states of over-nutrition, expansion of the adipose tissue is rapidly reaching its maximal storage capacity. As a consequence, adipose depots expand first by increasing cell size (hypertrophy) until signals are released to induce the proliferation (hyperplasia). Excess lipids are deposited in other peripheral tissues such as liver and pancreas where the release of lipid metabolites can exert toxic effects contributing to insulin resistance [31, 32].

1.2.2 Metabolic flexibility

Regulation of postprandial glucose levels underlies a tight mechanism dependent on insulin and other hormones. However, it has been shown that an impaired glucose uptake into insulin resistant tissues does not necessarily lead to chronic hyperglycemia [33, 34]. A possible explanation for these findings is the ability to adapt to such physiological changes. Especially the adipose tissue and the skeletal muscle, both playing a crucial role in energy metabolism, have been reported to be highly metabolic flexible. Their ability to switch between energy substrates in the transition from fasting to fed states (or during exercise) is predominantly driven by cellular processes in the mitochondria. In skeletal muscle, a shift from fatty acid to glucose oxidation including a distinct increase in glycolysis, has been demonstrated to be healthy in the transition from fasted to fed states. This shift is dependent on the content and amount of the available ingested nutrients, as well as on the genetically determined fuel oxidation and storage capacity [35]. Insulin resistance in skeletal muscle has a substantial impact on fuel oxidation, thereby causing metabolic inflexibility. The other way around, impaired metabolic flexibility can alter mitochondrial function, including fatty acid synthesis, further contributing to insulin resistance [36, 37].

In the adipose tissue, metabolic flexibility is closely linked to energy storage and supply for peripheral tissues. A well-regulated balance of lipids is essential as both, absence and excess is associated with metabolic complications [38, 39]. Especially in response to acute exercise, abdominal subcutaneous fat depots represent an important energy supplier as they are the biggest in size, containing higher amounts of free fatty acids that can be mobilized to the skeletal muscle and other tissues [40]. Similarly, also insulin resistance shows anabolic effects in adipose tissue that lead to an increasing rate of lipolysis, elevating the amount of free fatty acids. As a sign of metabolic flexibility, adipose tissue tries to counteract the development of dyslipidemia by expansion to further maintain insulin sensitivity and glucose homeostasis [41]. However, obesity-induced insulin resistance showed not only impaired adipose tissue inflexibility but also, as a cause of ectopically deposited fatty acids, metabolic changes in other tissues [42].

1.2.3 Organ crosstalk in glucose metabolism

Besides primary defects in the glucose or lipid metabolism, also cytokines have been shown to play a major role in the mechanisms of insulin resistance and its comorbidities such as diabetes. Depending on the tissue which is responsible for the secretion of these signalling proteins, one can differentiate between myokines (skeletal muscle), adipokines (adipose tissue), hepatokines (liver) and inflammatory cytokines (immune cells) [43]. In the skeletal muscle the two most studied myokines regarding glucose homeostasis, are interleukin 6 (IL-6) and myonectin. Both myokines have shown to increase myocellular insulin-stimulated glucose uptake and fat oxidation through AMPK and PI3K-AKT signalling pathways [44, 45]. Moreover, the endocrine effects of IL-6 have shown to modulate further key metabolic functions by an inter-organ crosstalk. Recent studies described that contraction-mediated IL-6 secretion contributes to the maintenance of blood glucose levels by regulating pancreatic insulin secretion as well as hepatic glucose production [46, 47]. In the context of T2D and obesity also adipokines like leptin and adiponectin play a major role in the regulation of metabolism and inter-organ signalling. While leptin is secreted solely by the adipose tissue to promote fatty acid oxidation and glucose uptake [48], adiponectin and its insulin-sensitizing effects reside in both adipocytes and hepatocytes [49, 50]. Similar effects across the tissues have been reported for the fibroblast growth factor 21 (FGF21) which is a protein mainly expressed in the liver. This hepatokine is known to induce several positive metabolic functions as it ensures intact insulin signalling by regulating lipid and energy metabolism. Furthermore, also in adipocytes FGF21 stimulates insulin-dependent glucose uptake and causes the inhibition of lipolysis by improving insulin

sensitivity [51, 52]. Quite the contrary is represented by the tumor necrosis factor alpha (TNF-α) which in contrast to the above mentioned positive regulators of the insulin signalling pathway rather mediates insulin resistance leading to impaired glucose tolerance [53]. TNF-α and other pro-inflammatory cytokines such as IL-1β or IL-6 have emerged as important pathophysiological factors of T2D and therefore emphasize the close link to our immune system [54, 55]. However, the question whether biosynthesis and secretion of all these cytokines are regulated by insulin itself remains unclear.

1.3 The use of mouse models for diabetes research

For the analysis of the genetic nature of T2D, animal models have been proven to be a powerful tool as their genome has a high homology with those of humans. The advantage over human studies is indicated by the ability to control the environment of the animals, their shorter generation time and the opportunity to investigate single gene variants *in vivo* [56]. One example of a monogenic mouse model in which obesity is derived from single gene mutation is the *ob/ob* mouse. Due to a spontaneous mutation in the gene encoding leptin, these mice develop severe obesity at early stages of life as a result of the dysregulated protein biosynthesis and the following increase in food intake. Also the onset of diabetes can be promoted by single mutations which is shown in *db/db* mice with defects in the leptin receptor [57, 58]. A similar diabetic phenotype but without any signs of obesity has been found in the Akita mouse model [59]. However, T2D research has become successful with the generation of mouse inbred strains that differ in the combinations of several gene variants to mimic the symptoms of the human disease. For this reason, different polygenetic mouse models have been established in the past, one of them the New Zealand Obese (NZO) mouse strain [60].
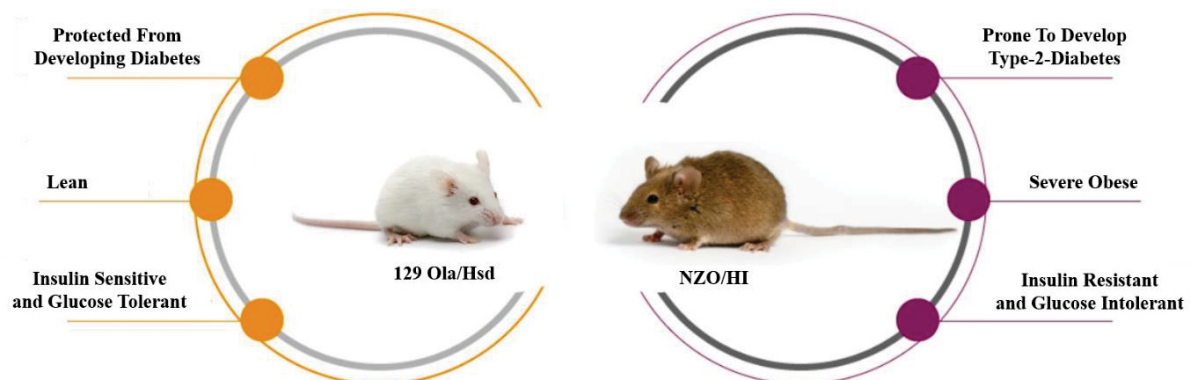
Fig. 2: Phenotypes of inbred 129P2/OlaHsd (Ola) and New Zealand Obese (NZO) mouse strains. (Adapted from Axton, 2020)**.**

The New Zealand Obese (NZO) mouse (Fig. 2) has its origin in a colony of randomly bred mice that were initially selected for their agouti coat color. In 1948, M. Bielschowsky started to inbreed these mice, whereby an adipogenic phenotype was observed after the F10 generation [61]. The following selection for an obese progeny led to the establishment of the current NZO mouse strain. About 60 % of male NZO mice develop a polygenic disease pattern, which is, in response to high-fat diet (HFD) consumption, very similar to the human metabolic syndrome. Depending on the extent of the developing symptoms, including obesity, dyslipidemia, hyperinsulinemia, hypertension and insulin resistance, animals also suffer from a varying degree of hyperglycemia [62, 63]. Furthermore, it has been shown that even on a low caloric diet, about one in two male NZO mice develops hyperglycemia with severe obesity. At later stages of the disease, pancreatic β-cell failure results in decreasing insulin contents leading to a hypoinsulinemic state. In contrast, female NZO mice exhibit obesity and insulin resistance but are protected from T2D development, which has been attributed to the protective influence of the hormone estrogen [63, 64]. Despite non-synonymous mutations in the leptin-encoding gene have been discovered in the NZO mouse strain, none of the known variants can explain the development of severe obesity. However, it is speculated that rather an interplay of several adipogenic genes are involved in the observed phenotype. Therefore, the NZO strain bears a high potential to discover novel disease genes for obesity and T2D [65, 66].

In contrary to NZO animals, the 129P2/OlaHsd (Ola) mouse strain is characterized by a lean phenotype, on both low-caloric and high-fat diet, and remains glucose tolerant (Fig. 2). Due to a low beta-cell mass, these mice maintain low plasma insulin concentrations which can be explained by a high insulin sensitivity of the peripheral tissues [67]. Even genetically induced disruptive mutations in the *Lepr* or *Insr* genes, respectively, have been shown to only result in mild symptoms in this mouse strain. Thus, the Ola mouse strain can be described as diabetes-resistant [68, 69]. Nowadays, there are numerous substrains available differing in their genetic architecture. However, all 129P2/OlaHsd strains share the mutations for a coat color ranging from albino to chinchillation and pink-coloured eyes [70].

1.4 Strategies for the identification of disease-related genes

Most common disorders are characterized by a phenotype variation of different quantitative traits that include aspects of morphology (body weight), physiology (blood glucose), behavior (depression), as well as molecular phenotypes (gene expression differences) [71]. These traits can be affected by the environment or the epigenome, but also the interaction of genomic

regions within the individual genetic background can lead to disease-related traits. The linkage of such genomic regions to a specific quantitative trait is referred to as quantitative trait locus (QTL).

To map the polygenic architecture of diseases like diabetes and adiposity to phenotype-associated genomic regions, the methodology of genome-wide association studies (GWAS) has been introduced in the early 21st century [72]. Although linkage studies have been accomplished already much earlier, usage of large-scale approaches with increased sample size showed much higher validity. The analysis of genetic variations in GWAS is based on the separation of individuals into at least two groups that differ in the traits of interest. Using single nucleotide polymorphisms (SNPs) the genomic DNA of these individuals is mapped to a chromosomal position. On this basis, computational methods are able to calculate the linkage of these SNPs with the investigated phenotype of interest to identify QTL regions that have a high probability to contribute to a certain disease [73] [56]. To confirm this linkage, a convenient threshold is calculated by the logarithm of the odds (LOD) score that evaluates the statistical significance of a QTL [74].

In terms of mouse genetics, the detection of such a QTL is highly variable as it depends on the used mouse population. Starting with the crossbreeding of two mouse strains that differ in the phenotypic trait of interest, the resulting offspring (F1) can be further crossed with either each other to receive an intercross (F2) or with one of the parental strains to produce a backcross (N2) population. Depending on the population (F2 or N2), genetic recombination leads to different combinations of the parental genome, thereby generating a heterogeneous genetic background. When using the F2 population, the offspring can consist of a allelic distribution of either 25 % heterozygous and 25 % homozygous animals of each parental genotype, while the N2 population generates an offspring of 50 % heterozygous and 50 % homozygous animals. When aiming to identify dominantly acting genes relevant for a specific disease, analysis of the N2 population is the better choice, which moreover requires only half of the animals of an F2 population but reaching the same degree of power [75].

Such linkage studies emphasize the advantage of mouse models across from human studies. Despite the aforementioned ability to control environmental factors, genetic variation within a single mouse cross remains quite low compared to human populations. As a result, only few hundred animals are required to identify a QTL region explaining a specific phenotype while human studies would need tens of thousands of individuals [76, 77]. However, the identification of the causal gene variant remains difficult as each QTL region often harbors several hundreds

of genes. Additionally, the last decades have shown that the underlying genetic risk of polygenic diseases is mainly composed of many gene variants with cumulative effect and just rarely at the basis of single genes with moderate effect [78]. Moreover, the identification of a QTL alone does not provide any information on the target tissue and the molecular function. Therefore, secondary analysis such as pathway analysis, aiming a more detailed biological understanding of the specific function and role within the examined disease of the identified risk loci or the generation of recombinant congenic strains (RCS) to further narrow down the genetic region, seem to depict promising solutions [79, 80]. Nevertheless, functional investigation of selected candidate genes *in vitro* or *in vivo* are essential to validate the before seen genetic association within a QTL.

1.4.1 Strategies to narrow down a critical genomic region

Once a potential QTL has been identified, further characterization of the genetic region needs to be assessed to find the underlying gene(s) for the observed phenotype. The generation of recombinant congenic strain (RCS) has shown to be a powerful tool to narrow down such genomic regions, whereby introgression of a selected chromosomal fragment onto the background of a reference strain is performed (Fig. 5). After repeated backcrossing the genetic background of the reference strain can be increased for up to 99 % so that these animals only differ in the genomic region of interest [81]. This procedure can be accelerated by a technique called "speed congenics", where the breeding animals are consistently genotyped to select animals carrying the maximal genomic background of the reference strain [82]. Using RCS for the identification of genetic modifier of a respective QTL has the advantage that the genomic variance is reduced to a minimum so that the phenotypic effect can be reliably referred to the introgressed chromosomal fragment. Based on the successful replication of the observed phenotype, the generation of RCS with even smaller fragments enables a further reduction of the number of candidate genes within the genomic region [83, 84].

Other strategies like haplotype or gene expression analysis are using the genetic information of the mouse genome with the general assumption that the underlying causative gene(s) of the identified QTL is differentially expressed in one of the strains. For these analyses one has to distinguish whether the genetic changes are expected to be of an inherited origin or due to newly developed mutations by recombination. The haplotype analysis is based on the assumption that phenotypic differences mostly occur due to the genetic inheritance from different ancestors rather than due to mutations [85]. Full genome sequences of common parental inbred strains

are freely available to perform a comparative analysis of strain-specific genes to identify polymorphic regions. By using informative SNP marker, genomic regions can be determined that are either identical (identical by descent, IBD) or polymorph (non-identical by descent, non-IBD) between the analysed mouse strains. While IBD regions are supposed to descend from a common ancestor, it is very likely that non-IBD regions may be more affected by mutations during genetic recombination [85, 86]. In contrast to haplotype analysis, whole-genome transcriptome profiling using microarray techniques represents a fast and high-throughput method that directly detects gene expression differences that occur due to mutation, single nucleotide polymorphisms and other genetic aberrations. In this context, a basic assumption is that phenotypic differences occur due to spontaneous alterations of causative genes reflected by marked differences in their mRNA expression. Another advantage is the opportunity to analyse gene expression of different tissues or isolated primary cells to identify genes of tissue-specific metabolic processes. In sum, several QTL studies have used haplotype or gene expression analyses (or a combination of both) to successfully identify potential risk genes for complex metabolic diseases [87-90].

1.4.2 Blood glucose-related QTL in mouse research

In context to clarify the genetic cause of T2D, a large number of animal studies were conducted in the past using different strains with varying susceptibility towards the development of diabetes, such as C57BL/6, C3H/HeJ, BALB/c, NON/Lt, NZO/HI, DBA/2, SJL/N and other. Although numerous QTL have been linked to T2D prevalence (such as blood glucose levels, glucose tolerance, plasma insulin levels or pancreatic insulin concentration), only a low percentage of the phenotypic association can be explained by a defined genetic modifier. Furthermore, these QTL display a broad chromosomal distribution with some overlapping regions between different mouse models (Suppl. Tab. 1). One example of accumulating QTL were found on mouse chromosome 15 with highly significant linkage to fasting blood glucose levels (FBG) as well as glucose tolerance (IPGTT). Thereby, linkage was found on two independent mouse crosses of Akita x A/J mice and LP/J x BALB/cJ mice with LOD scores of 6.17 and 7.03, respectively [91, 92]. A recent publication of Shi and colleagues showed that this QTL was previously found in multiple crosses, whereby screening of the causative genes led to the identification of three potential candidate genes [91]. Another prominent region for diabetes-related QTL has been found on chromosome 4, whereby most of these loci were based on mouse crosses with the diabetes-susceptible NZO mouse strain [87, 93-95]. Despite the close genomic relationship of these crosses, the causative gene variant that may explain the

comprehensively observed hyperglycemic and hyperinsulinemic traits within the overlapping QTL regions could not be elucidated up to today. This again highlights the complexity of T2D and the difficulty to uncover the underlying genes.

1.5 The collective diabetes cross

Individual crossbreeding approaches of inbred mouse strains have been proven to be useful for the identification of diabetic susceptibility genes in the recent years. In this context, it turned out that the characterization of multiple crossbreeding approaches in parallel represents an even more advantageous method to accelerate the process of gene discovery and to increase the evidence of identified polymorphic variants by the genomic diversity of the different mouse crosses. The collective diabetes cross was carried out within a collaborative project between the German Diabetes Center (DDZ) and the German Institute for Nutrition (DIfE) and has been funded by the German Center for Diabetes Research (DZD). This crossbreeding approach includes a comprehensive linkage study of four lean mouse strains (C57BL/6, C3H/HeJ, DBA/2, 129P2/OlaHsd) which were intercrossed with the diabetes-prone New Zealand Obese (NZO) mouse in four separate approaches. As theses mouse strains differ widely in their diabetes susceptibilities, comparison of genotypes and phenotypes facilitates the identification of novel genomic regions and the limitation of the causative gene variants. For this purpose, approximately 600 mice (300 males/females) of each backcross population (N2) underwent a deep phenotyping schedule after receiving a high-fat diet (HFD) at 3 weeks of age. To determine their genotypes, informative SNP markers were used with 10-20 Mb intervals and linkage analysis was performed separately for each crossbreeding experiment and gender.

Linkage analysis of these mouse populations led to the identification of multiple QTL, again underlying the complexity of diabetes development. Genome-wide QTL scans allowed the chromosomal distribution of the respective blood glucose-related traits which showed a predominant pattern in male compared to female mice. In detail, the most prominent genomic region with linkage to blood glucose levels was found on chromosome 4 within three of four crossbreedings (Fig. 3). Previous studies have identified *Zfp69* as a causative gene in a crossbreeding approach using lean Swiss Jum Lambert (SJL) and obese NZO mice [96] [94]. However, this genetic modifier seem to be uniquely expressed in SJL and therefore remains unlikely to be the only regulator of glucose homeostasis. Analysis of another mouse cross with DBA mice carrying the diabetogenic allele of *Nidd/DBA,* showed similar hyperglycemic features and an impaired insulin secretion. Investigations of a reduced fragment of the *Nidd/DBA* locus led to the identification of four potential candidate genes that might be relevant

for maintaining glucose homeostasis in these animals by influencing pancreatic beta-cell function [87]. Although other mouse populations, independently from the collective diabetes cross, have been analysed worldwide, relevant causal genes for the multiple diabetes-related QTL on murine chromosome 4 have only been insufficiently investigated so far.
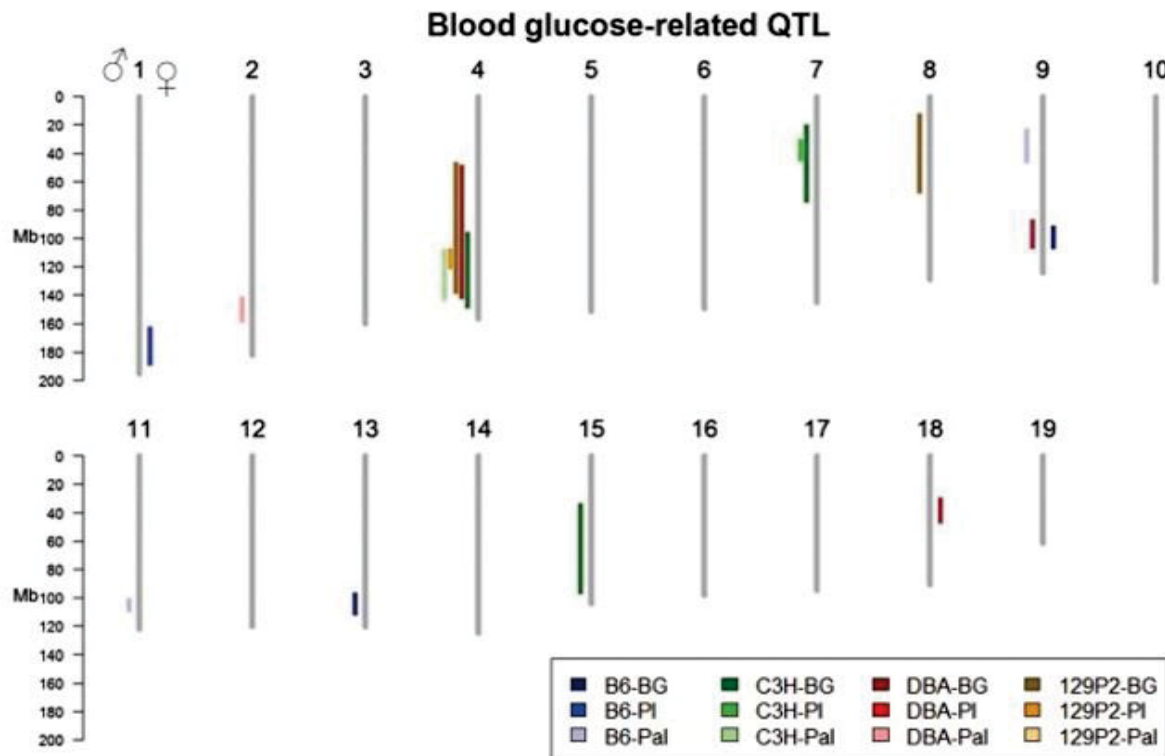
Fig. 3: Chromosomal distribution of blood glucose-related QTL in NZO crosses. Genome-wide QTL scans of NZO backcross populations with different diabetes-susceptible mouse strains were mapped to the corresponding chromosomal region. Genomic regions with linkage to glucose homeostasis such as blood glucose (BG), plasma insulin (PI) or pancreatic insulin (PaI) were assigned to either the left (males) or right (females) side of the indicated chromosome [97].

Another crossbreeding between NZO and T2D-resistant C3H mice that has been conducted in our research group, led to the identification of two further QTL for blood glucose levels. These susceptibility loci on chromosome 7 (*Nbg7*) and 15 (*Nbg15*) showed protective effects for T2D on mice carrying the respective C3H alleles on a NZO genomic background. Combined gene expression profiling with haplotype analysis led to the identification of new candidate genes which might explain the underlying diabetes-protective effect. For *Nbg7,* significant associations were observed for the candidates *Pop4* and *Atp4a*, which showed a distinct reduction in insulin secretion after siRNA-mediated knockdown in the Min6 insulinoma cell line [95]. Moreover, also the gene *Nudt19* has been considered to contribute to the phenotypic outcome of *Nbg7* by the regulation of fatty acid β-oxidation and was confirmed as described later in this study (4.3.2). Similar to *Nbg7*, the identified *Nbg15* locus seems to be characterized by protective pancreatic islet function and/or integrity which probably affects the severity of

hyperglycaemia and T2D. Candidate gene analysis revealed a potential contribution of the gene *Kdelr3* on *Nbg15* presumably by regulating insulin granules maturation and pro-insulin levels [88]. These findings show that the selected methods are more than promising when trying to find the causative genetic modifier for metabolic disorders which contribute to the overall understanding of polygenic diseases such as T2D.

1.5.1 *Nbg4* – A new susceptibility locus for T2D

In order to identify causative genes that associate with the pathogenesis of T2D, a crossbreeding between the diabetes prone NZO with the lean and T2D-resistant 129P2/OlaHsd (Ola) mouse was previously conducted in our research group [98]. Subsequent linkage analysis of the N2(NZOxOla) population revealed multiple QTL on chromosome 4 that associated with higher random (LOD 5.8 at 27.53 cM and 7.1 at 41.37 cM) and fasted (LOD 3.2 at 41.37 cM) blood glucose levels as well as liver weight (LOD 5.8 at 47.03 cM) in heterozygous NZO/Ola (N/O) allele carriers (Fig. 4). The identified genomic region, further designated as *Nbg4* (NZO blood glucose locus on chromosome 4), has a size of 57.91 Mb, carrying several hundreds of genes (Fig. 3). Based on the observed LOD scores, the locus can be separated into three distinct peak regions, namely at 58.07 cM, 41.37 cM and at 48.72 cM. Thereby, animals carrying the heterozygous N/O alleles showed higher blood glucose levels compared to animals carrying the N/N alleles, reaching a maximum average of 309.2 mg/dL compared to 252.6 mg/dL, respectively. At fasted states, the difference in blood glucose concentrations reached 44.5 mg/dL between the genotypes. Therefore, N/O-allele carriers showed a risk to develop T2D that was approximately 27.1 % higher compared to homozygous N/N-allele carriers. Although plasma insulin levels in fasted animals were significantly elevated in N/O-allele carriers (10.9 µg/L in N/O vs. 7.7 µg/L in N/N), linkage analysis revealed no significant association with the identified genomic region on chromosome 4 (LOD 2.1). The observed hyperglycemic phenotype was not associated with body weight or body composition, respectively, but showed linkage to liver weight with a maximum difference of 0.5 g between the genotypes [98]. These data led to the hypothesis that the Ola allele for *Nbg4* harbors risk genes that were predominantly expressed on an obese NZO genomic background, eventually leading to increased insulin resistance in peripheral tissues and therefore to the observed hyperglycemic phenotype.
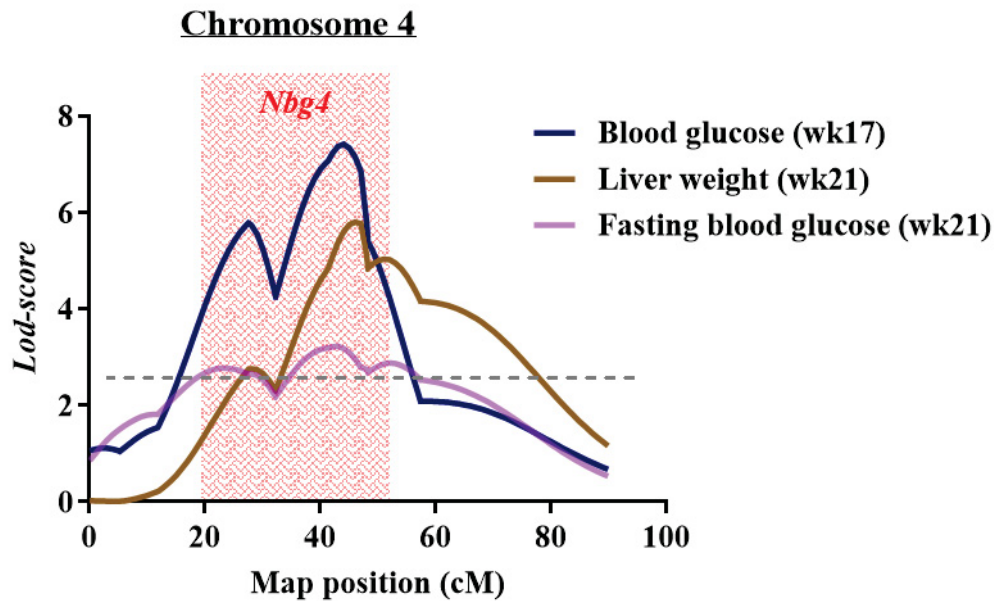
Fig. 4: *Nbg4* reveals linkage with blood glucose and liver weight. Linkage analysis of the N2(NZOx129Ola) genome with diabetes-related traits revealed significant associations on chromosome 4 with random (LOD 5.8 at 27.53 cM and 7.1 at 41.37 cM) and fasted (LOD 3.2 at 41.37 cM) blood glucose as well as liver weight (LOD 5.8 at 47.03 cM). The susceptibility locus in which these QTL were located was designated as *Nbg4* (NZO blood glucose on chromosome 4). wk = week, cM = centimorgan, LOD = logarithm of the odds. (Adapted from: Sandra Lebek PhD thesis 2018).

1.6 Aim of this work

The aim of this work was the identification and functional investigation of novel risk genes for the development of T2D using different approaches of mouse genetics. To provide a better overview of the key findings, the present study is separated into two parts. The first part aims the identification of novel risk genes for the blood glucose QTL *Nbg4*. Since this diabetes susceptibility locus spans a large genomic region, the first strategy was to narrow the critical genomic region by generating RCS lines carrying different fragments of the locus. Following, phenotypic characterization of the congenic lines was performed for the validation of the hyperglycemic phenotype observed in the backcross population. After, the target tissue(s) were identified by *ex vivo* metabolic investigation to localize the origin of the hyperglycemic effect of *Nbg4*. Further, a combination of *in silico* analyses of DNA variations with gene expression profiling was used to select potential causal genes. Finally, the second part of this work aims the validation of diabetes-related genes that have been identified from different crossbreeding approaches. In this context, functional *in vitro* characterization of the genes *Alad* and *Nudt19* aimed the confirmation of a potential contribution to *Nbg4* and *Nbg7*, respectively.

2. Materials and Methods

2.1 Materials

2.1.1 Mouse strains

The RCS.NZO.129Ola-*Nbg4* mouse strain used throughout this study was generated by selective breeding in the animal facility of the German Diabetes Centre (Düsseldorf, Germany).

2.1.2 Mouse diets

Mice were divided into different cohorts and received either a standard diet (SD, V1126) purchased from ssniff (Soest, Germany), which was composed of 11 kcal% fat, or a high-fat-diet (HFD, D12451) purchased from Research Diets Inc. (New Brunswick, NJ, USA) with 45 kcal% fat.

2.1.3 Mammalian cells

The murine liver cell line Hepa 1-6 (CRL-1830), originated from a C57BL/6J tumor (BW7756) and 3T3-L1 fibroblasts (CL-173) were purchased from ATCC (USA). Plat-E packaging cells used for retroviral overexpression were kindly provided from Prof. Dr. Stork from the University hospital of Düsseldorf (Germany).

2.1.4 Cultivation media, buffers and solutions

Tab. 1: Cell culture media, buffers and solutions

Name	Ingredients / Supplier
Cell culture media	
Dulbecco's Modified Eagle Medium (DMEM), high glucose and low glucose	Thermo Fisher Scientific (Schwerte, Germany)
CMRL medium without L-glutamine and HEPES	Thermo Fisher Scientific (Schwerte, Germany)
Dulbecco's Phosphate Buffered Saline (DPBS)	Thermo Fisher Scientific (Schwerte, Germany)
Fetal calf serum (FCS)	Biochrom (Berlin, Germany)
Newborn calf serum (NCS)	Sigma Aldrich (Steinheim, Germany)
3T3-L1 Maintaining medium (MM)	10 % NCS and 1 % PenStrep in DMEM (25 mM glucose)
3T3-L1 Differentiation medium I (DMI)	10 % FCS, 1 % PenStrep, 1 µg/mL insulin, 1 µM dexamethasone, 2 µM rosiglitazone and 0.5 µM IBMX in DMEM (25 mM glucose)

Name	Ingredients / Supplier
3T3-L1 Differentiation medium II (DMII)	10 % fetal calf serum, 1 % PenStrep and 1 μg/mL insulin in DMEM (25 mM glucose)
Fetal bovine serum (FBS)	Biochrom (Berlin, Germany)
Cultivation medium (for Hepa 1-6 and Plat-E cells)	10 % heat-inactivated FBS, 1 % PenStrep, 1.12 % 1 M HEPES, 1 % GlutaMAX, 1 % 100 mM sodiumpyruvate, 0.35 % 50 mM β-Mercaptoethanol in DMEM (high glucose)
Opti-MEM I reduced serum medium	Thermo Fisher Scientific (Schwerte, Germany)
Sodium acetate buffer	0.12 M sodium acetate solved in distilled H_2O, pH 4.8
TEA-buffer 200 mM	3.71 g triethanolamine hydrochloride (TEA) diluted in 100 mL dH_2O, pH 8.1
Trypsin-EDTA solution	Sigma Aldrich (Steinheim, Germany)
Trypan blue stain 0.4 %	Thermo Fisher Scientific (Schwerte, Germany)
Penicillin/streptomycin (Pen Strep)	Thermo Fisher Scientific (Schwerte, Germany)

Glucose uptake in isolated skeletal muscles

Krebs-Henseleit buffer (KHB)	Stock I: 118.5 mM NaCl, 4.7 mM KCl, 1.2 mM KH_2PO_4, 25 mM $NaHCO_3$, gassing with CO_2 for 20 minutes on ice; Stock II: 2.5 mM $CaCl_2 \cdot 2\ H_2O$, 1.2 mM $MgSO_4$ x 7 H_2O, 5 mM HEPES, gassing with CO_2 for 10 minutes on ice, mix I and II and add 1 % BSA
Hot incubation buffer	19 mM Mannitol, 1 mM 2-deoxyglucose with/without 120 nM Insulin, 2.5 μCi/mL [^{3}H]-2-deoxyglucose, 0.7 μCi/mL [^{14}C]-mannitol
Incubation buffer	15 mM Mannitol and 5 mM Glucose with/without 120 nM Insulin in KHB
Recovery buffer	15 mM Mannitol and 5 mM Glucose in KHB
Rinse buffer	20 mM Mannitol with/without 120 nM Insulin in KHB
Acid ethanol	0.18 M HCl in 75 % ethanol
Anticoagulant	25 mL 0.5 M EDTA, 92 mg aprotinin dissolved in 21 mL saline (0.15 M), 4 mL heparin (10.000 U/mL), 21.6 mg diprotin A

Name	Ingredients / Supplier
Glucose uptake in isolated adipocytes	
KRBH (Krebs-Ringer-Bicarbonate HEPES) buffer	120 mM NaCl, 4 mM KH_2PO_4, 1 mM $MgSO_4 \cdot 7\ H_2O$, 1 mM $CaCl_2 \cdot 2\ H_2O$, 10 mM $NaHCO_3$, 30 mM HEPES, 5 % BSA, 200 nM adenosine freshly added, with/without 120 nM Insulin (pH 7.4)
Lipid extraction solution	78 Vol. % 2-propanol, 20 Vol. % heptane, 2 Vol. % sulphuric acid
Primary hepatocytes isolation and assays	
Hanks' balanced salt solution (HBSS)	5.33 mM KCl, 0.44 mM KH_2PO_4, 0.34 mM N_2HPO_4, 138 mM NaCl, 4.17 mM $NaHCO_3$, 5.56 mM glucose, 0.5 mM EGTA and 25 mM HEPES
Plating medium	10% (v/v) FCS, 1.5 mM sodium pyruvate (final conc. 2 mM), 0.1 μM porcine insulin, 1 μM Dexamethasone, 2x Antibiotic-Antimycotic mix in DMEM/F-12 with GlutaMAX™ supplement
Glucose production medium	2.5 mM Glutamine, 15 mM HEPES, 3.7 g/mL $NaHCO_3$, 1x Antibiotic-Antimycotic mix in DMEM w/o glucose, L-glutamine, phenol red, sodium pyruvate and sodium bicarbonate
Starvation medium	0.2 % (v/v) BSA Fraction V, 1.5 mM sodium pyruvate (final conc. 2 mM), 2x Antibiotic-Antimycotic mix in DMEM/F-12 with GlutaMAX™ supplement
Pancreatic islet isolation and GSIS	
Collagenase Medium	2x Antibiotic-Antimycotic mix, 0.18 mg/mL collagenase IV in DMEM low glucose
KRH (Krebs-Ringer-HEPES) buffer	15 mM HEPES, 5 mM KCl, 120 mM NaCl, 24 mM $NaHCO_3$, 1 mM $MgCl_2$, 2 mM $CaCl_2$, freshly added 1 mg/mL BSA
Pancreatic islet medium	15 % FBS, 0.1 % 50 mM β-Mercaptoethanol, 1 % penicillin/streptomycin, 0.5 % 1.11 M glucose, 2 % $NaHCO_3$ solution (7.5 %) in CMRL medium without L-glutamine and HEPES

2.1.5 Solutions and chemicals for Seahorse experiments

Tab. 2: Solutions for Agilent Seahorse XF Extracellular Flux Assays

Name	Ingredients / Supplier
FCCP	Agilent Technologies (Waldbronn, Germany)
Oligomycin	Agilent Technologies (Waldbronn, Germany)
Rotenone / Antimycin A	Agilent Technologies (Waldbronn, Germany)
Seahorse XF Assay Medium	1 mM pyruvate, 2 mM glutamine, 10 mM glucose in Seahorse XF Base Medium, pH 7.4
Seahorse XF Base Medium	Agilent Technologies (Waldbronn, Germany)
Seahorse XF Calibrant	Agilent Technologies (Waldbronn, Germany)

2.1.6 Media and solutions for bacterial culture

Tab. 3: Media and solutions for bacterial culture

Name	Ingredients / Supplier
Luria-Bertani (LB) medium, liquid	10 g Peptone, 5 g Yeast Extract and 10 g NaCl were mixed with 1 L ddH$_2$O and autoclaved.
Luria-Bertani (LB) medium, solid	10 g Peptone, 5 g Yeast Extract, 10 g NaCl and 15 g Agar Agar were mixed with 1 L ddH$_2$O and autoclaved.
SOC medium	20 g Tryptone, 5 g Yeast Extract, 0.5 g NaCl and 0.19 g KCl were mixed with 1 L ddH$_2$O and autoclaved. After, 10 mL of 1 M MgCl$_2$ and 10 mL of 20 % Glucose were added.

2.1.7 Plasmids and siRNA

Plasmid-DNA, -shRNA and siRNA oligonucleotides were used for the genetic modification of cultivated mammalian cells (2.2.2.2).

Tab. 4: Plasmid-DNA and -shRNA

Plasmid name	Supplier (Ordering number)
pRS-*Alad* shRNA	Origene (#TR501272C)
pRS-NC	Origene (#TR30012)

Tab. 5: siRNA oligonucleotides

Target Gene	Sequence (5`→ 3`)	Ordering number/ product name (Dharmacon)
Nudt19	#1:CUUUUAACUUCUGAUGGCA #2:CUCUGCUCUGUAUAGAUUU #3:CCUGUGUCAUGUGUGUUUU #4:GCAAAGUCCUUAACCGAGU	E-040466-00-0005, Accell Mouse Nudt19 (110959) siRNA SMART pool
Non-target	UAGCGACUAAACACAUCAAUU	D-001210-01, siGENOME Non-Targeting Control siRNAs

2.1.8 SNP markers

For genotyping, allele-specific primers of different SNP markers were used to confirm the genotype of each genomic region of murine chromosome 4 (Tab. 6). These primers were purchased from LGC genomics (Teddington, United Kingdom) to perform a competitive allele-specific PCR (KASP) as described in section 2.4.2.

Tab. 6: KASP SNP markers for genotyping of RCS.NZOx129Ola-Nbg4. Mb = Megabase, A= Adenine, G= Guanine, C=Cytosine, T= Thymine

JAX Stock #	Position (Mb)	RS_ID	129P2/OlaHsd	NZO/HILtJ
04-032923355-M	33,36	rs3706812	T	C
04-039199957-M	39,40	rs3723778	G	C
04-056969111-M	58,07	rs4138670	G	C
04-075245266-N	77,61	rs16265	A	G
04-085096243-M	87,33	rs3697531	C	T
04-088959560-M	91,02	rs4136370	A	C
04-095346075-M	97,25	rs3726937	C	T
04-114064127-N	115,98	rs4224727	A	G
04-125988404-M	128,20	rs3711319	A	T
04-132955150-M	134,93	rs3679734	A	G
04-150152643-M	154,08	rs3693138	A	C

2.1.9 Oligonucleotides

Primer sequences for qPCR analysis (2.2.3.5) were designed with the help of the online tool Primer-Blast from NCBI and synthesized by Eurogentec (Seraing, Belgium). Primer were diluted in nuclease-free water for a final concentration of 10 nM. The sequences of all primers used in this study are listed in Tab. 7.

Tab. 7: Primer for qPCR

Primer	Locus ID		Sequences	Product size (bp)
CEBPa	NM_007678.3	Fwd:	AGAAGTCGGTGGACAAGAACAGCA	95
		Rev:	GCGTTGTTTGGCTTTATCTCGGCT	
Pparg	NM_011146.3	Fwd:	GCCTATGAGCACTTCACAAGAAAT	168
		Rev:	TGTGGAGCAGAAATGCTGGA	
Fatp1	NM_011977.3	Fwd:	CGCCGATGTGCTCTATGACT	138
		Rev:	ACACAGTCATCCCAGAAGCG	
Fabp4	NM_024406.3	Fwd:	AAGGTGAAGAGCATCATAACCCT	133
		Rev:	TCACGCCTTTCATAACACATTCC	
Slc2a4	NM_009204.2	Fwd:	CAGCGAGTGACTGGAACACT	106
		Rev:	CAATCACCTTCTGTGGGGCA	
Adipoq	NM_009605.5	Fwd:	GCACTGGCAAGTTCTACTGCAACA	114
		Rev:	AGAGAACGGCCTTGTCCTTCTTGA	
Plin1	NM_175640.2	Fwd:	CTGAGACTGAGGTGGCGGTC	101
		Rev:	ACATCCTTACTCTCCACGCTGTAA	
Plin2	NM_007408.3	Fwd:	GGCTGTAAACGTCTGTCTGGA	103
		Rev:	AGCACACGCCTTGAGAGAAA	
LPL	NM_008509	Fwd:	CAGCTGGGCCTAACTTTGAG	144
		Rev:	AATCACACGGATGGCTTCTC	
HSL	NM_010719.5	Fwd:	GGATTGACTCTAAGAGAGGAACTTG	190
		Rev:	GTGAGAACGCTGAGGCTTTG	
Fas	NM_007988	Fwd:	TTGCTGGCACTACAGAATGC	192
		Rev:	AACAGCCTCAGAGCGACAAT	
CD36	NM_007643.4	Fwd:	TGGCCTTACTTGGGATTGG	111
		Rev:	CCAGTGTATATGTAGGCTCATCCA	
IL-1ß	NM_008361.4	Fwd:	TGCCACCTTTTGACAGTGATG	136
		Rev:	ATGTGCTGCTGCGAGATTTG	
Chop	NM_001290183.1	Fwd:	ATCTTGAGCCTAACACGTCGATT	98
		Rev:	CCAGGTTCTCTCTCCTCAGGTT	
BiP	NM_022310.3	Fwd:	TTCAGCCAATTATCAGCAAACTCT	143
		Rev:	TTTTCTGATGTATCCTCTTCACCAGT	
Actb	NM_007393.3	Fwd:	CCACCATGTACCCAGGCATT	253
		Rev:	AGGGTGTAAAACGCAGCTCA	
Scp2	NM_011327.4	Fwd:	TAGGAGACCTTCGCTGCTGGA	231
		Rev:	GGAATCACCATACACATAGCCAACG	
18S	NR_003278.3	Fwd:	GCAATTATTCCCCATGAACG	123
		Rev:	GGCCTCACTAAACCATCCAA	
Aqp7	NM_001378638.1	Fwd:	CCTTGTTACCGTCCTTGGGG	132
		Rev:	AAAGAAGGAGGCCTGAACAC	
AI464131	NM_001085515.2	Fwd:	TGGCGGTCACTGAGACTTCA	155
		Rev:	TGAGACTTTTAGGGCCTGCG	
Cntfr	NM_016673.3	Fwd:	CAGCTGGTGGTAACGAGATGG	175
		Rev:	CCCAGACGCTCATACTGCAC	
Dctn3	NM_016890.4	Fwd:	TGTGTGGCGATCACTGAAGA	70
		Rev:	TGGAGAGAAGCATTGTAGTCTTG	
Ccl19	NM_011888.4	Fwd:	TCACTTGCACTTGGCTCCTGAA	107

Primer	Locus ID		Sequences	Product size (bp)
Ccl19		Rev:	GCAAGAATCTGAGAGGCCGAG	
Il11ra2	NM_010550.4	Fwd:	AATGTGACCGAGGTGAACCC	81
		Rev:	TGGATCGGGACGCAAGATG	
Fam219a	NM_001159583.2	Fwd:	GCAGCCTCTATCTCAGACCG	159
		Rev:	ATTAGGGACGACCAGCCTCG	
Unc13b	NM_021468.3	Fwd:	TGGGGAGAGCATCAGACCTTT	86
		Rev:	GCGCTATTGCTGGTCTCACT	
Atp8b5	NM_177195.3	Fwd:	CTGCCCATGAACCTGTTTGAA	87
		Rev:	GATCTGCGGGACCAACTGT	
Spaar	NM_001348108.1	Fwd:	ATTCCAGGCAGCACCAACAA	149
		Rev:	CCTCAGGACTTCAAGAGTTACTTGG	
Gne	NM_001190414.2	Fwd:	GGGGCTTGCAGAGGAACTC	83
		Rev:	GCTTTCGGTTGTTCCCGTTC	
Gabbr2	NM_001081141.2	Fwd:	TCTTCGGAGTCACGGGTCAA	162
		Rev:	CCGACCCCTGGAACCTTATG	
Invs	NM_010569.4	Fwd:	GGGCAGCCTTACTAGGTCAT	106
		Rev:	GCATAGTGCAAGGGTGTTGC	
Tmeff1	NM_001356272.1	Fwd:	CAAACGGGGACACCTACCAG	139
		Rev:	CCTTCCTCCTCTGCTCCTTCT	
AI314180	NM_001355696.1	Fwd:	CCAGGACGAGCTGAATTCTTT	125
		Rev:	CAGCATGGCCAAGTCGTAAA	
Svep1	NM_022814.2	Fwd:	CCAGACCTGTGAGGTTGTCC	94
		Rev:	GGCGGCATTGAAGTGGTTTT	
Hdhd3	NM_024257.1	Fwd:	CTCTTTTCCCGAGCCAGGATCT	76
		Rev:	GTAGGTCAGAGGGGTAGGCT	
Alad	NM_008525.5	Fwd:	GCGAGCAGCGTCCTTGGTA	89
		Rev:	CCTCAGCTCTTGTTCTGGGGT	
Pfkl	NM_008826.5	Fwd:	CTACGTGAAGGATCTGGTGGT	77
		Rev:	CTCCTCGCTGTACATGACCC	
Pccb	NM_025835.3	Fwd:	CGATTAGGATTCGGGCGGTG	192
		Rev:	CTGTTAGCTTCCCTCGCTTGT	
Acad11	NM_175324.4	Fwd:	CATCAAGCGATGCCACGAAC	168
		Rev:	TGTGCTGTCTGTGTCTGGATG	
Hibch	NM_146108.2	Fwd:	TTGCTATGCCAGAAACGGGA	184
		Rev:	TCCAACACACGCAACTTTTCC	
Sesn2	NM_144907.1	Fwd:	TGAACAACTCAGGGGGCTTTG	132
		Rev:	CCAGCTCAAAACGGTTCTCC	
Casp4	NM_001379319.1	Fwd:	CTGTCAAGCTGTCTTCACGGT	70
		Rev:	TGTCAGGGTGTTTGTTTTCAGC	
Fgfr1	NM_010206.3	Fwd:	GCGATACCACCTACTTCTCCG	134
		Rev:	GGGAGCTACAGGCCTACGG	
Ffar4	NM_181748.2	Fwd:	GCCCAACCGCATAGGAGAA	120
		Rev:	CGCGATGCTTTCGTGATCGTAA	
Adig	NM_145635.2	Fwd:	AAGTACCCTCTGGTGCCTCT	140
		Rev:	TCATCTTCCTTTGACTCTTGACT	
Insr	NM_001330056.1	Fwd:	TGGATTATTGTCTCAAAGGGCTGAA	244

Primer	Locus ID		Sequences	Product size (bp)
Insr		Rev:	GCACCATTGCCTGAAGAGGTT	
Tshr	NM_011648.5	Fwd:	GCAATGAAACCTTGACCCTGAAA	186
		Rev:	CGCTGGTGGAAGACACATCT	
Pde3b	NM_011055.2	Fwd:	ATCGAAAACTTCACAAGGGATTGA	132
		Rev:	ACCCTTACCACTGCTGCGAT	
Adcy5	NM_001012765.5	Fwd:	TGGTGGACCGTGTTCTTCATC	167
		Rev:	ATGAGGACATTGGAGACAAGCTGTT	
Crat	NM_007760.3	Fwd:	AGCTGGCATACTACAGGATCT	211
		Rev:	TCAGTGTAGGCTCGGTGGG	
Slc22a5	NM_001362711.1	Fwd:	GACATCAGGTTGGAGAACAGAA	108
		Rev:	AACAGTGGCAGCACCATGAA	
Cpt2	NM_009949.2	Fwd:	CGTACCCACCATGCACTACC	128
		Rev:	CTTCTGTCTTCCTGAACTGGCT	
Acox1	NM_015729.3	Fwd:	TCATGTGGTTTAAAAACTCTGTGC	70
		Rev:	AGGAACATGCCCAAGTGAAGG	
Plpp2	NM_015817.3	Fwd:	GCGTGTTGGTCGCCTCT	190
		Rev:	ACCAGGTAGGCTTCTCCCAA	
9130409I23Rik	NM_001033819.2	Fwd:	AGACCTTCCCTTGGTGAGGAA	183
		Rev:	TGCTTTGACTCTGACAGTGCT	
Dct	NM_010024.3	Fwd:	CAACCCTTCCACAGATGCCT	169
		Rev:	AACTGGAGCTTCTTCCTCTGAC	
Coq3	NM_172687.2	Fwd:	CTCGCCTAACTTCACGGTCG	161
		Rev:	CTTCCAAGGGGTCCTGTAAGT	
Nudt19	NM_033080.2	Fwd:	CTACCAGTGGTTGTCCCCAT	148
		Rev:	TGATGGGCGATCCGAACAAA	
Pdk4	NM_013743	Fwd:	CCTTTGGCTGGTTTTGGTTA	225
		Rev:	CCTGCTTGGGATACACCAGT	
Gckr	NM_001374741.1	Fwd:	AGATTGCGTGAGTGCAGAGG	130
		Rev:	TGCTTCATACCCTGACAACTCC	
Gys2	NM_145572.2	Fwd:	CCCTGCTGTGAATAGTCAGGTT	215
		Rev:	AAAGCAGCAGCCTTGGGATA	
Hsl	NM_010719.5	Fwd:	GGATTGACTCTAAGAGAGGAACTTG	190
		Rev:	GTGAGAACGCTGAGGCTTTG	
Atgl	NM_001163689.1	Fwd:	GATTCCTTAGGAGGAATGGCCTAC	75
		Rev:	CTTCCTGGGGGACAACTGG	
Pck1	NM_011044	Fwd:	TCAACACCGACCTCCCTTAC	235
		Rev:	CCCTAGCCTGTTCTCTGTGC	
Pck2	NM_028994.3	Fwd:	TGGCCGTGCAATCCAGAAAA	188
		Rev:	TTGGTGATGCCCAAAATCAGCAT	
Cpt1a	NM_013495	Fwd:	CTCAGTGGGAGCGACTCTTCA	105
		Rev:	GGCCTCTGTGGTACACGACAA	
Cpt1b	NM_013495.2	Fwd:	CAGCGCTTTGGGAACCACAT	105
		Rev:	CACTGCCTCAAGAGCTGTTCTC	
G6Pc	NM_008061.4	Fwd:	GCTGGAGTCTTGTCAGGCATT	124
		Rev:	AGAATCCAAGCGCGAAACCA	

2.1.10 Antibodies and Buffers for Western Blot analysis

Tab. 8: Antibodies

Antibody (Cat.-No.)	Supplier
Primary Antibodies	
Mouse anti-GLUT4	Cell Signaling (Danvers, MA, USA)
Rabbit anti-GAPDH (#2118)	Cell Signaling (Danvers, MA, USA)
Mouse total OXPHOS AB cocktail (ab110413)	Abcam (Cambridge, UK)
Rabbit anti-PDK4 (ab214938)	Abcam (Cambridge, UK)
Secondary Antibodies	
Goat-anti-rabbit IgG (#111-035-003)	Dianova (Hamburg, Germany)
Rabbit-anti-mouse IgG (#315-035-008)	Dianova (Hamburg, Germany)

Tab. 9: Buffers and solutions for Western Blot analysis

Buffer/Chemical	Ingredients
1-kb DNA Ladder	Thermo Scientific (Wilmington, MA, USA)
Agarose	Biozym (Hessisch Oldendorf, Germany)
Blocking solution	5 % powdered milk, TBS-Tween (1x)
Electrode buffer	25 mM Tris, 192 mM glycine, 0.1 % SDS
Laemmli sample buffer (4xLSB)	20 Vol. % glycerol, 8 % SDS, 10 mM EDTA, 0.25 M Tris, 6 % DTT, 0.2 % bromophenol blue (pH 6.8)
Lysis buffer	20 mM Tris-HCl, 150 mM NaCl, 1 mM EDTA, 1mM EGTA, 1 % Triton X-100 (pH 7.5) + 40 μl/ml cOmplete and 100 μl/ml PhosSTOP (freshly added)
Separating gel buffer	1.5 M Tris, 0.4 % SDS (pH 8.8)
Stacking gel buffer	0.5 M Tris, 0.4 % SDS (pH 6.8)
TBS-Tween buffer (TBS-T, 1x)	10 mM Tris, 150 mM NaCl, 0.05 Vol. % Tween 20
Transfer buffer	25 mM Tris, 192 mM glycine, 20 % methanol

2.1.11 Chemicals

Tab. 10: Chemicals

Chemical	Supplier
^{3}H-2-deoxyglucose	Hartmann Analytic (Braunschweig, Germany)
^{14}C-D-glucose	Hartmann Analytic (Braunschweig, Germany)
^{14}C-mannitol	PerkinElmer (Waltham, MA, USA)
2-deoxyglucose (2-DOG)	Sigma Aldrich (St. Louis, MO, USA)
Acetic acid	Merck (Darmstadt, Germany)
Ampicilin	Roth (Karlsruhe, Germany)
Antibody diluent, background reducing	Dako (Hamburg, Germany)
Avertin (2,2,2-Tribromoethanol)	Sigma Aldrich (St. Louis, MO, USA)
Bovine serum albumin (BSA)	Thermo Fisher Scientific (Darmstadt, Germany)
Bromphenol blue	AppliChem (Darmstadt, Germany)
Collagenase	Serva (Heidelberg, Germany)
Chloralhydrate	AppliChem (Darmstadt, Germany)
Chloroform (pure)	AppliChem (Darmstadt, Germany)
Citric acid	Sigma Aldrich (Steinheim, Germany)
Cold water fish skin (CWFS) gelatin	Aurion (Wageningen, Netherlands)
Cytochalasine B	Sigma Aldrich (Steinheim, Germany)
D-(+)-Glucose	Sigma Aldrich (Steinheim, Germany)
3,3'-Diaminobenzidine tablets	Sigma Aldrich (Steinheim, Germany)
Desoxy-ribonucleotide triphosphate (dNTP)	Promega (Madison, USA)
Dinonyl Phthalate	PHYWE (Göttingen, Germany)
Ethylenediamine tetra-acetic acid (EDTA)	Roth (Karlsruhe, Germany)
Ethylene glycol-bis (β-aminoethyl ether)-N, N, N',N'-tetraacetic acid (EGTA)	Roth (Karlsruhe, Germany)
Eosin yellowish	Merck (Darmstadt, Germany)
Ethanol absolut (EMSURE®)	Merck (Darmstadt, Germany)
Fetal Bovine Serum (FBS)	Thermo Fisher Scientific (Darmstadt, Germany)
Glycin	Serva (Heidelberg, Germany)
Glucose (20 %)	Braun (Meslungen, Germany)
Glucose-6-Phpsphyte dehydrogenase	Sigma Aldrich (Steinheim, Germany)
Glycerol	MP Biomedicals (Santa Ana, CA, USA)
Glycine	AppliChem (Darmstadt, Germany)
Hematoxylin	Merck (Darmstadt, Germany)
HEPES (4-(2-hydroxyethyl)-1-piperazineethanesulfonic acid)	Sigma Aldrich (Steinheim, Germany)
Heptane (Isomers)	Roth (Karlsruhe, Germany)
Hexanucleotide primer	Roche (Mannheim, Germany)
Histopaque-1077	Sigma Aldrich (Steinheim, Germany)
Hydrochloric acid (HCL)	Roth (Karlsruhe, Germany)

Chemical	Supplier
Insulin Actrapid® HM Penfill®	Novo Nordisk Pharma GmbH (Mainz, Germany)
Isoflurane	Piramal Healthcare (Morpeth, UK)
Isopropanol ($\geq$ 99.5 %)	AppliChem (Darmstadt, Germany)
Kaiser's glycerol gelatin	Merck (Darmstadt, Germany)
L-Glutamine	Sigma Aldrich (Steinheim, Germany)
Liberase TL Research Grade	Roche (Mannheim, Germany)
Lipofectamine RNAimax	Thermo Fisher Scientific (Darmstadt, Germany)
Magnesium chloride ($MgCl_2$)	Promega (Madison, USA)
Mannitol	AppliChem (Darmstadt, Germany)
Methanol	Roth (Karlsruhe, Germany)
nicotinamide-adenine-dinucleotide phosphate (NADP)	Sigma Aldrich (Steinheim, Germany)
Normal serum goat	Aurion (Wageningen, Netherlands)
Paraffin (Paraplast Plus©)	Sigma Aldrich (Steinheim, Germany)
Paraformaldehyde (PFA) extra pure	Merck (Darmstadt, Germany)
Penicillin/Streptomycin solution	Thermo Fisher Scientific (Darmstadt, Germany)
Peroxidase-conjugated Streptavidin	Dianova (Hamburg, Germany)
Phosphatase inhibitor tablets (PhosSTOP)	Roche (Mannheim, Germany)
Potassium aluminum sulfate	Merck (Darmstadt, Germany)
Potassium chloride (KCl)	Sigma Aldrich (Steinheim, Germany)
Polybrene	Merck (Darmstadt, Germany)
Powdered milk	Roth (Karlsruhe, Germany)
Protease Inhibitor Cocktail (cOmpete)	Roche (Mannheim, Germany)
Puromycin 1 mg/mL	Thermo Fisher Scientific (Darmstadt, Germany)
QIAzol® Reagent	QIAGEN (Hilden, Germany)
Resazurin	Sigma Aldrich (Steinheim, Germany)
Rotiszint eco plus	Carl Roth (Karlsruhe, Germany)
Shandon EZ-Mount	Thermo Fisher Scientific (Darmstadt, Germany)
Sodium chloride (NaCl)	Roth, Karlsruhe (Germany)
Sodium hydroxide (NaOH)	Roth, Karlsruhe (Germany)
Sodium iodate	AppliChem (Darmstadt, Germany)
Sodium lactate	AppliChem (Darmstadt, Germany)
Sodium pyruvate	AppliChem (Darmstadt, Germany)
Sterile glucose 20 %	Braun (Melsungen, Germany)
Tetramethylendiamine (TEMED)	Roth, Karlsruhe (Germany)
Tris(hydroxymethyl)-aminomethane (TRIS)	Merck (Darmstadt, Germany)
Triton-X-100	Serva (Heidelberg, Germany)
TRIzol® Reagent	Thermo Fisher Scientific (Darmstadt, Germany)
Tween 20	AppliChem (Darmstadt, Germany)
Xylene	AppliChem (Darmstadt, Germany)
Wax Paraplast® PLUS	Roth (Karlsruhe, Germany)

2.1.12 Reaction kits

Tab. 11: Molecular biological reaction kits

Kit	Application	Supplier
Ambion WT Expression and WT Terminal Labeling Kit	Microarray	Agilent (Taufkirchen, Germany)
GoScript® Reverse Transcription System	cDNA synthesis	Promega (Madison, USA)
GoTaq® qPCR Master Mix	RT qPCR	Promega (Madison, USA)
Invisorb® Genomic DNA Kit II	DNA isolation	STRATEC (Berlin, Germany)
KASP V4.0 2X Master mix, low Rox	Genotyping	LGC group (Teddington, UK)
QIAGEN® Plasmid Maxi Kit	DNA isolation	QIAGEN (Hilden, Germany)
RNAse free DNAse Set	RNA isolation	QIAGEN (Hilden, Germany)
RNeasy Mini Kit	RNA isolation	QIAGEN (Hilden, Germany)

Tab. 12: Biochemical reaction kits

Kit	Application	Supplier
Adiponectin ELISA (Mouse)	Plasma adiponectin	Abcam (Cambridge, UK)
Cholesterol Liquicolor kit	Plasma cholesterol	Human Diagnostics (Wiesbaden, Germany)
Insulin ELISA (Mouse)	Insulin from isolated pancreatic islets	DRG (Marburg, Germany)
Insulin ELISA Ultrasensitive (Mouse)	Plasma insulin	DRG (Marburg, Germany)
NEFA standard	Plasma free fatty acid	Wako Chemicals (Neuss, Germany)
NEFA-HR (2) R1 set	Plasma free fatty acid	Wako Chemicals (Neuss, Germany)
NEFA-HR (2) R2 set	Plasma free fatty acid	Wako Chemicals (Neuss, Germany)
Glucose Liquicolor kit	Liver glycogen	Human Diagnostics (Wiesbaden, Germany)
Pierce™ BCA Protein Assay kit	Total protein	Thermo Fisher Scientific (Schwerte, Germany)
Triglycerides (TRIGS) GPO-PAP kit	Plasma triglyceride	RANDOX Laboratories Ltd. (Ardmore, UK)
Western Lightning Enhanced Chemiluminescence (ECL)	Western blot imaging	PerkinElmer (Waltham, MA, USA)

2.1.13 Equipment

Tab. 13: Equipment

Instrument	Supplier
Camera Olympus DP73	Olympus Corporation (Tokyo, Japan)
Cell dissociation sieve	Sigma Aldrich (Steinheim, Germany)
Centrifuge GPKR	Beckman Coulter (Krefeld, Germany)
Centrifuge Megafuge 1.0	Heraeus (Hanau, Germany)
ChemiDoc XRS+	Bio-Rad (Hercules, CA, USA)
Contour XT glucometer	Bayer (Leverkusen, Germany)
Cooling table centrifuge 5425 R	Eppendorf (Hamburg, Germany)
Electronic scale	Sartorius, Göttingen, Germany)
FeedTime	TSE-Systems (Bad Homburg, Germany)
GelDoc XR+	Bio-Rad (Hercules, CA, USA)
HERAcell 240i CO_2 Incubator	Thermo Fisher Scientific (Schwerte, Germany)
Histoembedder	Leica Mikrosysteme (Wetzlar, Germany)
Infinite® 200 PRO Multimode Reader	Tecan Trading AG (Männedorf, Switzerland)
iMark™ Microplate reader	Bio-Rad (Munich, Germany)
Light microscope	Leica Mikrosysteme (Wetzlar, Germany)
Mini-PROTEAN®	Bio-Rad (Hercules, CA, USA)
Multipipette® E3	Eppendorf (Hamburg, Germany)
Multipipette® M4	Eppendorf (Hamburg, Germany)
Multitron incubation shaker	Infors HT (Bottmingen-Basel, Switzerland)
NanoDrop® 2000	Thermo Fisher Scientific (Schwerte, Germany)
Neubauer-Kammer improved Assistent	VWR International (Langenfeld, Germany)
NMR	EchoMRI (Houston, USA)
QuantStudio 7 Flex	Applied Biosystems (Foster City, USA)
Reacti-Therm/-Vap Evaporating Unit	Pierce (Rockford, IL, USA)
Rotary microtome HM360	Thermo Microm (Schwerte, Germany)
Scintillation counter	Beckman Coulter (Krefeld, Germany)
Seahorse XFe96 Analyzer	Agilent Technologies (Waldbronn, Germany)
Seahorse XFe96 PrepStation	Agilent Technologies (Waldbronn, Germany)
Shaking waterbath	Köttermann (Uetze/Hänigsen, Germany)

Instrument	Supplier
Shandon™ Excelsior™ Tissue Processor	Thermo Fisher Scientific (Schwerte, Germany)
SlideScanner Olympus VS200	Olympus Corporation (Tokyo, Japan)
StepOnePlus™ System	Applied Biosystems (Foster City, USA)
Stereomicroscope SMZ1500	Nikon Instruments (Amsterdam, Netherlands)
Tankblot Eco-Mini	Biometra (Göttingen, Germany)
Thermomixer comfort 1.5 mL	Eppendorf (Hamburg, Germany)
TissueLyser II	QIAGEN (Hilden, Germany)
Uniprep Gyrator	UniEqui (Planegg, Germany)
Vortex-Genie 2	Scientific Industries (New York, USA)
XFe96e extracellular flux analyzer	Agilent Technologies (Waldbronn, Germany)

2.1.14 Software

Tab. 14: Software

Software	Application	Supplier
ClustVis 2.0	Heatmaps	BIIT
EndNote X9	Literature research	Thomson Reuters
Excel 2016	Statistical analysis	Microsoft Office
GraphPad Prism 9	Statistical analysis	Graph Pad
ImageJ by Fiji	Fat cell size analysis	Fiji
ImageLab 6.0.1	Western blot analysis	Bio.Rad Laboratories
Microplate Manager® 5	Biochemical measurements	Bio-Rad Laboratories
QuantStudio™ Real-Time PCR Software v1.7.2	qPCR analysis	Applied Biosystems
QuPath 0.2.3	Image preparation	QuPath
R version 4.3	Microarray analysis	R Development Core Team
SnapGene Viewer 5.0.7	Plasmid maps	GSL Biotech LLC
T.Base 4D v18.2	Animal management	4D SAS
TAC 4.0	Transcriptome analysis	Applied Biosystems
Wave 2.4.0	Seahorse analysis	Agilent Technologies

2.2 Methods

2.2.1 Animal experiments

2.2.1.1 General animal housing

All animal experiments were performed in accordance with the National Institutes of Health for the care and use of laboratory animals and were approved by the Ethics Committee of the State Ministry of Agriculture, Nutrition and Forestry (State of North Rhine-Westphalia, Germany) (Ref.-No.: 84-02.04.2015.A354 and 81-02.04.2021.A168). Mice were bred and housed in the animal facility of the German Diabetes Center in Düsseldorf in Macrolon type III cages with two to six mice per cage. For constant environmental parameters, a 12 h day-night-cycle (lights on at 6 a.m.) and a temperature of 22 °C with 50 ± 5 % air humidity were chosen. All mice had access to food and water *ad libitum*. In this study, different cohorts were used to analyze different parameter on different time points (Fig. 9). Therefore, the 19-21-days old animals received either a standard diet (SD) or a high-fat diet (HFD) consisting of 45 kcal% fat (soy oil), 35 kcal% carbohydrates (with 4.73 kcal/g energy) and 20 kcal% protein (2.1.2).

2.2.1.2 Generation of the RCS.NZO.129Ola-*Nbg4* mouse line

For the generation of the recombinant congenic RCS.NZO.129Ola-*Nbg4* mouse strain, repeated backcrossing of heterozygous NZOxOla mice selected for the region of interest (*Nbg4*) with the donor strain NZO was performed[63]. Following a so-called "speed congenics" approach, the percentage of the genomic background was determined with the help of informative SNP markers (with a distance of 5-20 Mb between each marker) and a selective breeding was conducted with animals of the N2 and N3 population. The portion of NZO alleles in the genome was increased by selecting male mice for Ola alleles on chromosome 4 which were then backcrossed five times with NZO females. By using the competitive allele-specific PCR (KASP) technology (2.4.2) and defined SNP markers (Tab. 6), genotyping of these mice was conducted. To produce homozygous Ola alleles on the *Nbg4* locus, siblings were intercrossed in the N5 and N6 generation (theoretically ~95 % NZO background). In total three lines were generated with this breeding strategy (see also Fig.4), carrying different fragments of the *Nbg4* locus on the genetic NZO background: 1.) The congenic strain (*Nbg4con*) with mice carrying the whole *Nbg4* locus from 33 to 134 Mb, 2.) The proximal strain (*Nbg4prox*) with mice carrying just the proximal part of *Nbg4* from 33 to 77 Mb, and 3.) The distal strain (*Nbg4dis*) with mice carrying just the distal part of *Nbg4* from 91 to 134 Mb. All three lines were further used for metabolic characterization throughout this study.
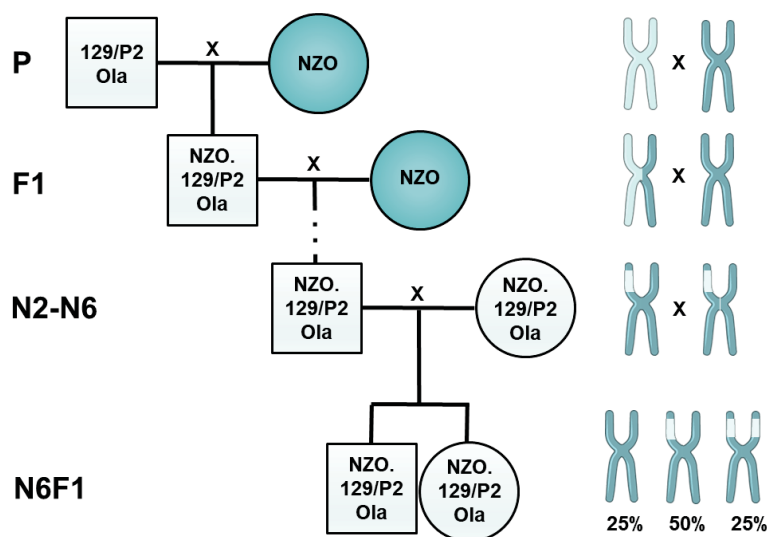
Fig. 5: Graphical crossbreeding scheme for the generation of recombinant congenic mice (RCS). P=parental mice, F1=first filial generation, N2-N6=Number of repeated backcrosses, N6F1= first filial generation of the sixth backcross.

2.2.1.3 Determining body weight and body composition

Body weight was determined weekly by electronic scales (Tab. 11), whereas the body composition was measured at 3, 6, 9 and 15 weeks of age by Nuclear Magnetic Resonance (NMR) technology using the program Echo2000 (Tab. 11). The principle of the NMR-method is based on the non-invasive measurement of fat mass, lean mass and body liquids in the living mice by the acquirement of radio frequency signals generated by the hydrogen spins from adipose tissue and muscles and uses the respective relaxation times to estimate the whole body composition [100].

2.2.1.4 Determining blood glucose levels and T2DM-prevalence

Random blood glucose levels were measured weekly in the morning hours between 8 to 10 a.m. and determined by placing a droplet of blood from the mouse tail tip on a glucose test strip of a Contour XT glucometer (Tab. 11). The T2DM-prevalence was expressed as a percentage of all animals exceeding a random blood glucose value of > 300 mg/dl for at least three weeks in a row.

2.2.1.5 Fasting and refeeding

In order to determined parameters in the fasted state, mice were fasted overnight for 16 hours and were granted food *ad libitum* the next morning for 2 hours. Tail blood was collected for both the fasted and the refed state and transferred into a micro tube containing calcium-disodium EDTA (Tab. 8) to avoid coagulation of the blood. The blood samples were centrifuged at 9000 x g for 5 minutes and 4 °C for insulin measurements and 2348 x g at room temperature

for measurements of free fatty acids (FFA) and triglycerides (TG) using the respective kits (Tab. 10). Subsequently, the plasma samples were collected in a micro tube and stored at -80 °C until further processing.

2.2.1.6 Intraperitoneal glucose tolerance test (i.p. GTT)

To estimate the ability of metabolising glucose, intraperitoneal glucose tolerance tests (i.p. GTT) were performed at either 6 or 13 weeks of age. This method follows the same principle as in humans and is therefore used as a substantial indicator of diabetes. During this intervention, mice were fasted for 16 hours (overnight) and basal blood glucose levels (time point zero) were measured the next morning as described in 2.2.1.4. Next, mice received an intraperitoneal injection of a 20 % sterile glucose solution (2 g/kg body weight) and blood glucose levels were measured at time points 15, 30, 60, 120 and 240 minutes after this injection. Mice were kept without access to food during the test period but with ad libitum access to water. Tail blood was collected for each time point using a micro tube coated with Lithium-Heparin (Microvette CB 300 µL, Saerstedt) and centrifuged at 9000 x g for 5 minutes and 4 °C. Plasma samples were stored at -80 °C until further determination of plasma insulin levels (2.6.1).

2.2.1.7 Intraperitoneal insulin tolerance test (i.p. ITT)

For the determination of whole-body insulin sensitivity, intraperitoneal insulin tolerance tests (i.p. ITT) were conducted in either 7 or 15 weeks old animals. Therefore, mice were fasted for 6 hours during the morning (from 2 to 8 a.m.) to measure basal fasting blood glucose levels (time point zero) before the intraperitoneal injection of 1 Unit/ kg body weight insulin (Tab. 8). Blood glucose was measured at time points 15, 30 and 60 minutes after the injection. Mice were kept without access to food during the test period but with *ad libitum* access to water.

2.2.1.8 Sacrificing and tissue harvest

Before sacrificing at life week 6 or 18, all mice were fasted for 6 hours during the morning (between 2 to 8 a.m.) unless otherwise stated and final fasting blood glucose level as well as final body weight was measured. Afterwards, the mice were sacrificed by either decapitation or heart puncture after isoflurane narcosis and the blood was collected into a 2 mL reaction tube containing 75 µL anticoagulant cocktail (Tab. 8). For plasma separation, samples were centrifuged for 10 minutes at 4000 *x* g and 4 °C and supernatants were aliquoted into 0.5 mL reaction tubes. The plasma and harvested tissues (liver, subcutaneous and gonadal white adipose tissue, brown adipose tissue, pancreas and Quadriceps muscle) were stored at -80 °C until further analysis. For further investigation, primary hepatocytes, pancreatic islets of

Langerhans, scWAT, gWAT, EDL and soleus muscle were isolated and treated as described below.

2.2.1.9 Isolation of intact skeletal muscles and *ex vivo* glucose uptake analysis

Mice were fasted for 4 hours (from 4 to 8 a.m.) and anesthetized by intraperitoneal injection of 20 mg/g body weight Avertin (Tab. 8). To keep muscle stress as low as possible, a high skill level as well as the usage of very precise forceps are crucial to accurately pick the muscles during the transfer. Therefore, EDL (*Extensor digitoris longum*) and Soleus muscles were dissected by the help of Lena Espelage throughout this study. To measure glucose transport, radioactive labelled ^{3}H-2-desoxyglucose (2-DOG) and ^{14}C mannitol were used. Thereby, all conditions were performed in 2 mL pre-gassed 1x Krebs-Henseleit bicarbonate buffer (KHB) in a shaking water bath at 30°C under constant gassing (95 % O_2, 5 % CO_2). Incubation buffers (Tab. 1) were separated into basal and insulin stimulated conditions, so that one EDL and one Soleus muscle per mouse could be measured for both conditions to enable a paired analysis. Therefore, insulin (Tab. 8) was added to the pre-incubation, rinse and hot incubation buffers in maximal concentrations (120 nM, 20 µU/ mL). After dissection, muscles were immediately transferred to the recovery buffer for 30 minutes at 30 °C under constant gassing. Next, muscles were transferred to the pre-incubation buffer with or without insulin for another 30 minutes. Muscles were rinsed for 10 minutes at constant conditions and subsequently incubated with the labelled ^{3}H-2-DOG and ^{14}C-Mannitol incubation buffer for 20 minutes (Tab. 1). Glucose uptake was stopped by cutting the muscle tendons and freezing the muscles in liquid nitrogen. Processing of the muscles was done by adding 300 µL protein lysis buffer containing proteinase and phosphatase inhibitors (Tab. 1) and homogenized in 2 mL Eppendorf tubes with a steel ball using the tissue lyser (Tab. 11) for 5 minutes and 25 Hz.. Centrifugation was performed for 10 minutes at 13,000 rpm and 4 °C and supernatants were transferred to new tubes. 40 µL of each sample was counted with 1.5 mL scintillation fluid (Tab. 8) in a scintillation counter (Tab. 11). The resulting counts per minutes (cpm) were normalized to the protein concentration, which was determined by BCA Protein Assay Kit (Tab. 10). The calculation of 2-DOG uptake was performed by the amount of extracellular bound 2-deoxyglucose, which is estimated via the detection of the extracellular space by ^{14}C-mannitol and subtracted from the intracellular 2-deoxyglucose [101]. Final values for glucose uptake are given as nmol/mg protein/20 minutes.

2.2.1.10 Isolation of mature murine adipocytes and *ex vivo* glucose uptake analysis

Glucose uptake into isolated primary adipocytes was assessed by measuring incorporated radioactively labelled ^{14}C-D-glucose. Similar to the assay of skeletal muscle glucose uptake, mice were fasted for 4 hours following an Avertin narcosis. To isolate the primary adipocytes, parts of the epididymal white adipose tissue (WAT) were dissected and immediately transferred to vials with 3 mL of pre-warmed (37 °C) KRBH buffer with 5 % BSA and 200 nM adenosine (Tab.1). The fat pads were sheared with scissors and digested by adding 16 mg of collagenase (Tab. 1) with an incubation time of 1 hour at 37 °C in a shaking water bath (Tab. 11). Following, the cell suspension was filtered through 400 µm polyamide nylon tissue and centrifuged at 50 x g for 1 minute at RT to remove any excess tissue. The lower aqueous solution was carefully removed and the cells were washed three times with 5 mL of fresh KRBH buffer by shortly centrifuging the cells. Thereafter, remaining adipocytes were mixed in a 1:1 ratio with KRBH buffer and further diluted to generate a 6.25 % adipocyte cell suspension. For the stimulation of glucose uptake, 200 µL of the adipocyte suspension were mixed in a 1:1 ratio with either only KRBH buffer (basal) or with KRBH buffer supplemented with 120 nM of insulin (Tab. 8) and incubated for 30 minutes at 37 °C in a shaking water bath. After that, 200 µL of adipocyte suspension were transferred to 2.7 mL of lipid extract solution and kept at 4 °C overnight to determine the lipid weight for normalization of the samples. The remaining adipocyte cell suspension was incubated for 30 minutes with 0.1 µCi/µL ^{14}C-D-glucose at 37 °C for further glucose uptake. The assay was stopped by transferring 280 µL of the adipocyte cell suspension into small tubes supplemented with 125 µL of dinonyl phthalate oil (Tab. 8), followed by a centrifugation step at 9391 x g for 10 minutes at RT. To measure the incorporated ^{14}C-D-glucose, the tubes were bisected and the upper adipocyte cells-containing piece of the tube was transferred to counting vials containing 3 mL of scintillation liquid (Tab. 8). The tubes were thoroughly vortexed and radioactivity was determined by a scintillation counter (Tab. 11). To normalize the results (cpm) to the lipid weight of the samples, 1.2 mL heptane (Tab. 8) and 800 µL ddH$_2$O were added to the overnight lipid extract solution. The samples were mixed and centrifuged at 201 x g for 5 minutes at RT. 1 mL of the supernatant was transferred to tared glass tubes and let dry. Thereafter, tubes were evaporated by heating and gassing with nitrogen for 15 minutes using a Reacti-Therm and Reacti-Vap Evaporating Unit and the weight of the dried lipids were measured to further calculate the glucose uptake as cpm/ mg lipid. The glucose uptake assays in isolated mature murine adipocytes were performed by Anette Kurowski and Heidrun Podini.

2.2.1.11 Fat cell size analysis

After dissection, subcutaneous (scWAT) and gonadal white adipose tissues (gWAT) were placed in an embedding cassette and fixed with 4 % paraformaldehyde (Tab. 8) for at least 24 hours at 4 °C. The fixation was mediated by the reaction of primary amines on proteins and nucleic acids to form reversible crosslinks. The stabilization of the proteins by adding methanol to PFA is important to protect them against the reversible redox-reaction of formaldehyde to formic acid and *vice versa* and to maintain the actual status of the tissue. Embedding of the fixed adipose tissues was performed using an automatic sample handling device (Shandon Excelsior, Tab. 13). Fixed tissues were dehydrated using ascending alcohol series and treated with the amphoteric intermedium xylene to substitute the alcohol (Tab. 15). Using a manually operated embedding station (Tab. 13), the tissues were transferred to liquefied paraffin on specialized molds to obtain an equal block. Embedding of the tissues was partly conducted with the help of Carmen Weidlich.

Tab. 15: Embedding protocol

Solution	Temperature	Time
Ethanol 70 %	RT	1 h
Ethanol 70 %	RT	1 h
Ethanol 96 %	RT	1 h
Ethanol 96 %	RT	1 h
Ethanol 100 %	RT	1 h
Ethanol 100 %	RT	2 h
Xylene	RT	1 h
Xylene	RT	1 h
Paraffin	60 °C	1 h
Paraffin	60 °C	1 h
Paraffin	60 °C	2 h

With the help of a rotary microtome (Tab. 13), the embedded WAT tissues were cut into slices of 10 µm (scWAT) and 16 µm (gWAT) thickness. Before collection of the slices, the embedded tissues were trimmed until a rudimentary profile of the tissue was reached. Subsequently, 2 levels á 3 slices were collected with 100 µm distance between the two levels. The slices were transferred into a water bath of 45 °C to prevent overlapping of the tissue by stretching, before they were collected on a microscope slice and dried overnight at RT.

Staining of the adipose tissues was executed with hematoxylin and eosin (Table 8) to visualize the outer membrane of the single fat cells. For this purpose, the slices were deparaffinized and rehydrated before they were stained with hematoxylin and eosin as described below (Tab. 16). The stained tissues were covered with a xylene-containing mounting medium (Tab. 8) and sealed with coverslips. Due to the flammability and toxicity of xylene, all steps, including the final overnight drying, were conducted under the fume hood.

Tab. 16: HE-staining protocol

Solution	Incubation time
Xylene	5 minutes
Xylene	5 minutes
Ethanol 100 %	5 minutes
Ethanol 100 %	5 minutes
Ethanol 96 %	5 minutes
Ethanol 96 %	5 minutes
Ethanol 70 %	5 minutes
Ethanol 70 %	5 minutes
Mayer's Hematoxylin	2 minutes
Aqua ddH2O	Wash up
Tap water	10 minutes
Ethanol 70 %	2 minutes
Eosin yellowish 0.1 %	30 sec
Ethanol 96 %	Wash up
Ethanol 96 %	2 minutes
Ethanol 100 %	2 minutes
Ethanol 100 %	2 minutes
Xylene	5 minutes
Xylene	5 minutes

Stained samples were imaged with an Olympus VS200 Slidescanner (Tab. 13) using a 20x objective. To determine the fat cell size, single images were created for each slice using the QuPath 0.2.3 software (Tab. 12). Subsequently, images were opened in ImageJ (Tab. 12) and adipocyte size was calculated using a plugin generated by Maguire and colleagues (available in

linked GitHub repository; github.com/asm0028/Adipocyte_QuPath) [102]. The plugin works by running the 'Find Edges' command three times, turning the image binary and then using the 'Analyze Particles' command with the user-defined restrictions. To exclude cells that were crushed or otherwise distorted, as well as blood vessels, measurement was adjusted to cells with areas from 400 (scWAT) or 600 (gWAT) to 15,000µm² and a degree of circularity from 0.04 to 1.0. 'Count' and 'Average Size' results from the 'Summary' window were recorded, as well as the area of each adipocyte from the 'Results' window. Total counts of adipocyte size distribution were used for percentile analysis to divide the adipocytes into three groups according their size [103, 104]. The three groups were defined according to the size percentiles as follows: small (0-25th percentile; P_{25} = 500-3,000 µm²), medium (25-75th percentile; P_{25-75} = 3,000-8,000 µm²) and large (75-100th percentile; P_{75} = 8,000-15,000 µm²) adipocytes.

2.2.1.12 Isolation of primary hepatocytes

The protocol for the isolation of primary hepatocytes was adapted from Akie and Cooper [105] and conducted with the help of Dr. Delsi Altenhofen. After 6 hours of fasting (from 2 to 8 a.m.) mice were decapitated before abdominal cavity was opened to expose the liver and the abdominal IVC (*inferior vena cava*) and to clamp the thoracic IVC. A peristaltic pump for HBSS isolation buffer (Tab. 1) was started at low pump rate (approx. 0.2 - 0.5 mL/minute) to get rid of any air completely. Subsequently, the needle was carefully inserted into the abdominal IVC and the portal vein was cut while the pump rate was increased to approx. 7.5 mL/minute to start open perfusion for up to 10 minutes until no blood was left in the organ and the liver appeared yellowish. Following, the peristaltic pump was changed to switch from HBSS to collagenase medium (Tab. 1) to initiate digestion of the liver with a pump rate of 7.5 mL/minute until the liver appeared reddish and enlarged (approx. 5 - 15 minutes depending on liver size). Afterwards, the gall bladder was removed before the digested liver tissue was dissected from the dead animal and transferred to a petri dish. Subsequently, 5 mL of plating medium (Tab. 1) was added and the tissue was scraped with a scalpel blade to dissociate the whole tissue into the medium. To remove any excess tissue, the hepatocyte cell suspension was filtered through cell strainer units with 70 µm pore size and rinsed with additional 10-15 mL plating medium. After a centrifugation step at 500 g for 5 minutes at 4 °C, the hepatocyte pellet was again washed with 10 mL plating medium (Tab. 1) followed by additional centrifugation at 500 g for 5 minutes at 4 °C. By density gradient centrifugation using a percoll gradient (Tab. 8), viable cells were separated from dead cells and cell debris. Therefore, the cells were resuspended in 10 mL plating medium and carefully coated with 9 mL cold percoll working solution. The mixture was slowly inverted 5 times before another centrifugation step was performed at 500 g

for 10 minutes at 4 °C with low settings for acceleration and deceleration. Thereafter, cells were washed again with 10 mL plating medium as described above and the final cell pellet was resuspended into 10 mL plating medium to count the number of viable cells using trypan blue and a Neubauer hemocytometer. Cells were seeded in plating medium on rat tail collagen I (50 µg/mL diluted in 1x PBS) coated cell culture plates at assay dependent cell densities and cultivated for at least 3 hours at 37 °C, 5 % CO_2 to enable adhereance of the cells to the bottom of the culture plates.

2.2.1.13 *De novo* Lipogenesis (DNL) assay

DNL of primary mouse hepatocytes was quantified using radioactively labelled substrate to analyse their ability to synthesize fatty acids. Therefore, cells were seeded into 24-well plates in a density of $9x10^4$ cells per well. The assay protocol was adapted to the method described by Akie and Cooper [105] which was adjusted as follows: After overnight incubation of the cells in 400 µL starvation medium with or without 100 nM insulin (Tab. 10), culture medium was exchanged to assay medium supplemented with 10 µM cold acetate and 0.5 µCi ^{14}C-acetate per well (Tab. 1). After an incubation time of 2 and 4 hours at 37 °C and 5 % CO_2, the cells were washed once with 500 µL 1x PBS followed by cell lysis with 120 µL/well 0.1 N HCl. To extract the lipids, 500 µL chloroform:ethanol in a ratio of 2:1 (v/v) was added to 100 µL lysate, carefully inverted and incubated 5 minutes at RT. Next, 250 µl ddH_2O was added to the homogenate which was again mixed and incubated another 5 minutes at RT. Homogenates were centrifuged at 2,500 g for 10 minutes at RT to separate phases. With the help of a syringe, the lower organic phase including cellular lipids was transferred into a new 2.0 mL tube containing 1.5 mL scintillation fluid and ^{14}C activity was measured using a scintillation counter (Tab. 13).

2.2.1.14 Glucose production assay

Isolated primary hepatocytes were seeded at a density of 250,000 cells/4 cm^2 and cultivated for at least 3 hours in plating medium (Tab. 1). Afterwards, the medium was changed to serum-free medium (Tab. 1) for an overnight serum starvation of the cells. The next day cells were washed twice with pre-warmed glucose production medium (Tab. 1). Cells were incubated either just with glucose production medium for basal control or treated as follows: To start the assay, cells were first incubated with 10 nM porcine insulin (Tab. 8) for 5 hours in total to suppress glucose production. After 1 hour, 2 mM pyruvate and 2 mM lactate (Tab. 8) were added to stimulate glucose production for 4 hours. At the end of the incubation period the supernatant was collected and centrifuged at maximal g for 20 minutes at 4 °C to remove any particles and debris. Glucose concentration of the supernatants was measured using the Glucose

Assay Kit (Tab. 10) according to the manufacturers' manual at 540 nm with the help of a Tecan reader.

2.2.1.15 Isolation of pancreatic islets of Langerhans

The dissection of the pancreas was conducted by Dr. Delsi Altenhofen from the German Diabetes Center. Mice were decapitated after 6 hours of fasting (from 2 to 8 a.m.) and subsequently the abdomen was opened. To ensure that the collagenase will only reach the pancreas and not the gastrointestinal tract, the first step was to clamp the *Papilla duodeni* major. For the digestion of the pancreas, 3 mL of the diluted collagenase (0.18 mg/mL in DMEM, Tab. 1) was injected into the *Ductus coledochus.* The pancreas was dissected and directly transferred into a 50 mL falcon stored on ice. Digestion of the tissue was initiated by a shaking waterbath at 37 °C. After 15 to 18 minutes incubation time, the reaction was stopped by adding 30 mL of DMEM (containing 15 % FCS). After 3 minutes of centrifugation at 900 x g at RT, the supernatant was discarded and the pellet was resuspended in 10 mL DMEM. To get rid of excess tissue, the cell suspension was filtered using a tissue sieve with a mash size of 380 µm and filling up with DMEM, followed by another centrifugation step for 3 minutes at 900 x g at RT. The cell pellet was then resuspended in 10 mL Histopaque-1077 (Tab. 8) and carefully covered with 13 mL DMEM to separate the cells by density gradient. After a 25 minutes centrifugation step at 1200 x g with deactivated brake, the two liquid phases were transferred into a new falcon tube and washed with DMEM, followed by another centrifugation step at 900 xg for 3 minutes. The resulting pellet was resuspended in 10 mL islet medium (Tab. 1) and transferred into a disposable petri dish with 10 cm diameter. Using a microscope (Tab. 11), morphologically intact islets were picked and carefully transferred into a new petri dish containing 10 mL islet medium to separate them from other remaining tissues and further overnight cultivation at 37 °C, 5 % CO_2 and 90 % humidity.

2.2.1.16 Glucose-stimulated insulin secretion (GSIS)

One day after isolation of the Langerhans islets from the mouse pancreas, a glucose-stimulated insulin secretion (GSIS) assay was executed. For this purpose, eight islets of similar size were transferred in a total volume of 20 µL medium into a well of a 96-well plate prepared with 80 µL warm KRH buffer (Tab. 1). Afterwards, the islets were washed three times by removing and adding fresh KRH buffer (80 µL each well). Subsequently, the islets were incubated in 80 µL KRH buffer containing 1 mM glucose (Tab. 8) for one hour at 37 °C and 5 % CO_2. For low-glucose (LG) stimulation, the islets were again supplemented with 80 µL KRH buffer containing 1 mM glucose, whereas for high-glucose (HG) stimulation, 80 µL of KRH buffer

containing 25 mM glucose was added to the islets and incubated for one hour at 37 °C. Thereafter, 80 µL of the supernatant were transferred into 1.5 mL reaction tubes and stored on ice until centrifugation for 5 minutes at 2000 x g and 4 °C. The islets were lysed by adding 80 µL ice cold lysis buffer (Tab. 8) and were further transferred into new reaction tubes containing 150 µL lysis buffer (final volume: 250 µL). Islets were shaken for 10 minutes in a gyrator (Tab.11) and the lysates were then centrifuged for 10 minutes at maximal speed and 4 °C. Finally, the supernatant were transferred into new reaction tubes and stored at -20 °C until quantification of the insulin content via the mouse insulin ELISA Kit (Tab. 3). All samples were measured in technical triplicates.

2.2.2 Cell biological methods

2.2.2.1 Cultivation of 3T3-L1 cells

3T3-L1 fibroblasts (2.1.3) were cultured in Maintaining Medium (Tab. 1) at 37 °C and 5 % CO^2 until reaching confluence. For differentiation to adipocytes, the fibroblast were incubated with differentiation medium I (Tab. 1) until day 7 of differentiation, where the medium was replaced to differentiation medium II (Tab. 1). Cells were cultured for additional 7 days for the maturation of adipocytes until functional investigation.

2.2.2.2 Glucose uptake into 3T3-L1 adipocytes

3T3-L1 fibroblasts were seeded into black collagen-coated 96-well plates with a density of 7.5 x 10^3 cells per well and differentiated into mature adipocytes. After starvation for 24 hours with DMEM without serum and antibiotics (Tab. 1), cells were either kept untreated (basal state), stimulated with 100 nM insulin or 50 mM cytochalasin B (Tab. 10) for 1 hour at 37 °C. Thereafter, uptake of 1 mM 2-Deoxy-D-glucose (Tab. 10) was allowed for 10 minutes at RT and subsequently stopped by washing the cells twice with ice-cold PBS following lysis with 0.1 M NaOH for 1 hour at 37 °C. Neutralization of the cell suspension was achieved by adding 1 M HCl in 200 mM TAE buffer, pH 8.1 (Tab. 1). Following, the Assay Reagent (Tab. 17) was added and cells were incubated for 30 minutes at 37 °C. Fluorescence was determined at the excitation spectra of 545 nm, which was proportional to the concentration of 2-deoxyglucose-6-phosphate (2DG6P).

Tab. 17: 3T3-L1 glucose uptake assay reagent

Component	Volume per well
TEA-buffer 200 mM	50 µL
KCl 200 mM	0.75 mg
BSA 0.4 %	10 µL
NADP 10 mM	2 µL
Diaphorase 100 U/mL	0.4 µL
Resazurin 2 mM	0.6 µL
G6PDH 6420 U/mL	0.48 µL
dH_2O	136.52 µL

2.2.2.3 Cultivation of Hepa 1-6 and Plat-E cells

Hepa 1-6 and Plat-E cells (2.1.3) were constantly cultivated in T75 flasks at 37 °C and 5 % CO_2 with the respective cultivation medium (Tab. 1). Three times a week, when cells were confluent, a new subculture was produced. Therefore, cells were washed with prewarmed PBS and detached by adding 1 mL trypsin (Tab. 10). Subsequently, cells were split 1:8 to 1:10 in fresh medium. For dissemination, trypsinated cells were centrifuged for 5 minutes at 1000 rpm and the pellet was resuspended in 10 mL cultivation medium. To determine the cell concentration, cells were diluted in trypan blue (Tab. 10) and counted in a Neubauer chamber. Plat-E cells were solely used to generate stable 3T3-L1 *Alad* KD cells by retroviral transduction.

2.2.2.4 Extracellular flux assay

Hepa 1-6 cells were seeded in XF96e microplates in a density of $5x10^4$ cells per well and cultivated for 24 hours. The day after, knockdown of the *Nudt19* mRNA was conducted within the microplates as described below (2.2.2.5) and used for extracellular flux analysis 48 hours after the transfection. Retroviral 3T3-L1 adipocytes and primary isolated murine hepatocytes were seeded into XF24e microplates with a density of $2x10^4$ or $1x10^4$ cells per well, respectively and cultivated overnight. After cultivation of the cells in the respective microplates, cells were washed twice with Seahorse XF DMEM medium containing 5 mM HEPES (Tab. 2) supplemented with 10 mM glucose, 2 mM glutamine and 1 mM sodium pyruvate (Tab. 10) and incubated for 1 hour at 37 °C under the restriction of CO_2. For the extracellular flux assay, cells were incubated with 0.15 mmol/L BSA-coupled palmitate or oleate or the equivalent amount of 25 µmol/L fatty acid-free BSA alone immediately before starting the assay. Afterwards, cells were placed in the Extracellular flux analyzer (Tab. 13) for real time cell metabolic analysis.

Cellular oxygen consumption rates (OCR) and extracellular acidification rates (ECAR) were recorded at baseline and after additional injections at 6 minutes intervals. For the mitostress test assay, 1.0 µmol/L oligomycin A, 1.0 µmol/L carbonyl cyanide 4-(trifluoromethoxy)phenylhydrazone (FCCP), and 0.5 µmol/L rotenone/antimycin A were injected (Tab. 2). The compounds used in the assays were dissolved in DMSO, and stored as aliquots at -20 °C before use. After the assay, the medium was aspirated and the cells were lysed in 50 µL 20 mM Tris-HCl, 1 mM EDTA, 1 mM EGTA, 150 mM NaCl, 1 % Triton X-100, pH 7.5 (Tab. 1) for normalization of the extracellular flux data. Therefore, cell lysates were cleared by centrifugation for 5 minutes at 1000 rpm and protein content was determined using the Pierce™ BCA™ protein assay (Tab. 10). The data were analyzed using WAVE software (Tab. 14). ECAR values were converted to proton extrusion rates (PER). To calculate determinants of ATP production rate, mitochondrial function and glycolysis, the protein and baseline-adjusted OCR and PER values were used as described elsewhere [106, 107].
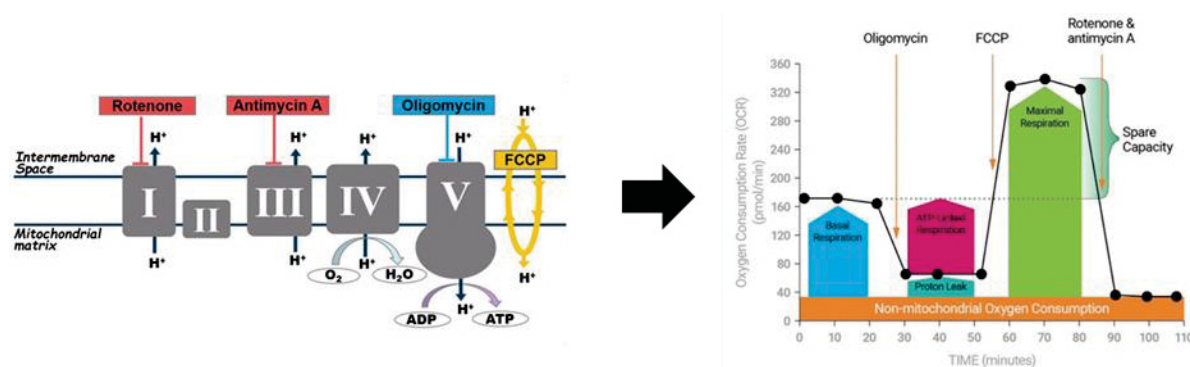
Fig. 6: Analysis of mitochondrial function using the Seahorse Mito Stress Test Assay. Simplified drawing of the electron transport chain (ETC) and the targets of the used compounds (left). The oxygen consumption rate (OCR) shows the characteristic responses of the mitochondrial inhibitors and the uncoupler FCCP (right). I-V represent the different complexes of the ETC. (Aapted from: www.agilent.com).

2.2.2.5 Lipofection

By using a lipid complex to deliver DNA to the cells, the also called 'liposome-based transfection' represents a common method for gene modification *in vitro*. In this study, Hepa 1-6 cells were seeded in a density of $1x10^5$ or $5x10^4$ cells per 6-or 96-well, respectively and cultivated overnight at 37 °C and 5 % CO_2. For gene knockdown (KD) Lipofectamine RNAiMAX (Tab. 10) was used to enable the transfection of siRNA oligonucleotides into the cells (Tab. 5). Therefore, mixture A which is composed of Lipofectamine and Opti-MEM was transferred to mixture B which contains Opti-MEM and the siRNA oligonucleotides (Tab. 18). During the incubation of the Lipofectamine-siRNA solution for 10 minutes at RT, the cells were washed once with prewarmed PBS and 2 mL (6-well) or 80 µL (96-well) of fresh cultivation media was added. After adding 500 µL or 20 µL (6- or 96-well, respectively) of the

reaction mix to the wells, cells were cultivated for at least 24 hours at 37 °C and 5 % CO_2 before conducting further analyses.

Tab. 18: Pipetting scheme for lipofection. Listed volumes were used per well.

Mix	Component	6-well	96-well
A	Opti-Mem medium	250 µL	10 µL
	Lipofectamine RNAiMAX reagent	7.5 µL	0.3 µL
B	Opti-Mem medium	250 µL	10 µL
	siRNA (50 µM)	2.5 µL	0.1 µL

2.2.2.6 Retroviral transduction

In this study, functional analysis of *Alad* KD in 3T3-L1 adipocytes was investigated to analyse a potential impact of this gene in adipose tissue glucose uptake and lipid metabolism. Therefore, a customized shRNA sequence on retroviral pRS vector (Tab. 4) was used without any need of previous adaptation. To produce infectious viruses, the retroviral pRS-Alad shRNA plasmid was transfected into Plat-E packaging cells (2.1.3) using Lipofectamine 2000 with the same method as mentioned above (2.2.2.5). 48 hours post transfection, the virus-containing supernatant was centrifuged for 4 minutes at 300 x g. Afterwards, 6 µg/mL polybrene (Tab. 10) was added, and the virus-containing supernatant was added to 3T3-L1 fibroblasts. After overnight infection, drug selection was initiated by adding 4 µg/mL puromycin (Tab. 10) to the cultivation medium for several days. 3T3-L1 fibroblasts with stable *Alad* KD were preserved as a newly generated cell line in liquid nitrogen (2.2.2.7).

2.2.2.7 Cryopreservation of mammalian cell lines

For future use and to minimize genetic change in continuous cell lines, cryopreservation was performed as follows: Cells were grown until 50 % confluency, washed with PBS, trypsinized and centrifuged for 5 minutes at 1000 rpm. The pellet was resuspended in the respective cultivation medium supplemented with 20 % FCS and 10 % DMSO and aliquoted into cryopreservation tubes. The samples were incubated overnight in a container filled with isopropanol at -80 °C and transferred to liquid nitrogen the next day.

2.3 Microbiological methods

2.3.1 Cultivation of *Escherichia coli*

Cultivation of *Escherichia coli* (*E.coli*) cells was conducted overnight in liquid Luria-Bertani (LB) medium (Tab. 3) supplemented with appropriate antibiotics. Flasks were incubated at 37 °C and 220 rpm constant shaking (Tab. 13). Short-term storage of bacteria was performed at 4 °C on solid LB culture plates. Test cultures were produced from 1 volume of a fresh overnight culture and 1 volume 40 % glycerol and stored at -80 °C.

2.3.2 Transformation

To manifold plasmid-DNA of the genes of interest, transformation into electrocompetent *E.coli* DH5α cells (produced by Samaneh Eickelschulte) was conducted by electroporation. Therefore, 1 - 2 µL of the plasmid-DNA diluted in 30 µL ice-cold dH$_2$0 was placed on ice together with 100 µL-cuvettes. 30 µL of electrocompetent *E.coli* cells were thawn on ice, mixed carefully with the ice-cold DNA and the mixture was transferred to the cuvettes. Immediately, samples were electroporated (1700 V) and subsequently 500 µL SOC medium (Tab. 3) was added and transferred to new 1.5 mL tubes. To secure efficient transformation, time constant (tau value) during electroporation should be between 5 and 6 ms. Bacteria were outgrown by incubating the tubes in a 37 °C shaker (220 rpm) for 1 hour, plated onto LB plates (Tab. 3) with the appropriate antibiotics and incubated overnight at 37 °C laying upside down.

2.3.3 Isolation of plasmid DNA from *E.coli* cultures

Isolation of plasmid-DNA from overnight cultures of *E.coli* was conducted the Maxi-Prep Kit from Qiagen (Tab. 11). The concentration of isolated plasmid-DNA was determined photometrically on a NanoDrop device (Tab. 13).

2.4 Molecular biological methods

2.4.1 DNA isolation from mouse tail tips

For genotyping of the animals, DNA of the mouse tail tip was isolated. Therefore, approx. 2 mm of the mouse tail tip from 3 weeks-old mice was cut and transferred into a reaction tube of the Invisorb® Genomic DNA Kit II (Tab. 11). Further steps of the DNA isolation were performed according to the manufacturer`s instructions. The DNA concentration was determined photometrically in the Nanodrop (Tab. 13) at a wavelength of 260 nm.

2.4.2 Genotyping by Competitive Allele Specific PCR (KASP)

By using a universal fluorescence resonance energy transfer (FRET) cassette reporter system, the KASP technique allows an accurate bi-allelic differentiation of analyzed polymorphic

Single Nucleotide Polymorphisms (SNPs). RCS.NZO.129Ola mice were genotyped using the KASP Assay Mix and KASP Master Mix (Tab. 11) according to the manufacturer's manual. For this purpose, isolated DNA from mice tail tips was used in a concentration of 10 ng/µL. To each well of a 384-well plate, 3 µL DNA was pipetted and further supplemented with 3 µL 2x KASP Master Mix (Low Rox) and 00.084 µL KASP Assay Mix (Tab. 11). The amplification was performed using the StepOnePlus^{TM}-PCR System (Tab. 13) with following settings:

Tab. 19: KASP amplification protocol

Step	Temperature	Time	Number of cycles
Hot-start activation	94 °C	15 minutes	1
Touchdown	94 °C	20 sec	10
	61-55 °C	60 sec	
	(dropping 0.6 °C per cycle)		
Amplification	94 °C	20 sec	20
	55 °C	60 sec	
Read stage	30 °C	60 sec	1

2.4.3 RNA isolation from mouse tissues

For RNA isolation of murine tissues, about 100 mg (fat) or 40 mg (liver) tissue was placed into a 2 mL tube containing a steelball and 700 µL TRIzol$^{®}$ (Tab. 10). Samples were homogenized for 5 minutes at 25 Hz with a Tissue-Lyser (Tab. 13) and afterwards incubated at RT for further 3 minutes. The homogenates were transferred to a QiaShredder-column, centrifuged for 2 minutes at 18,407 x g and the flow-through was transferred to new 1.5 mL tubes containing 100 µL chloroform (Tab. 10). After the inversion of reaction tubes for 15 seconds and an incubation period of 3 minutes at RT, phase separation was achieved by another centrifugation step for 15 minutes at 12,000 x g and 4 °C. The RNA-containing aqueous phase was then transferred into new reaction tubes and mixed with 350 µL isopropanol (Tab. 10), followed by an incubation period of 10 minutes at RT. After centrifugation for 15 minutes at 12,000 x g and 4 °C, the supernatant was discarded and the pellet was washed twice with 500 µL of 75 % ethanol (Tab. 10). A centrifugation step of 5 minutes and 7,500 x g at 4 °C was performed, supernatant was again discarded and the pellet was dried for 30 minutes at RT. The pellet was dissolved in 30 µL RNase-free H$_2$O and incubated in a thermos mixer (Tab. 13) for 2 minutes at 55 °C and 400 rpm. RNA concentration was determined at 260 nm using the Nanodrop device (Tab. 12) and samples were stored at -80 °C.

2.4.4 RNA isolation from cultured cells

Cells were washed once with PBS and lysated by adding 500 µL of the TRIzol® Reagent (Tab. 10) to each 6-well. Hereby no manually homogenization step is necessary, since TRIzol® already disrupts and breaks down the cells and cell components by itself. After adding 100 µL chloroform, 15 seconds of inversion and 2 minutes incubation at RT, the tube was centrifuged for 15 minutes at 12,000 x g and 4 °C. The RNA-containing pellet was then washed twice in 500 µL of ethanol 75 % (centrifugation at 7,500 x g and 4 °C) and dried at RT for 30 minutes. After incubation of the open tube for 5 minutes at 55 °C, the pellet was resuspended in 20 µL RNAse-free water. Finally, the tube was incubated for 5 minutes at 55 °C to dissolve the pellet and the RNA concentration was measured using a Nanodrop device (Tab. 13). Samples were stored at -80 °C.

2.4.5 cDNA synthesis

To synthesize complementary DNA (cDNA) from isolated RNA preparations, 25 mM dNTPs, 12.5 mmol hexanucleotide primers (Tab. 10) and RNA (500 ng isolated from cells and 1 µg from tissues) were mixed and incubated for 5 minutes at 65 °C to allow the annealing of the primers to the RNA template. Subsequently, the reaction mix was incubated on ice for 1 minute and spinned down, before the reverse transcriptase, its corresponding buffer and 25 mM $MgCl_2$ were added (Tab. 10). With the help of a PCR thermocycler (Tab. 13), the cDNA-synthesis was performed using the following conditions (Tab. 20).

Tab. 20: cDNA-synthesis protocol

Step	Temperature	Time
Annealing	25 °C	5 minutes
Elongation	42 °C	60 minutes
Enzyme-inactivation	70 °C	15 minutes
Hold	4 °C	∞

2.4.6 Quantitative Real-Time PCR (qPCR)

The quantitative Real-time PCR (qPCR) represents a highly sensitive method for the determination of relative gene expression levels. By the use of a fluorescent dye, which intercalates with the DNA, the relative amount of cDNA in a sample can be measured. With each amplification cycle, the fluorescence intensity increases proportionally in response to the increased amplicon concentration. The cycle of threshold (Ct), which is given at the end of the reaction, represents the amplification cycle, in which the fluorescence significantly exceeds the

baseline fluorescence and correlates reversely with the amount of cDNA in a sample. For each reaction, 4-5 ng cDNA (volume of 4 µL) were mixed with 5 µL 2x GoTaq® qPCR Master Mix (Tab. 11) and 0.5 µL of both forward and reverse primer (Tab. 7), reaching a total volume of 10 µL. Tab. 21 shows the settings of the thermocycler used for the amplification of the targeted cDNA. In this work, the mean values of the relative gene expression were calculated using the $2^{(-\Delta\Delta Ct)}$-method [65].

Tab. 21: qPCR amplification protocol

Step	Temperature	Time	Number of cycles
Lid heating	105 °C	∞	-
Hot-start	95 °C	2 minutes	1
Denaturation	95 °C	15 sec	40
Annealing/Elongation	60 °C	60 sec	
Dissociation/Melt curve	65-95 °C	75 sec	1

2.4.7 Agarose gel electrophoresis

For gradient PCR products, a gel of 1% agarose in TAE buffer (Tab. XY) was used. For this purpose, agarose (Tab. 10) was mixed with 1xTAE buffer (Tab. 9) and heated in a microwave until boiling. After cooling down to approx. 60 °C, 0.1 µg/mL ethidium bromide (Tab. 10) was added and gel was further cooled down until loading. Samples were supplemented with 5x Gel loading buffer (Tab. 10) and loaded into the gel pockets. Electrophoresis was performed at 120 V (Tab. 13) for approx. 30 minutes. Fragments size was determined by a 1 kb-Ladder (Tab. 10). DNA bands were visualized on a UV Transluminator (Tab. 13) and if needed, specific DNA fragments were excised from agarose gel for further isolation with a sterile scalpel. Therefore, weight of DNA fragments was determined and isolation was performed using the Qiagen Gel Extraction Kit (Tab. 11) according to the manufacturer`s instructions.

2.5 Biochemical methods

2.5.1 Quantification of plasma parameters

To quantify insulin levels in murine blood plasma, the ultrasensitive enzyme-linked immunosorbent assay (ELISA) was used, which was executed following the manufacturer's instructions (Tab. 12).

Further parameters measuring components of the lipid metabolism were plasma triglycerides (esterified fatty acids), free fatty acids (FFA, non-esterified fatty acids; NEFA) and cholesterol. For this purpose, colorimetric kits were used following the corresponding manuals (Tab. 12).

2.5.1.1 Determination of total pancreatic insulin

Pancreatic insulin concentration was analysed using the whole snap-frozen pancreas, which was homogenized with 1 mL ice-cold acid ethanol and a stainless steel ball for 5 minutes at 25 Hz in a TissueLyser (Tab.13). After further shaking of the homogenates overnight at 4 °C, samples were centrifuged for 15 minutes at 4000 g and 4 °C and the supernatant was stored at -20 °C until further processing. Pancreatic insulin concentration was determined using the Mouse Insulin ELISA Kit (Tab. 11) and normalized to the protein content according to the manufacturer's instructions.

2.5.1.2 Determination of liver glycogen

In order to determine glycogen content in murine livers, 40 mg of frozen pulverized tissue was transferred into a 2 mL safe-lock tube and hydrolysed with 300 mL of 30 % KoH (wt/vol) for 30 minutes at 100 °C. After returning to RT, samples were washed with 100 µL of 1 M Na_2SO_4 and 800 µL of ethanol (100 %), followed by incubation for 3 minutes at 100 °C. After centrifugation (15 minutes at maximal speed and 4 °C), the supernatant was discarded and the pellet was washed three times in 200 µL dH_2O. The final pellet was dried for 10 minutes in a vacuum-centrifuge and subsequently dissolved in 200 µL of 0.12 M sodium acetate buffer supplemented with 0.3 mg/mL amyloglucosidase (Tab 10). After 3 hours at 40 °C, samples were again centrifuged and the supernatant was collected to determine the glycogen concentration using the colorimetric glucose liquicolor kit (Tab 12) according to the manufacturer's instructions.

2.5.1.3 Determination of liver triglycerides

For the analysis of the hepatic triglyceride content, 40 mg of frozen pulverized liver tissue was lysed in 1.5 mL of a cold chloroform/methanol mixture (2:1 vol/vol) with a steel bead using the Tissue-Lyser (Tab. 13) at 25 Hz for 5 minutes. The homogenates were horizontally inverted for 2 hours at RT in order to extract the lipids. After adding 200 µL of dH_2O, the solution was mixed and centrifuged at 3,381 x g for 15 minutes to allow a clear phase separation. The supernatant was discarded and 250 µL of the lower organic phase was transferred in a new reaction tube and dried for 1 hour in a vacuum centrifuge. Lastly, the lipid pellet was dissolved in 1 mL of chloroform and quantified using the Triglyceride kit (Tab. 12) according to the manufacturer's protocol.

2.5.2 Protein analyses

2.5.2.1 Preparation of protein lysates

Protein extraction was achieved by adding 300 µL lysis buffer (Tab. 1) and a steel bead to the respective tissue sample (approx. 30-50 mg gWAT and liver). After an incubation period of 20 minutes on ice, samples were homogenized for 10 minutes at 4 °C using a Tissue-Lyser (Tab. 12), followed by centrifugation at maximal speed for 10 minutes at 4 °C. gWAT samples were centrifuged twice to get rid of the fat layer. Supernatants were transferred into new tubes after each centrifugation step and stored at -80 °C or directly used for the determination of the protein content using the BCA Protein Assay Kit (Tab. 5) according to the manufacturer's instructions.

2.5.2.2 Western Blot analysis

For the separation of proteins, SDS-PAGE was performed. Therefore, 20 µg of the protein lysates were diluted with 5 µL of 4x LSB and total sample volume (20 µL) was adjusted with ddH$_2$O. Protein samples were incubated for 30 minutes at RT, followed by a short centrifugation step before they were loaded on 12 % SDS gels (Tab. 22). Additionally, a pre-stained protein standard was loaded on the gels to estimate the molecular weight of the separated protein bands. Electrophoretical separation was carried out in electrode buffer at initial 100 V for 15 minutes following 150 V for 45 - 60 minutes using the Mini-PROTEAN Tetra Vertical Electrophoresis Cell system (Tab. 13).

Tab. 22: Composition of 12 % SDS gels

Compound	Separating gel	Stacking gel
Separating buffer	2.34 mL	780 µL
Acrylamide (30 %)	3.6 mL	390 µL
APS	18 µL	6 µL
TEMED	9 µL	3 µL
ddH$_2$O	9 µL	3 µL

By using the Tank-blot procedure, separated proteins were transferred to a nitrocellulose membrane. Protein transfer was performed at 200 mA and 4 °C overnight using the transfer buffer (Tab. 9). Thereafter, membranes were incubated in 5 % blocking solution (Table 8) for 1 hour at RT. The membranes were washed twice with 1x TBS-T buffer (Tab. 9) and

subsequently incubated with the respective primary antibody (Tab. 8) diluted in 5 % skim milk at a ratio of 1:1,000 or 1:5,000 (GAPDH). After overnight incubation, membranes were again washed for three times 10 minutes with 1x TBS-T buffer and incubated for 1 hour at RT with the respective secondary antibody (Tab. 8) diluted in 5 % skim milk at a ratio of 1:20,000. The membranes were repeatedly washed as described above and immunochemical detection of the antibody-conjugated protein bands was performed using Enhanced Chemiluminescence (ECL) Substrate (Tab. 10) as described in the manufacturer's instructions. Visualization and quantification of the protein bands was conducted using the ChemiDoc System (Tab. 13) and Image Lab software (Tab. 14). Thereby, each band was normalized to the abundance of GAPDH as housekeeping protein and given as percentage.

2.6 Identification of causal gene variants

2.6.1 Haplotype and VEP-analysis

In order to identify genes within the proximal region of the *Nbg4* locus (40-77 Mb), *in silico* haplotype analysis was performed. For this purpose, publicly accessible DNA sequences (origin) of parental Ola and NZO mice were used to dissect the genomic region of *Nbg4p* into regions that are either identical by descent (IBD) or polymorphic (non-IBDs) between the two strains. Therefore, SNPs were counted for an interval of 250 kbp and a threshold of 200 SNPs per interval. For this purpose, the reference sequence from C57BL/6J was used to count the total number of annotated SNPs for each interval. Regions below this SNP frequency were considered as IBDs, whereas non-IBDs were defined for regions exceeding the threshold.

To predict the functional effect of gene variants, a freely available tool called variant effect predictor (VEP) from Ensembl was used. Therefore, the identification number (rs number) of every Ola-specific non-IBD SNP within the proximal *Nbg4* locus was used to annotate and analyse the variations in coding and non-coding DNA regions and thereby predict the impact on transcripts and protein level. Predictions were calculated by using VEP interface (https://www.ensembl.org/Tools/VEP) with C57BL/6J as reference strain (GRCm39 assembly) and standard filters options of Ensembl/GENCODE and RefSeq transcripts data bases [108].

2.6.2 Microarray analysis

Total RNA from 100 or 40 mg of gonadal adipose tissue (gWAT) or liver samples, respectively (collected from 6-weeks old animals) was isolated and purified using the RNeasy Mini Kit (Tab. 11) including DNAse digestion according to the manufacturer`s instructions. For microarray analysis, the quality of isolated RNA was tested using a RNA 6000 nano kit. Only

samples with RIN values greater than 8 were selected for subsequent microarray analysis. Genome wide expression analyses (n=6 per genotype) were performed with 200 ng of total RNA using the Ambion WT Expression Kit and the WT Terminal Labeling Kit. Hybridization was conducted on Affymetrix Mouse Gene ST 1.0 arrays as previously described [109] that included about 66,000 probe IDs. Staining and scanning were performed according to the Affymetrix expression protocol. TAC Expression console 4.0 was used for quality control and to obtain annotated normalized RMA gene-level data (standard settings including sketch-quantile normalization). Statistical analyses were performed by utilizing the statistical programming environment R (R Development Core Team 47) implemented in CARMAweb48 (1.5-fold, p-value ≤ 0.01). Data were analyzed pairwise, $Nbg4p^{N/N}$ vs. $Nbg4p^{O/O}$.

2.7 Statistics

The generated data for this thesis are represented as mean values with respective standard errors of the mean (SEM). The number of biological replicates (n) and the statistical test is described in the respective figures legend. Significant differences were reported either by two-tailed student´s t-test with Welch correction or by one/two-way analysis of variance (ANOVA) followed by an appropriate post hoc test (Sidak or Bonferroni). For all statistical tests applied, marginal significance were expressed by p-values ≤ 0.05. For some data, p-values between 0.05-0.08 were highlighted within the figure to indicate a tendency for an effect. All tests were calculated using the GraphPad Prism 9 software.

3. Results

3.1 Metabolic characterization of RCS.NZO.129Ola-*Nbg4* mouse lines

To validate the linkage of the *Nbg4* locus with the phenotype observed in animals of the N2 population, recombinant congenic strains were generated as described in 2.2.1.2. Briefly, the *Nbg4* genomic region of 129Ola mice was introgressed into the NZO genome to generate a RCS.NZO.129Ola-*Nbg4* mouse line. As a strategy to further narrow down this diabetes susceptibility locus, two more RCS subgroups were generated by further backcrossing to the NZO recipient strain. **1**. The consomic line carrying the entire *Nbg4* locus (33-134 Mb; *Nbg4c*), **2.** The proximal subline (33-77 Mb; *Nbg4p*) and **3.** The distal subline (91-134 Mb; *Nbg4d*) with respective parts of the *Nbg4* locus (Fig. 7).
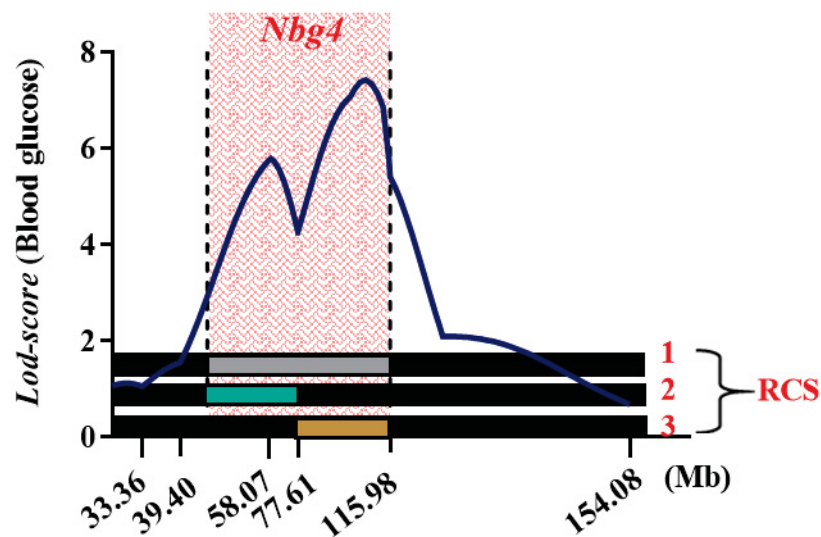
Fig. 7: Generation of recombinant congenic strains (RCS) to narrow down the critical region. Three different RCS mouse lines were generated by segregation of the *Nbg4* locus. 1: Mice carrying the whole (consomic) *Nbg4* ranging 33-134 Mb of chromosome 4 (*Nbg4c*), 2: Mice carrying the proximal sublocus of *Nbg4* ranging 33-77 Mb (*Nbg4p*) and 3: Mice carrying the distal sublocus of *Nbg4* ranging 91-134 Mb (*Nbg4d*). Within these lines, mice are homozygous for either the NZO or 129Ola genomic region of the respective segment.

After weaning at 3 weeks of age, male mice were fed a standard diet (SD) to prevent a severe disease progression. Furthermore, a metabolic phenotyping was performed until 21 weeks of age (Suppl. Tab. 2-4) to analyze their individual susceptibility for T2D development. Thereby, body weight and blood glucose levels were measured weekly for random fed values as well as at 21 weeks of age after 6 hours of fasting. Comparing the different RCS mouse lines (Fig. 8), only mice carrying the Ola-alleles of proximal *Nbg4* (*Nbg4p*^O/O) developed significant differences in blood glucose concentrations compared to NZO-allele carriers (*Nbg4p*^N/N). Similar to the N2(NZOxOla) population, Ola-allele carrier exhibited significantly elevated

blood glucose levels at 17 weeks of age which were increased by an average of 51.78 mg/dL compared to NZO-allele carriers (*Nbg4p*$^{O/O}$ 168.6 ± 11.32 mg/dL vs. *Nbg4p*$^{N/N}$ 116.82 ± 3.74 mg/dL, p=0.02) (Fig. 8A, Suppl. Fig. 1B). Likewise, a fasting period of 6 hours at 21 weeks of age resulted into increased circulating glucose concentrations in Ola-allele carriers of *Nbg4p* (*Nbg4p*$^{O/O}$ 180.50 ± 11.20 mg/dL vs. *Nbg4p*$^{N/N}$ 148.46 ± 5.41 mg/dL, p=0.05). In contrast, blood glucose levels in *Nbg4c* and *Nbg4d* mice were not different between the genotypes (Fig. 8A+D). In line with the blood glucose levels, similar results were observed in the measurement of 6-hours fasted plasma insulin values where *Nbg4p*$^{O/O}$ mice exhibited a 2.17 µg/L higher plasma insulin concentration compared to *Nbg4p*$^{N/N}$ mice (*Nbg4p*$^{O/O}$ 3.09 ± 1.40 µg/L vs. *Nbg4p*$^{N/N}$ 1.70 ± 1.13 µg/L, p=0.034) (Fig. 8E). Although, whole-body glucose as well as insulin tolerance were not different between the genotypes, insulin concentrations raised after glucose injection in Ola- compared to NZO-allele carriers of *Nbg4p* (Suppl. Fig.1F-H). To verify the rate of insulin resistance within the groups, the calculation of the HOMA-IR (Homeostatic Model Assessment for Insulin Resistance) value was used. Thereby, values of 6-hours fasted blood glucose (FBG) and plasma insulin (FPI) levels were calculated using the following formula developed by Matthews and colleagues [110].

$$\text{HOMA} - \text{IR} = \frac{\text{FPI (µU/mL) x FBG (mg/dL)}}{405}$$

The calculation revealed that insulin resistance in Ola-allele carriers of *Nbg4p* was almost twice as high as for NZO-allele carriers (*Nbg4p*$^{O/O}$ 32.48 ± 5.34 vs. *Nbg4p*$^{N/N}$ 16.17 ± 3.38, p=0.017), but was not significantly different comparing the other two lines carrying consomic or distal *Nbg4* (Fig. 8C). Furthermore, also the body weight was exclusively different in the proximal line, whereby *Nbg4p*$^{O/O}$ mice were in total 5.25 g heavier at 17 weeks of life compared to *Nbg4p*$^{N/N}$ mice (Fig. 8B). Further analysis of the body composition of these mice showed increased lean mass from week 10 of life and increased fat mass at week 15 of life (Suppl. Tab.2, Suppl .Fig. 1C-E). In line with the observed QTL, liver weight was only significantly different in animals carrying distal *Nbg4* locus with this time higher values for NZO-allele carriers (*Nbg4d*$^{O/O}$ 1.89 ± 0.11 g vs *Nbg4d*$^{N/N}$ 2.23 ± 0.05 g, p=0.006) (Fig. 8F).
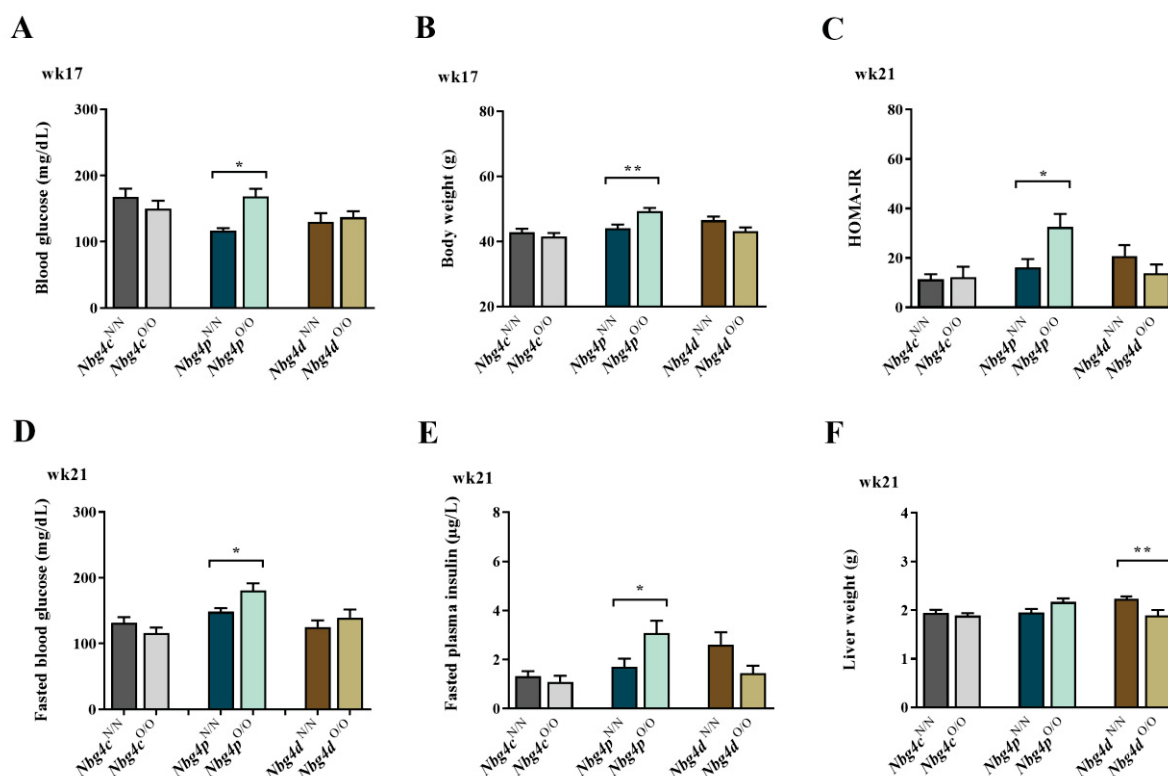
Fig. 8: Metabolic characterization of RCS.NZO.129Ola-*Nbg4* lines. RCS-lines carrying either consomic (*Nbg4c*), proximal (*Nbg4p*) or distal (*Nbg4d*) *Nbg4* were analyzed for blood glucose, plasma insulin, body and liver weight as well as the prevalence to develop insulin resistance via the HOMA-IR. Data are shown as mean ± SEM of 8-10 animals per group. One-way ANOVA followed by Sidak's multiple comparison post-hoc-test, *p<0.05, **p<0.01.

3.1.1 Phenotyping of RCS.NZO.129Ola-*Nbg4p* mice

The metabolic characterization of the different RCS lines on SD, validated the observed phenotype from the N2 population and ascribe the phenotypic effects of the proximal *Nbg4* sublocus. Therefore, deep phenotyping of the RCS.NZO.Ola-*Nbg4p* line was performed on a high-fat diet (HFD) containing 45%cal of fat (2.1.2) (Suppl. Tab. 3) according to the schedule shown in Fig. 9. The analysed metabolic parameters included blood glucose and plasma insulin levels for different ages for fasting, refed or random conditions, as well as further plasma components. Determination of body composition (2.2.1.3) were conducted at weeks 3, 6, 9, and 15 using nuclear magnetic resonance spectroscopy (NMR). Fasting-refeeding experiments (2.2.1.5) were executed at week 11, glucose tolerance test (GTT) either at week 6 or 13 (2.2.1.6) and insulin tolerance test (2.2.1.7) either at week 7 or 15 (different cohorts for different time points). Final experiments were performed at either week 6 or 18 of life, where mice were 6-hours fasted and sacrificed to harvest tissues for either subsequent functional *ex vivo* assays or gene and protein expression analysis.

♂ RCS.NZO.Ola-*Nbg4p* → 45% HFD

Weekly measurement of blood glucose & body weight

Fig. 9: Phenotyping schedule for RCS.NZO.Ola-*Nbg4p* mice on HFD. To analyse several parameter on different time points, different cohorts were generated. Juvenile mice were analysed until week 6 of life (cohort 1), while two other cohorts were analysed until 18 weeks of life (cohorts 2 and 3). Blood glucose and body weight was measured weekly. Nuclear magnetic resonance spectroscopy (NMR) was used to determine the body composition and was executed at weeks 3, 6, 9, and 15. Fasting-refeeding experiments were conducted at week 11, glucose tolerance test (GTT) either at week 6 (cohort 2) or 13 (cohort 3) and insulin tolerance test either at week 7 (cohort 2) or 15 (cohort 3). Animals were sacrificed either at 6 or 18 weeks of age for the collection of blood and tissues and further *ex vivo* experiments.

3.1.1.1 Plasma parameters and body weight development of RCS.NZO.129Ola-*Nbg4p* mice

Weekly measurements showed that Ola-allele carriers for *Nbg4p* displayed higher blood glucose levels already at week 5 of life with 287.00 ± 15.72 mg/dL compared to NZO-allele carriers with 227.91 ± 9.29 mg/dL. The state of hyperglycaemia (blood glucose >300 mg/dL) was reached at week-of-life 6 in $Nbg4p^{O/O}$ mice ($Nbg4p^{O/O}$ 300.66 ± 20.29 mg/dL vs. $Nbg4p^{N/N}$ 246.66 ± 15.98 mg/dL), whereas $Nbg4p^{N/N}$ mice started to be hyperglycaemic two weeks later ($Nbg4p^{O/O}$ 337.18 ± 42.25 mg/dL vs. $Nbg4p^{N/N}$ 325.58 ± 35.48 mg/dL) (Fig. 10A). In detail, gain of blood glucose concentrations were significantly elevated in the time between week 3 and 11 of life (Fig. 10B). In contrast to mice fed a SD, blood glucose development was independent from the body weight during HFD feeding (Fig.10C). The prevalence of T2D was higher in $Nbg4p^{O/O}$ mice for the whole time period and reached a difference of up to 35.7 % at week 15 of life ($Nbg4p^{O/O}$ 85.71 % vs. $Nbg4p^{N/N}$ 50 %) (Fig. 10D).
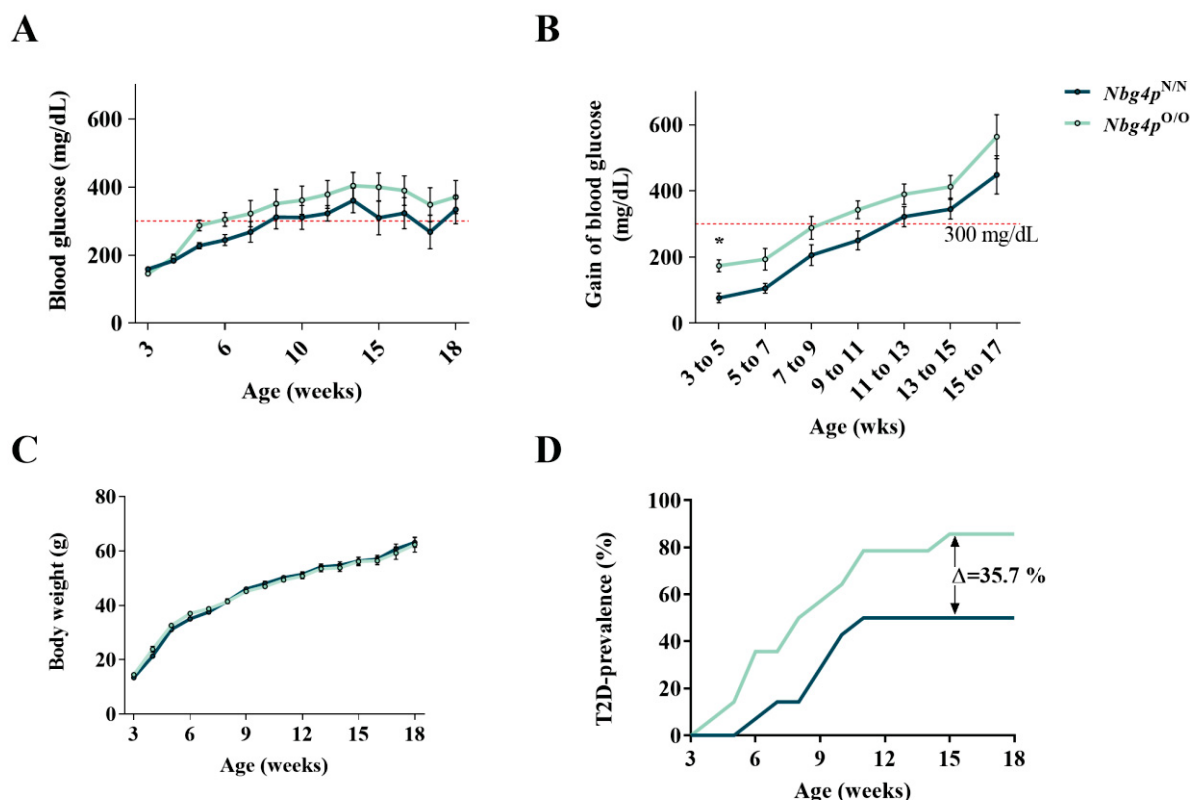
Fig. 10: Blood glucose levels, body weight and T2D prevalence of *Nbg4p* mice. After weaning at week 3 of life, mice were fed a high-fat diet (HFD). Blood glucose levels (A) as well as body weight (C) were measured weekly until week 21 of age. Gain of blood glucose concentrations (B) in a period of every 2 weeks was calculated for a detailed view on the development of hyperglycemia. T2D prevalence (D) was calculated by the percentage of animals reaching blood glucose concentrations over 300 mg/dLfor at least three weeks in a row. Data are shown as mean values ± SEM from 12-14 mice per genotype. Two-way ANOVA followed by Sidak's multiple comparison post-hoc-test, *p<0.05.

Plasma parameters from final 6-hours fasted measurements of juvenile and adult *Nbg4p* mice are summarized in Table 23. Although fasted blood glucose levels were not markedly different between the genotypes at both ages, plasma insulin levels at 6 weeks of age were 2.53 µg/L higher in Ola- compared to NZO-allele carriers (*Nbg4p*$^{O/O}$ 7.72 ± 0.88 µmol/L vs. *Nbg4p*$^{N/N}$ 5.19 ± 0.55 µmol/L, p=0.03). Despite of a decrease in the amount of circulating ketone bodies in mice carrying the Ola-allele (*Nbg4p*$^{O/O}$ 335.20 ± 29.28 µmol/L vs. *Nbg4p*$^{N/N}$ 440.30 ± 41.26 µmol/L, p=0.04), further plasma measurements were not different between the genotypes.

Tab. 23: Final plasma parameter of juvenile and adult *Nbg4p* mice. Plasma parameters were measured after 6 hours of fasting. Data are shown as mean ± SEM (n=9-25). Statistical analyses were done by two-tailed, unpaired Student's t-test, *p < 0.05 for N/N vs O/O; #p<0.05, ##p<0.01, ###p<0.001 for 6 vs 18 weeks. TG: triglyceride, NEFA: non-esterified fatty acids, wks: weeks.

Parameter	6 wks		18 wks	
	Nbg4p$^{N/N}$	*Nbg4p*$^{O/O}$	*Nbg4p*$^{N/N}$	*Nbg4p*$^{O/O}$
Blood glucose (mg/dL)	138.89 ± 4.61	143.18 ± 5.63	**265.25 ± 46.93**$^{\#}$	**325.73 ± 47.36**$^{\#\#}$
Insulin (µg/L)	5.19 ± 0.55	**7.72 ± 0.88***	8.93 ± 3.06	5.84 ± 1.71
TG (mg/dL)	135.38 ± 19.20	109.53 ± 10.80	118.65 ± 12.07	**152.75 ± 14.80**$^{\#}$
NEFA (mmol/L)	1.01 ± 0.09	0.82 ± 0.11	0.90 ± 0.07	1.0 ± 0.13
Ketone bodies (µmol/L)	440.30 ± 41.26	**335.20 ± 29.28***	358.44 ± 74.09	379.59 ± 55.17
Cholesterol (mg/dL)	4.56 ± 0.33	4.93 ± 0.39	**8.76 ± 0.34**$^{\#\#\#}$	**8.29 ± 0.86**$^{\#\#}$
Adiponectin (µg/mL)	5.27 ± 0.42	5.36 ± 0.28	-	-

3.1.1.2 Metabolic characterization of RCS.NZO.129Ola-*Nbg4p* mice during fasting and refeeding

To analyse the effect of intermittent periods of fasting and refeeding on the glucose metabolism of *Nbg4p* mice, 11-weeks old animals were fasted for 16 hours overnight, following a 2-hours period with *ad libitum* access to the HFD. The fasting period was characterized by low blood glucose and plasma insulin levels for both genotypes with concentrations around 140 mg/dL and 2.3 µg/L, respectively. Since blood glucose levels were already trending higher in Ola-allele carriers of *Nbg4p* after fasting (*Nbg4p*$^{O/O}$ 172.77 ± 32.94 mg/dL vs. *Nbg4p*$^{N/N}$ 107.08 ± 12.39 mg/dL), refeeding led to a significant increase which was about 30 % higher compared to NZO-allele carriers (*Nbg4p*$^{O/O}$ 378.14 ± 43.51 mg/dL vs. *Nbg4p*$^{N/N}$ 244.64 ± 17.03 mg/dL, p=0.015). As expected, plasma insulin levels were elevated after refeeding, however no differences were observed when comparing the genotypes. Body weight was monitored to determined excessive food consumption during the time of refeeding and was shown to be unaltered during the whole experiment (Fig. 11A-C).
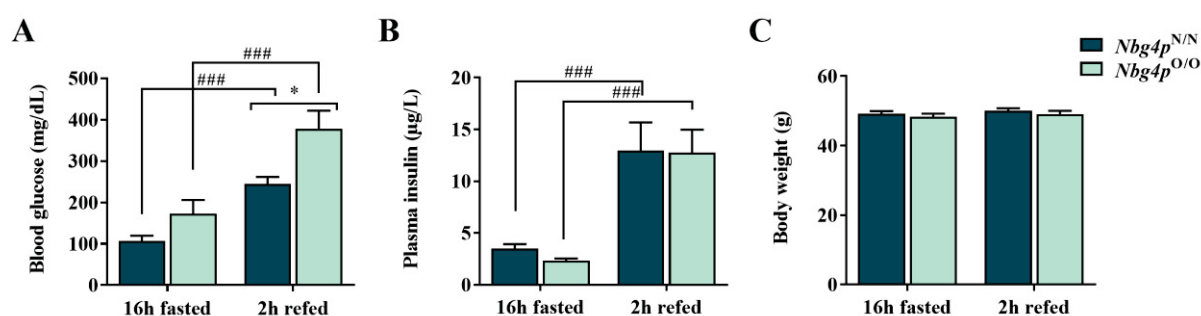
Fig. 11: Fasting and refeeding experiments in *Nbg4p* mice. Blood glucose (A), plasma insulin (B) and body weight (C) were measured after 16 hours of fasting as well as after 2 hours of *ad libitum* refeeding. Data are shown as mean ± SEM (n =10-14)

and analysed using two-way ANOVA followed by Sidak's multiple comparisons test. *p< 0.05 for N/N vs. O/O; ###p<0.001 for fasted vs. refed states.

3.1.1.3 Glucose and insulin tolerance tests in RCS.NZO.129Ola-*Nbg4p* mice

The intraperitoneal glucose tolerance test (i.p.GTT) is a very common measurement to analyse whole-body glucose homeostasis and therefore serves as a first indicator of peripheral insulin resistance in T2D. Mice were fasted for 16 hours before the administration of 2 g/kg body weight glucose in either week-of-life 6 or 13, respectively. Blood glucose levels were measured after fasting subsequently before the glucose injection, as well as 15, 30, 60, 120 and 240 minutes after the injection (2.2.1.6). While the overall glucose tolerance was not different in young (6-weeks old) animals, measurements in 13-weeks old animals reached a statistical significant difference in blood glucose levels at 15, 30 and 240 minutes after the glucose injection between Ola-and NZO-allele carriers (*Nbg4p*$^{O/O}$ 88597 ± 3166 AUC vs. *Nbg4p*$^{N/N}$ 79337 ± 1885 AUC, p=0.02) (Fig. 12A+B). Interestingly, juvenile mice carrying the Ola-allele showed increased plasma insulin levels for several time points after glucose injection with a significantly higher AUC, although corresponding blood glucose levels were not different. In contrast, insulin concentrations of adult Ola-allele carriers with impaired glucose tolerance were unaltered during the experiment (Fig. 12C+D).

Similar results were observed during the intraperitoneal insulin tolerance test (i.p.ITT). Mice were fasted for 6 hours and subsequently injected with 1 U/kg body weight insulin in week-of-life 7 and 15 (2.2.1.7). The results showed that adult mice (15-weeks old) carrying the Ola-allele for *Nbg4p* had a lower insulin sensitivity by higher blood glucose levels after insulin injection compared to NZO-allele carriers, indicating that whole-body glycaemia was impaired in *Nbg4p*$^{O/O}$ mice (*Nbg4p*$^{O/O}$ 11964 ± 1846 AUC vs. *Nbg4p*$^{N/N}$ 6923 ± 1039 AUC, p=0.038) (Fig.12 E+F).
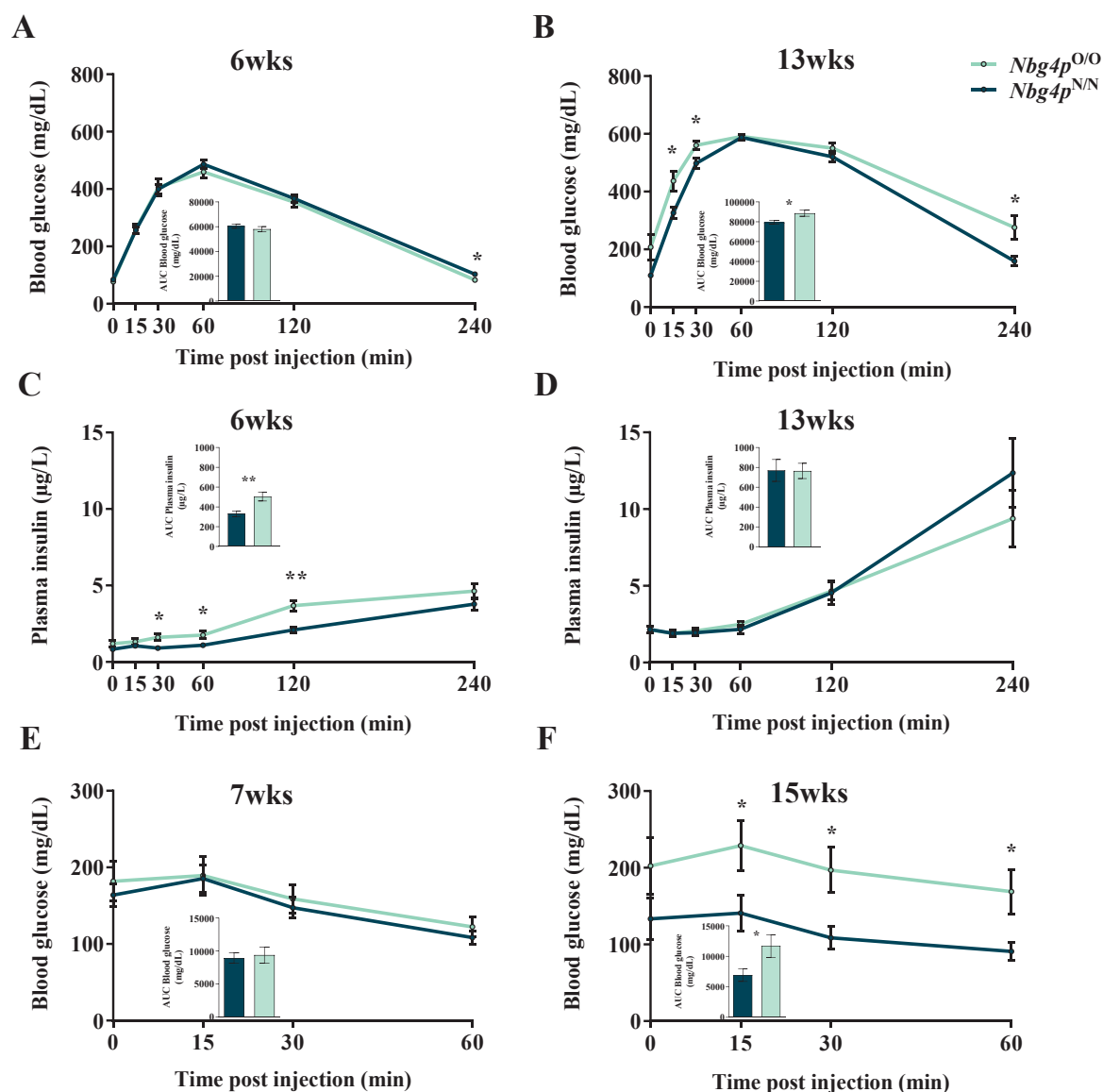
Fig. 12: Glucose and insulin tolerance of *Nbg4p* mice. Juvenile and adult mice were analysed for their whole-body glucose tolerance by measuring blood glucose and plasma insulin concentrations for several time points after the injection of 2 g/kg glucose (A-D). Insulin sensitivity was examined by measuring blood glucose levels after intraperitoneal injection of 1 U/kg insulin (E+F). AUC was determined for quantification of each experiment. Data are shown as mean ± SEM (n =9-12). Data were analysed using two-way ANOVA with Bonferroni's multiple comparisons test and two-tailed unpaired Student's t-test (AUC). *p< 0.05, **p<0.01.

3.1.2 Metabolic characterization of juvenile RCS.NZO.129Ola-*Nbg4p* mice

To prevent the development of a severe disease and undesired side effects of a chronic hyperglycaemic state, further analyses were performed at week 6 of life. At this stage, randomly measured blood glucose levels were 66.16 mg/dL higher in Ola- compared to NZO-allele carriers for *Nbg4p* (*Nbg4p*[O/O] 296.13 ± 18.83 mg/dL vs. *Nbg4p*[N/N] 229.97 ± 13.33 mg/dL, p=0.01), whereby 6 hours of fasting did not show any difference between the genotypes (Fig. 13A). Despite the unaltered body weight of both genotypes, body composition was

strikingly different. Thereby, Ola-allele carriers showed increased accumulation of body fat (*Nbg4p*$^{O/O}$ 10.43 ± 0.38 g vs. *Nbg4p*$^{N/N}$ 8.64 ± 0.25 g, p=0.001), whereas lean mass remained similar when comparing with NZO-allele carriers (Fig. 13B+C).
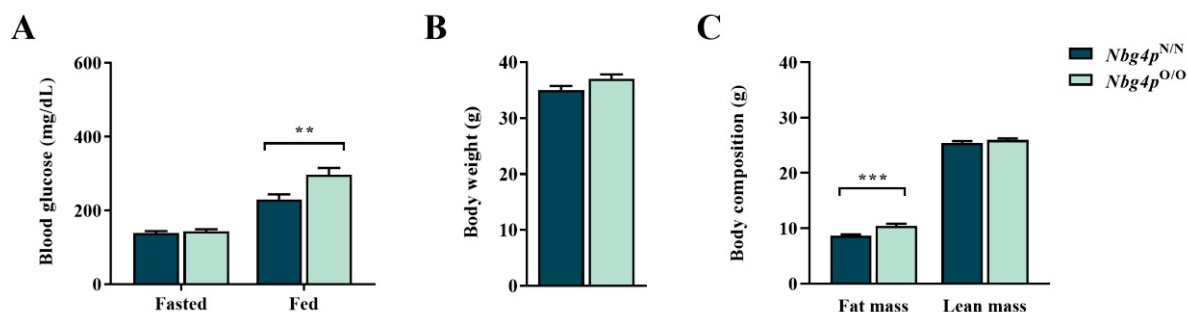
Fig. 13: Metabolic characterization of juvenile *Nbg4p* mice. At 6 weeks of age, blood glucose (A) levels were measured at random-fed states as well as after a fasting period of 6 hours. Body weight (B) was measured using an electronic scale and body composition (C) was determined by a nuclear magnetic resonance (NMR) spectrometer. Data are shown as mean ± SEM of 12-43 animals. Data were analysed using multiple unpaired t-test with Welch correction. **p<0.01, ***p<0.001.

To investigate glucose-related insulin action in 6 weeks old *Nbg4p* mice, concentrations of plasma insulin as well as the amount of pancreatic insulin secretion were determined. Thereby, a 6 hours fasting period showed increased plasma insulin concentrations in Ola- compared to NZO-allele carriers (*Nbg4p*$^{O/O}$ 7.72 ± 0.88 µg/L vs. *Nbg4p*$^{N/N}$ 5.19 ± 0.55 µg/L, p=0.03) (Fig. 14A). However, random fed plasma insulin levels showed a contrary effect (*Nbg4p*$^{O/O}$ 18.84 ± 1.92 µg/L vs. *Nbg4p*$^{N/N}$ 26.55 ± 2.16 µg/L, p=0.03). At final experiments, insulin secreting pancreatic islets were isolated and cultivated overnight. The next day, islets were incubated at low (LG) or high glucose (HG) concentrations of either 1 mM or 25 mM glucose, respectively. Although glucose-stimulated insulin secretion (GSIS) showed significantly increased amounts of insulin when comparing low to high glucose concentrations, no significant differences were observed between the genotypes (Fig. 14B).
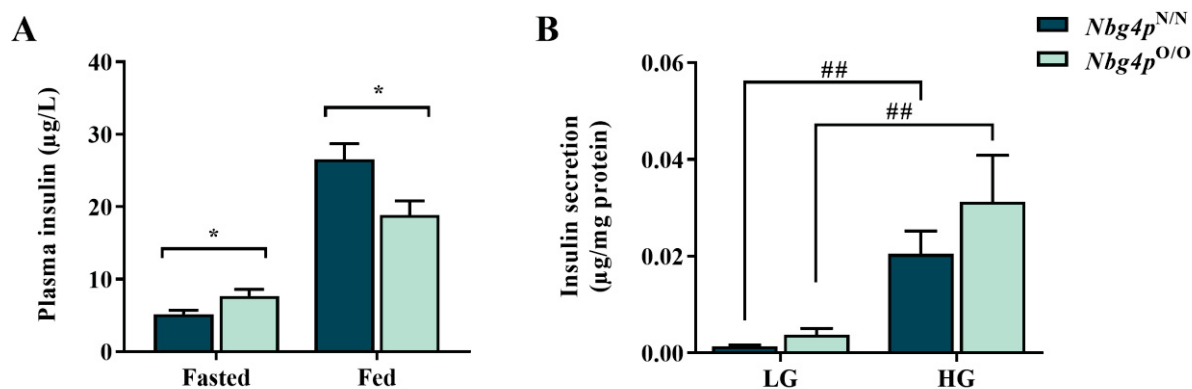
Fig. 14: Insulin concentrations at fasted (low) and glucose-stimulated (high) states. Plasma insulin levels (A) were determined after 6 hours of fasting and at random-fed states in 6 weeks old *Nbg4p* mice. Glucose-stimulated insulin secretion (GSIS) of isolated pancreatic islets (B) was executed in final experiments from 6 weeks old *Nbg4p* mice. Thereby, low (LG) or high glucose (HG) concentrations were used of either 1 mM or 25 mM glucose, respectively. Data are shown as mean ± SEM (n =11-31) and analysed using Data were analysed using multiple unpaired t-test with Welch correction (A) or two-way ANOVA followed by Sidak's multiple comparisons test (B). *p< 0.05 for N/N vs. O/O; ##p<0.01 for LG vs. HG condition.

3.1.2.1 *Ex vivo* glucose uptake into skeletal muscles from RCS-NZO.129Ola-*Nbg4p* mice

In response to insulin, circulating glucose is predominantly taken up by the skeletal muscle. As insulin binding and glucose uptake can differ widely between the different muscle types, we isolated extensor digitorum longus (EDL) and soleus muscles from 6 weeks old *Nbg4p* mice and examined their ability to take up ^{3}H-2-Deoxy-D-glucose (2-DOG) *ex vivo* (2.2.1.9). Figure 15A shows that in EDL muscle both genotypes exhibited a significantly increased insulin-stimulated glucose uptake of approximately 28 % compared to basal states (*Nbg4p*$^{O/O}$ 2.40 ± 0.08 nmol/mg/20 minutes at basal vs. 3.32 ± 0.14 nmol/mg/20 minutes at insulin-stimulated states compared to *Nbg4p*$^{N/N}$ 2.54 ± 0.26 nmol/mg/20 minutes at basal vs. 3.53 ± 0.31 nmol/mg/20 minutes at insulin-stimulated states). However, there was no difference in the glucose uptake within the two genotypes. Similar results were observed in soleus muscle with a little more variation between the single measurements (Fig. 15B).
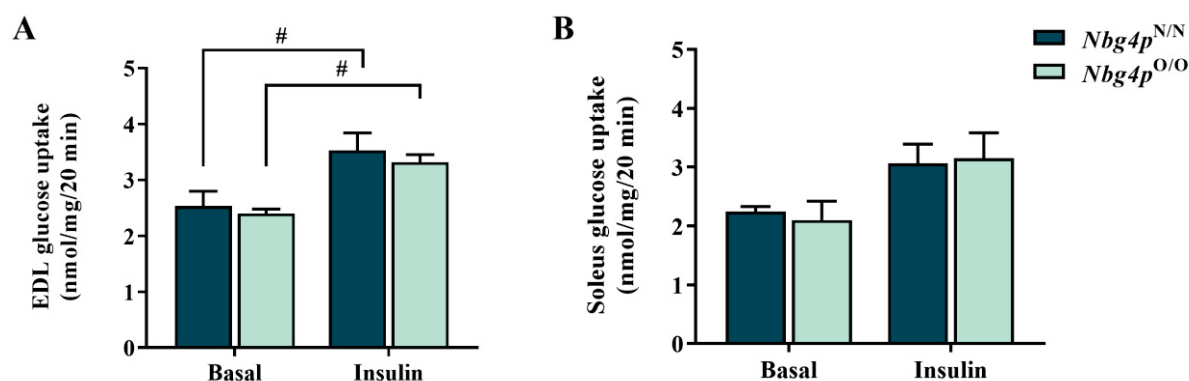
Fig. 15: *Ex vivo* glucose uptake in EDL and soleus muscle. Uptake of ^{3}H-2-DOG was measured at basal or insulin stimulated states in either isolated EDL (A) or soleus muscles (B) of *Nbg4p* mice. Data are shown as mean ± SEM (n = 4-7) and analysed using two-way ANOVA with Bonferroni's multiple comparisons test. #$p<0.05$ for basal vs. insulin-stimulated condition.

3.1.2.2 Investigation of glucose and lipid metabolism in the adipose tissue from RCS.NZO.129Ola-*Nbg4p* mice

In addition to skeletal muscle, also the white adipose tissue (WAT) is able to take up glucose. Therefore, *ex vivo* ^{14}C-D-glucose uptake was measured in isolated primary adipocytes (2.2.1.10) which showed already at basal states a tendentially lower rate in Ola- compared to NZO-allele carriers. This effect became significantly different between the genotypes after insulin stimulation. At this condition, Ola-allele carriers showed a reduced glucose uptake of approximately 53 % compared to NZO-allele carriers (*Nbg4p*$^{O/O}$ 112.85 ± 11.29 cpm/mg lipid vs. *Nbg4p*$^{N/N}$ 239.34 ± 39.38 cpm/mg lipid, p=0.03) (Fig. 16A).

GLUT4 is the main glucose transporter protein in the adipose tissue that catalyzes insulin-mediated glucose uptake. In order to investigate the cause of a decreased glucose uptake into the WAT of *Nbg4p*$^{O/O}$ mice, GLUT4 protein abundance was measured in the respective tissues of both genotypes. The Western Blot analysis resulted in a 31 % lower GLUT4 protein abundance in the WAT from Ola- compared to NZO-allele carriers (*Nbg4p*$^{O/O}$ 89.41 ± 3.7 % vs. *Nbg4p*$^{N/N}$ 61.85 ± 7.42 %, p = 0.04) (Fig. 16B), consistent to the observed decrease in adipocyte glucose uptake.
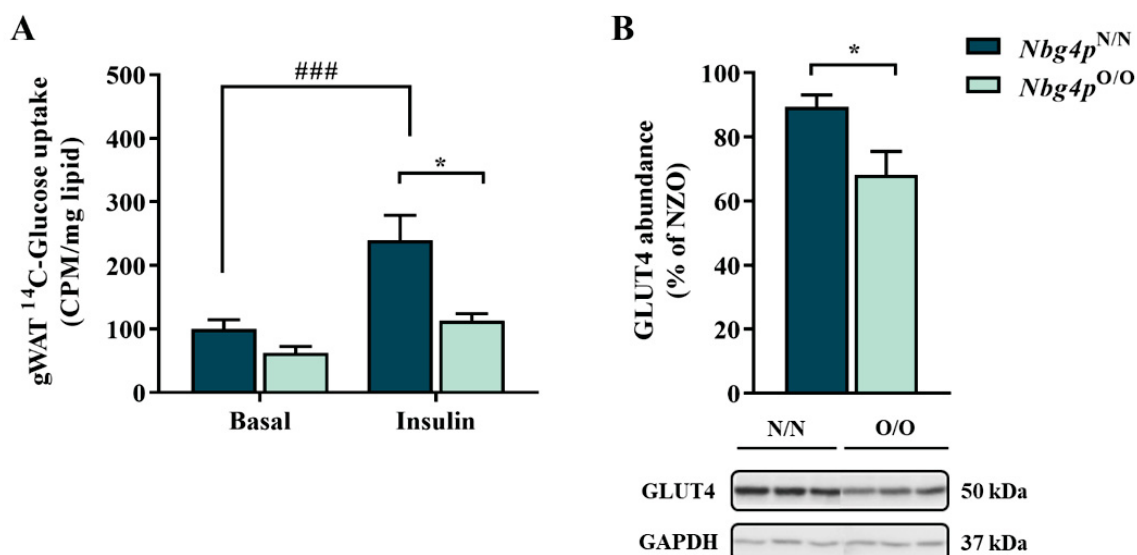
Fig. 16: *Ex vivo* glucose uptake and GLUT4 protein abundance in WAT. ^{14}C-Glucose uptake was measured in isolated adipocytes from gWAT at basal and insulin-stimulated states (A). GLUT4 protein abundance was quantified by the normalization to GAPDH and given as percentage of NZO controls (B). Data are shown as mean ± SEM (n = 5-8) and analysed using two-way ANOVA with Bonferroni's multiple comparisons test (A) or two-tailed, unpaired Student's t-test (B). *p <0.05 for N/N vs. O/O; ###p<0.001 for basal vs. insulin-stimulated condition.

Since the measurements of body composition revealed a higher body fat mass in *Nbg4p*$^{O/O}$ mice (3.1.2.), histological analyses were performed to uncover whether this increase occurs due to hypertrophy or hyperplasia. In states of insulin resistance, adipose tissue mass is usually increased due to bigger adipocytes. To verify this hypothesis, gonadal (gWAT) as well as subcutaneous (scWAT) white adipose tissue were dissected during the final experiments at 6 weeks of age and subsequently fixed in PFA to maintain the original morphology of the tissues. Ultra-thin slices were stained with hematoxylin and eosin (HE) to dye the adipocyte membranes. Multi-layer analysis was performed to quantify the adipocyte size of both genotypes (2.2.1.11). The representative images show that in general, adipocytes of the gWAT are larger compared to those of the scWAT depots (Fig.17A). Calculation of mean values from analysed adipocytes area further validated that Ola-allele carriers of *Nbg4p* mice have an increased adipocyte size in gWAT compared to NZO-allele carriers (*Nbg4p*$^{O/O}$ 3421.53 ± 246.95 µm² vs. *Nbg4p*$^{N/N}$ 2611.29 ± 239.66 µm², p=0.05). In contrast, adipocytes of the scWAT showed a similar size of around 1000 µm² per adipocyte for both genotypes (Fig. 17B). Dissecting of the different adipocytes into smaller groups defined by percentiles showed that the higher average of adipocyte size might emerge from less small (500-3000 µm²) and more bigger (3000-15000 µm²) adipocytes (Fig. 17C).

To explain the differences of adipocyte size in the gWAT of *Nbg4p*[O/O] mice, gene expression analysis was performed. For this purpose, major adipogenesis marker involved in adipocyte differentiation and maturation as well as known inflammation marker, that might play a role in the regulation of adipocyte size, were analysed. Despite this broad-ranging examination of key regulators, no significant differences were observed (Fig. 17D).
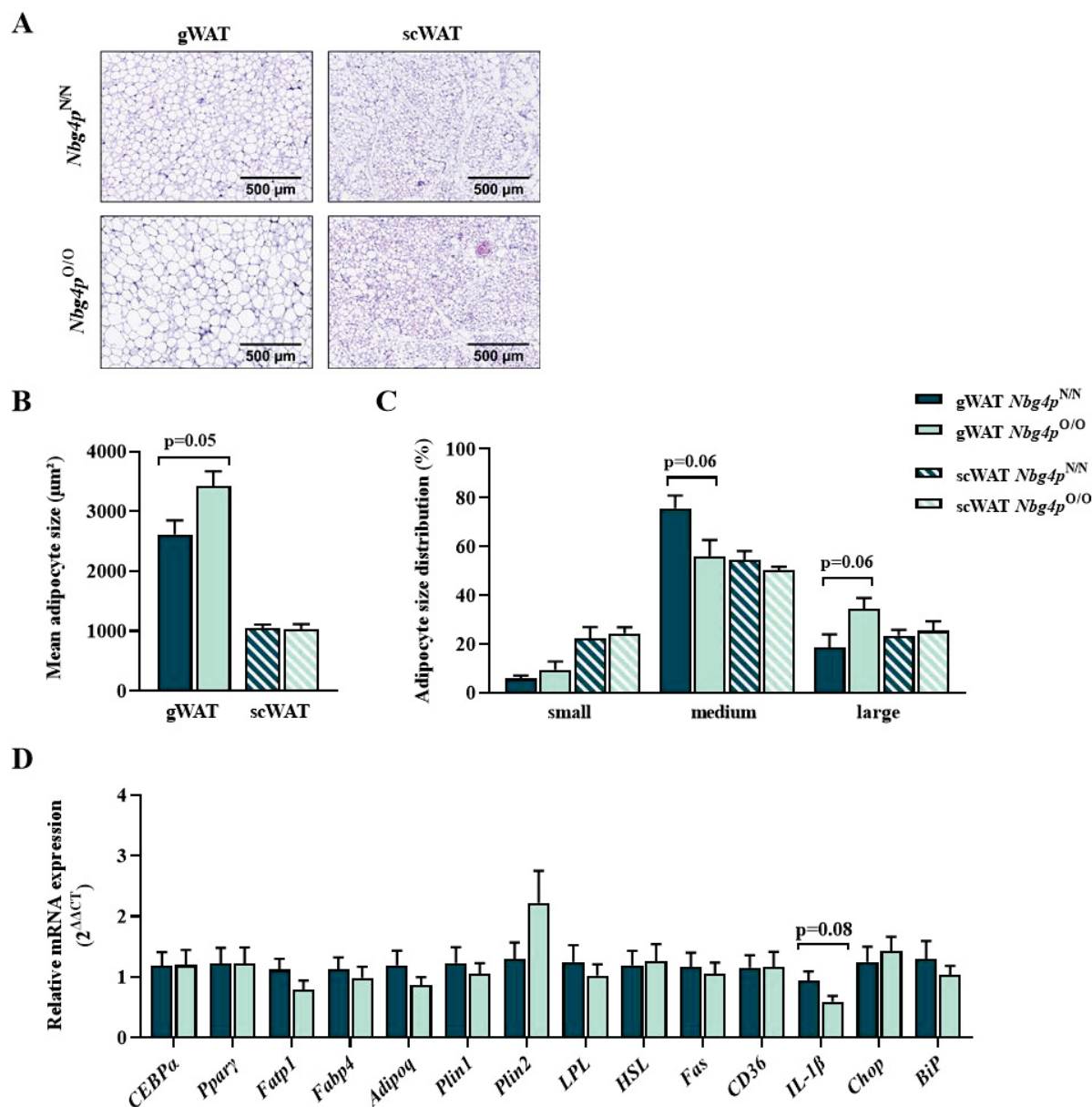
Fig. 17: Investigation of adipocyte size from gonadal and subcutaneous fat depots. Representative images of hematoxylin and eosin-stained sections of gWAT and scWAT tissues from 6 weeks old *Nbg4p* mice. At least 3 different areas per fat pad section of each mouse were quantified for 4 mice per genotype. Mean adipocyte area (B) and size distribution (C) were calculated using ImageJ. Adipocyte size was separated into three groups depending on their percentiles to define small (0-25), medium (25-75) and large (75-100) adipocytes. Gene expression of major adipogenesis and inflammation marker (D). Data are shown as mean ± SEM and analysed using two-tailed, unpaired Student's t-test with Welch's correction.

3.1.2.3 Investigation of glucose and lipid metabolism in primary hepatocytes from RCS.NZO.129Ola-*Nbg4p* mice

Disturbances in the hepatic lipid metabolism can lead to an excessive accumulation of hepatic lipids in form of triglycerides (TGs). Abnormally high concentrations of TGs can therefore lead to severe metabolic features, such as fatty liver disease. To investigate the regulation of lipids and glucose metabolism in the hepatic tissue, livers were dissected at week 6 of age as mentioned before (2.2.1.12). While the physiological appearance of the tissues seem to differ between the genotypes, measurements of liver weight remained unaltered (Fig. 18A+B).

Besides a restricted uptake of glucose into the peripheral tissues, also abnormally increased gluconeogenesis can contribute to hyperglycaemia and T2D. To verify that the liver also plays a role in the observed phenotype of *Nbg4p* mice, isolated primary hepatocytes were monitored for their capacity to produce and release glucose *ex vivo* (2.2.1.12.2). Therefore, glucose-starved cells were incubated either with insulin to inhibit gluconeogenesis or with pyruvate/lactate to stimulate the production of glucose. Figure 18C shows that at basal states equal amounts of glucose were measured for the two genotypes. However, after the addition of insulin, glucose production was significantly increased in Ola- versus NZO-allele carriers (*Nbg4p*$^{O/O}$ 0.040 ± 0.002 µg/µL vs. *Nbg4p*$^{N/N}$ 0.034 ± 0.002 µg/µL, p=0.02). As expected, supplementation with pyruvate/lactate significantly increased gluconeogenesis twice as much as in basal conditions for both genotypes. Also under these conditions, hepatocytes of Ola-allele carriers produced a higher amount of glucose compared to those of NZO-allele carriers (*Nbg4p*$^{O/O}$ 0.084 ± 0.003 µg/µL vs. *Nbg4p*$^{N/N}$ 0.074 ± 0.003 µg/µL, p=0.02). To elucidate if insulin-mediated inhibition of gluconeogenesis has an impact on the hepatic functionality, cells were treated with insulin for one hour and subsequently supplemented with pyruvate/lactate. Similar to the condition of pyruvate/lactate alone, the primary hepatocytes of the two genotypes still produced different amounts of glucose with the same pattern as before (*Nbg4p*$^{O/O}$ 0.078 ± 0.003 µg/µL vs. *Nbg4p*$^{N/N}$ 0.065 ± 0.003 µg/µL, p=0.04) (Fig. 19A). Besides gluconeogenesis, the liver is also able to convert stored glycogen back to glucose in a process called glycogenolysis. Therefore, hepatic glycogen contents were measured which showed a slight increase in Ola-compared to NZO allele carriers (*Nbg4p*$^{O/O}$ 4.60 ± 0.82 µg/mg vs. *Nbg4p*$^{N/N}$ 2.75 ± 0.46 µg/mg, p=0.07) (Fig. 18D). These data indicate, that Ola-allele carriers of *Nbg4p* seem to suffer from an impaired hepatic glucose metabolism when comparing to NZO-allele carriers.
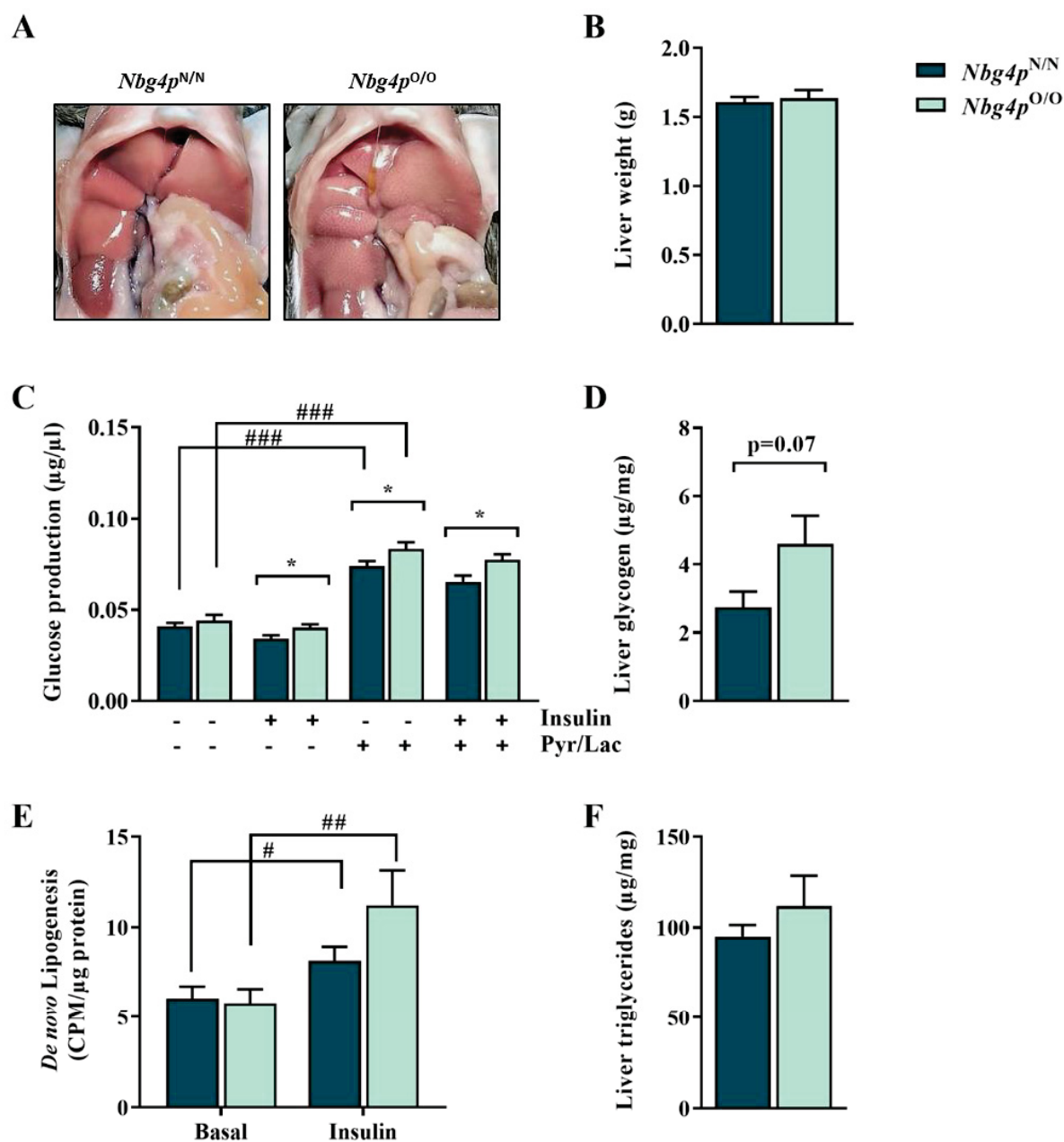
Fig. 18: Liver parameter of juvenile *Nbg4p* mice. Representative external appearance of liver tissue from 6 weeks old *Nbg4p* mice (A) Endogenous glucose production was determined in primary isolated hepatocytes with or without supplementation of insulin and/or pyruvate/lactate (C). For hepatic *de novo* lipogenesis (DNL) primary hepatocytes were supplemented with radiolabelled acetate as substrate and the amount of synthesized lipids was measured in the absence (basal) or presence of 100nM insulin (E). Liver weight (B), glycogen (D) and triglyceride (F) content was determined for both genotypes. Data are shown as mean $\pm$ SEM (n = 7-28) and analysed by two-way ANOVA with Bonferroni's multiple comparisons test (C+E) or two-tailed, unpaired Student's t-test with Welch correction (B, D, F). *$p < 0.05$ for N/N vs. O/O; #$p<0.05$, ##$p<0.01$ and ###$p<0.001$ for basal vs. insulin stimulated condition.

Glucose and lipid metabolism are closely related to each other and therefore also the crosstalk between organs must be taken into account when it comes to the regulation of whole-body glucose homeostasis. It is well established that in states of elevated blood glucose levels, hepatocytes are able to respond with the activation of transcription factors to induce lipogenic

genes involved in hepatic *de novo* lipogenesis (DNL). Insulin resistance and excessive fat accumulation as a result of a dysregulation in hepatic DNL may further influence metabolic health and contribute to diseases like non-alcoholic fatty liver disease (NAFLD) or severe T2D. In order to examine the potential effects of hyperglycaemia in $Nbg4p^{O/O}$ mice on hepatic lipid metabolism, isolated primary hepatocytes were provided with ^{14}C-acetate as substrate for fatty acid synthesis. In this way, ^{14}C-acetate was measured at basal states and after 4 hours of insulin stimulation, which was proportional to the rate of synthesized fatty acids during DNL (2.2.1.12.1). As expected, insulin increased DNL in hepatocytes of $Nbg4p^{O/O}$ mice twice as much compared to the basal state (5.79 ± 0.77 cpm/µg protein at basal vs. 11.22 ± 1.93 cpm/µg protein at insulin conditions). This effect was much smaller in hepatocytes of $Nbg4p^{N/N}$ mice (6.05 ± 0.66 cpm/µg protein at basal vs. 8.15 ± 0.76 cpm/µg protein at insulin conditions). Although, insulin-stimulated DNL tended to be higher in Ola-allele carries, genotype specific differences did not reach significance. In line with the DNL assay, also hepatic TG content showed similar amounts for both genotypes, concluding that the hepatic lipid metabolism was not affected in 6 weeks old $Nbg4p$ mice (Fig. 18E-F).

To investigate a possible relationship between the differences in hepatic glucose metabolism and mitochondrial function, a mitostress test assay of primary isolated hepatocytes was performed (2.2.2.4). Thereby, mitochondrial respiration was expressed by the oxygen consumption rate (OCR) which was measured for basal conditions, as well as after the inhibition of different targets of the electron transport chain. As shown by the overall OCR-trace, hepatocytes from $Nbg4p^{O/O}$ mice showed tendentially higher rates of mitochondrial respiration compared to hepatocytes from $Nbg4p^{N/N}$ mice (Fig. 19A). Calculation of the key parameters of mitochondrial function further observed significantly increased OCR-rates for maximal respiration, non-mitochondrial respiration and spare respiratory capacity in hepatocytes from $Nbg4p^{O/O}$ compared to $Nbg4p^{N/N}$ mice (Fig. 19B).

In addition to the metabolic assays of primary hepatocytes, gene expression analysis of key regulator of the hepatic glucose and lipid metabolism was performed in liver samples of 6 weeks old $Nbg4p$ mice. Interestingly, a significantly decreased expression was observed for the hepatic phosphofructokinase *Pfkl* when comparing Ola- with NZO-allele carriers of $Nbg4p$. Furthermore, gene expression of the glucokinase regulatory protein *Gckr* was strikingly elevated in $Nbg4p^{O/O}$ compared to $Nbg4p^{N/N}$ mice. In contrast, key regulator of the hepatic lipid metabolism remained unchanged (Fig. 19C).
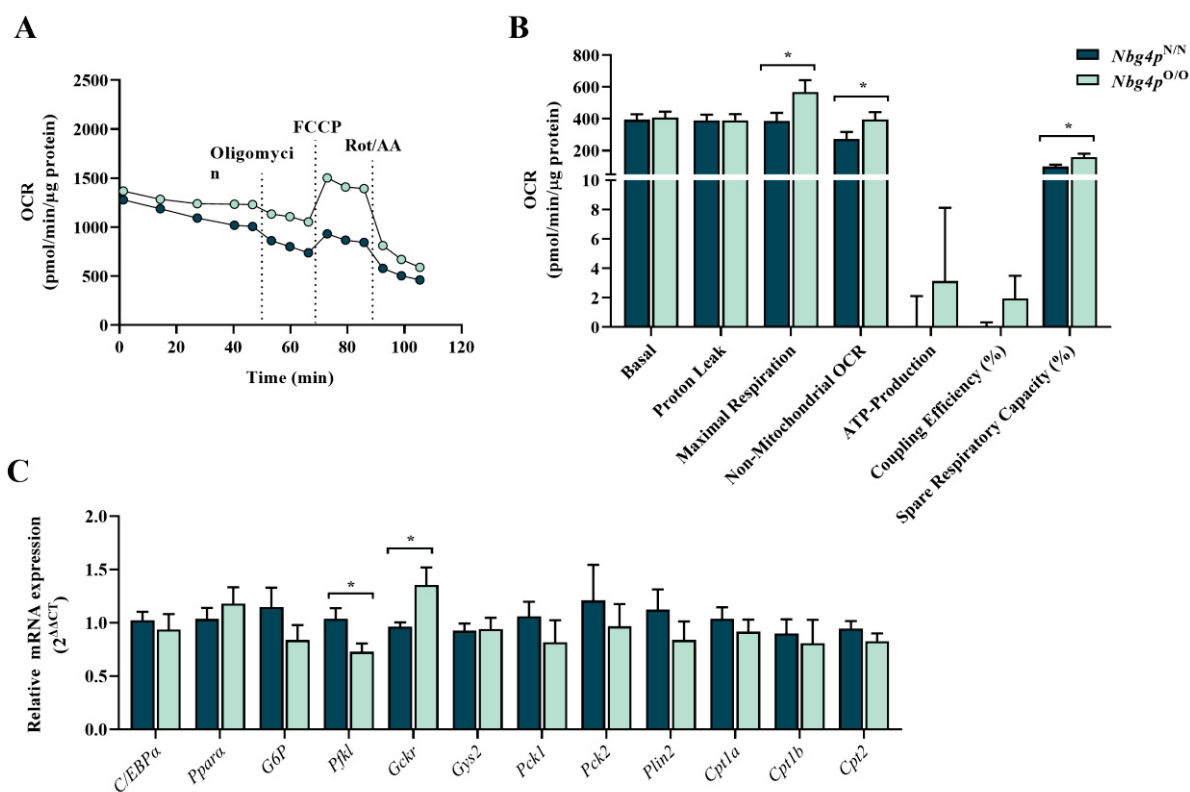
Fig. 19: Mitochondrial function and gene expression analysis in livers from *Nbg4p* mice. Mitochondrial stress test was performed in primary hepatocytes of 6 weeks old *Nbg4p* mice. Oxygen consumption rates (OCR) were shown for each time point of basal conditions and after the injection of inhibitors of the electron transport chain (A). Basal respiration, proton leak, maximal respiration, non-mitochondrial respiration, ATP-production, coupling efficiency and spare respiratory capacity were calculated after normalization to the total protein concentration of 5 independent experiments (B). Gene expression analysis of 6-9 liver samples from 6 weeks old *Nbg4p* mice was performed by qPCR and normalized to *Scp2* (C). Data are shown as mean ± SEM and analysed by multiple Student's t-test with Welch correction. *$p < 0.05$.

Summarizing the metabolic characterization of RCS.NZO.129Ola-*Nbg4p* mice, the results indicate that both gWAT and the liver are highly affected by a disturbed lipid and glucose metabolism. Thereby, significantly impaired glucose uptake and increased hypertrophy in adipocytes as well as a decreased insulin inhibition of hepatic glucose production have shown to be main metabolic characteristics of Ola-allele carriers of *Nbg4p*. If these effects contribute to insulin resistance and the hyperglycemic phenotype remains to be discussed. The investigation of potential candidate genes for *Nbg4p* aim to clarify a potential link to the underlying mechanisms.

3.1.3 Identification of genetic determinants for *Nbg4p*

To investigate the underlying genetic determinants of *Nbg4p*, a combination of different approaches were chosen. Firstly, haplotype mapping based on the SNP information of the different genomes from parental Ola and NZO mice was performed for the *in silico* identification of Ola-polymorphic regions within the *Nbg4p* locus. Afterwards, gene expression profiling of the affected tissues from juvenile RCS.NZO.129Ola-*Nbg4p* mice were analysed to estimate the real state (*ex vivo*) of gene transcription for both genotypes. In the end, matching data were used for the identification of potential candidate genes that were chosen for further functional analysis.

3.1.3.1 Haplotype mapping of the diabetogenic *Nbg4p* locus

By the investigation of common SNP databases a haplomap was generated (2.6.1) to identify genes within the *Nbg4p* locus that were polymorph between Ola and NZO (Fig. 20). With the dissection of the *Nbg4p* locus into regions that are either identical by descent (IBD) or polymorph between the strains (non-IBD), the frequency of accumulating polymorphic SNPs was determined within 250 kbp intervals. In this context, regions exceeding a threshold of 200 SNPs/window were considered to be specifically polymorph for the Ola mouse strain (using C57BL/6J as a reference strain). Thus, the haplotype analysis revealed 84 Ola-specific SNPs that were mapped within the polymorphic regions of *Nbg4p*. This number accounts to 36.8 % of the total SNPs within the analysed fragment. Interestingly, the identified polymorphic SNPs were accumulating rather at regions before the highest peak position (58.07 Mb) of the *Nbg4p* QTL (Fig. 20).
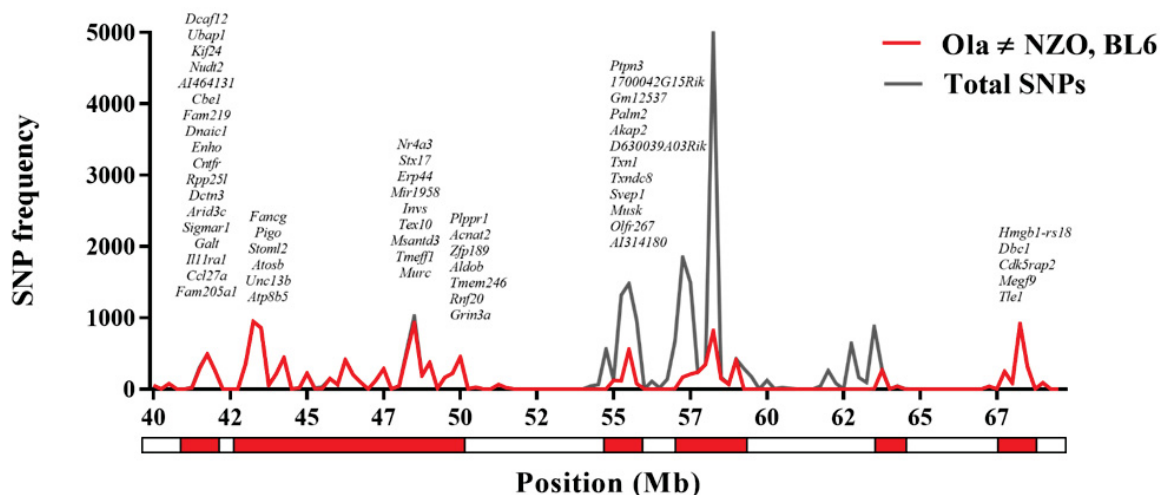
Fig. 20: Haplotype mapping of Ola-polymorphic genes within Nbg4p. Total (grey line) and polymorphic (red line) SNPs (Ola ≠ NZO, BL6) were mapped for Nbg4p (33-70 Mb) by investigating cross databases using C57BL/6J (BL6) as reference strain (GRCm39 assembly). Mb= mega base pairs.

3.1.3.2 Tissue-specific gene expression profiling in RCS.NZO.129Ola-*Nbg4p* mice

To detect gene expression differences that may explain the blood glucose QTL in *Nbg4p* mice, a microarray analysis was conducted (2.6.2). For this purpose, genome-wide gene expression was analysed in gWAT and liver samples from Ola- and NZO-allele carriers of 6 weeks old RCS.NZO.129Ola-*Nbg4p* mice. In the gWAT, 188 out of 40,148 analysed genes were significantly different expressed, whereof 27 genes were upregulated in Ola- and 162 in NZO-allele carriers of *Nbg4p* mice (Fig. 21A, Suppl. Fig. 5). Compared to the adipose tissue, a markedly lower amount of differentially regulated genes was found in the liver. Of 58 identified genes, 25 were upregulated in Ola- and 33 in NZO-allele carriers (Fig. 21B, Suppl. Fig. 6). As expected, most of these genes were located on chromosome 4 but also genes affecting other chromosomal regions were differentially regulated between the two genotypes.
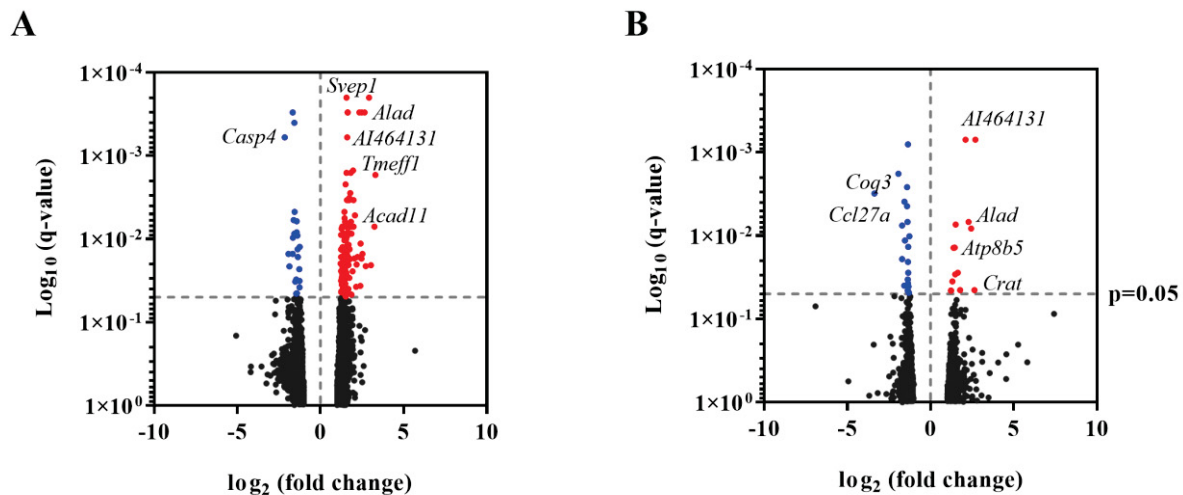
Fig. 21: Differentially expressed genes in gWAT and liver of *Nbg4p* mice. Volcano plot of differentially expressed genes analyzed by Affymetrix chip microarray from gWAT (A) and livers (B) of 6 weeks old *Nbg4p* mice. Dots represent fold change values of the analysed genes. Red indicates upregulation in NZO- and blue in Ola-allele carriers, whereas black dots represent genes without genotype-specific expression differences (defined by q-value). Differentially expressed genes located on chromosome 4 were advertised.

To get a first overview of the most likely pathways that are differentially regulated in gWAT and livers of *Nbg4p* mice, the mouse database of the Consensus PathDB (CPDB) was used. Therefore, expression ratios from significantly different genes of the microarray data were used to perform a gene enrichment analysis. The resulted interaction network showed prediction of main changes in adipocyte and hepatic fatty acid metabolism which were estimated for up to 50 % in the gWAT and about 17 % in the liver of *Nbg4p* mice. Furthermore, minor differences were predicted to affect cytokine response, abnormal carnitine and sphingolipid metabolic processes, as well as minor differences in pigment biosynthesis (Fig. 22A+B). Validation of several key regulators of the predicted pathways by qPCR revealed major changes in the regulation of lipolysis due to the substantial increase in *caspase 4* (*Casp4*) gene expression within the adipose tissue of *Nbg4p*$^{O/O}$ mice. Furthermore, different pathways of the hepatic fatty acid (FA) metabolism were shown to be differentially regulated in *Nbg4p* mice. Representative for the calmodulin binding, *Invs* was found to be downngulated in Ola-compared to NZO-allele carriers (Fig. 24B). Similar expression pattern were found for *Crat* and *Acox1* as representatives for the carnitin metabolic process. Alterations of the sphingolipid metabolism could be validated by the genes *Plpp2* and *9130409I23Rik,* whereby the latter revealed the strongest expression difference in the liver with a converse expression pattern showing significantly higher values for Ola- compared to NZO-allele carriers (Fig. 22C).

A

Pathway	Set size	Candidates	FDR (q-value)
BCAA metabolism	20	9 (45.0 %)	$3.72 \times E^{-10}$
CoA metabolism	6	3 (50.0 %)	0.000159
Regulation of lipolysis	56	7 (12.5 %)	0.000766
Fat cell differentiation	236	11 (4.7 %)	0.00731
FGFR signalling	9	2 (22.0 %)	0.0252
Cytokine response	292	3 (1.0 %)	0.0492

B

Pathway	Set size	Candidates	FDR (q-value)
Calmodulin binding	190	2 (1.1 %)	0.0072
Carnitine metabolism	13	2 (16.7 %)	0.0286
Sphingolipid metabolism	50	2 (4.0 %)	0.0452
Cytokine response	292	3 (1.0 %)	0.046
Pigment biosynthesis	52	2 (3.8 %)	0.168

C
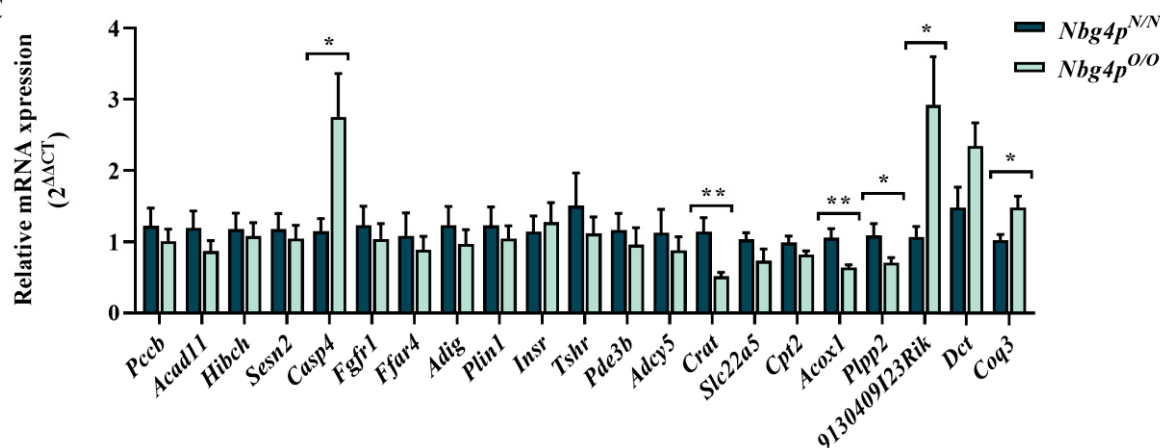
Fig. 22: *In silico* pathway analysis using CPDB. Pathway analysis using the Consensus PathDB (CPDB) mouse network revealed the most affected canonical pathways for the gWAT (A) and the liver (B) of Nbg4p mice. (C) Validation of genes that are annotated to the respective pathways was conducted by qPCR analysis. Data are shown as mean ± SEM (n = 7-9) and analysed using two-tailed, unpaired Student's t-test. *p<0.05 and **p<0.01.

Assuming that *Nbg4p* mice should only differ in the genomic interval of the proximal *Nbg4* locus, genes were selected mapping within 40 to 77 Mb of the susceptibility locus on chromosome 4. A summary of the differentially expressed genes between the genotypes is given in Figure 23. In total 19 genes were found in gWAT, whereof one was upregulated in Ola- and 18 in NZO-allele carriers. In the liver 3 out of 11 genes showed an increased expression in Ola- and 8 in NZO-allele carriers (Fig. 23).

In order to validate the results of the microarray data, expression levels of the identified genes were further analysed by qPCR. In the gWAT, two out of 19 genes (*Alad* and *Hdhd3*) have been

validated to be significantly differentially expressed with lower expression levels in Ola-
compared to NZO-allele carriers of *Nbg4p* mice. (Fig. 24A).

Gene-ID	Mb-Pos.	Fold change	
		gWAT	liver
Aqp7	41.03	1.49*	1.05
AI464131	41.50	1.82***	2.10***
Fam219a	41.52	1.42***	1.04
Cntfr	41.66	1.48***	1.03
Dctn3	41.71	1.62***	1.02
Ccl27a	41.77	1.17	1.38***
Fam205a4	41.97	1.29**	1.40*
Fam205a3	42.32	1.27*	1.20
Fam205a2	42.52	1.27*	1.96***
Ccl19	42.63	1.46**	1.30
Ccl27b	42.65	1.07	1.37**
Il11ra2	42.66	1.03	1.23**
Fam205a1	42.85	1.43*	1.48**
Unc13b	43.06	1.19	1.37*
Atp8b5	43.27	1.03	1.39**
Spaar	43.73	1.63**	1.05
Gne	44.03	1.48**	1.13
Gabbr2	46.66	1.32*	1.38
Invs	48.28	1.21	2.03***
Tmeff1	48.59	1.96***	1.08
Svep1	58.04	1.56***	1.05
AI314180	58.80	1.24**	1.08
Hdhd3	62.50	1.33**	1.19
Alad	62.51	2.66***	2.28***

Fig. 23: Differentially expressed genes in liver and gWAT of *Nbg4p* mice. Fold change of significantly differentially expressed genes within the 37 Mb of *Nbg4p* analysed in gWAT and liver samples of 6 weeks old mice. Red mark indicates an upregulation of the gene in 129- and blue for an upregulation in NZO-allele carriers. Data are shown as the mean fold change of 5 to 6 animals per genotype. Statistical testing is shown by the FDR-value with *q<0.05; **q<0.01 and ***q<0.001

From the liver tissue, 6 out of 11 genes (*AI464131, Il11ra2, Unc13b, Atp8b5, Invs and Alad*) were validated. Thereby, expression of *AI464131* and *Unc13b* showed to be upregulated in Ola-allele carriers, whereas for *Il11ra2, Atp8b5, Invs* and *Alad* a contrary expression pattern could be observed (Fig. 24B).
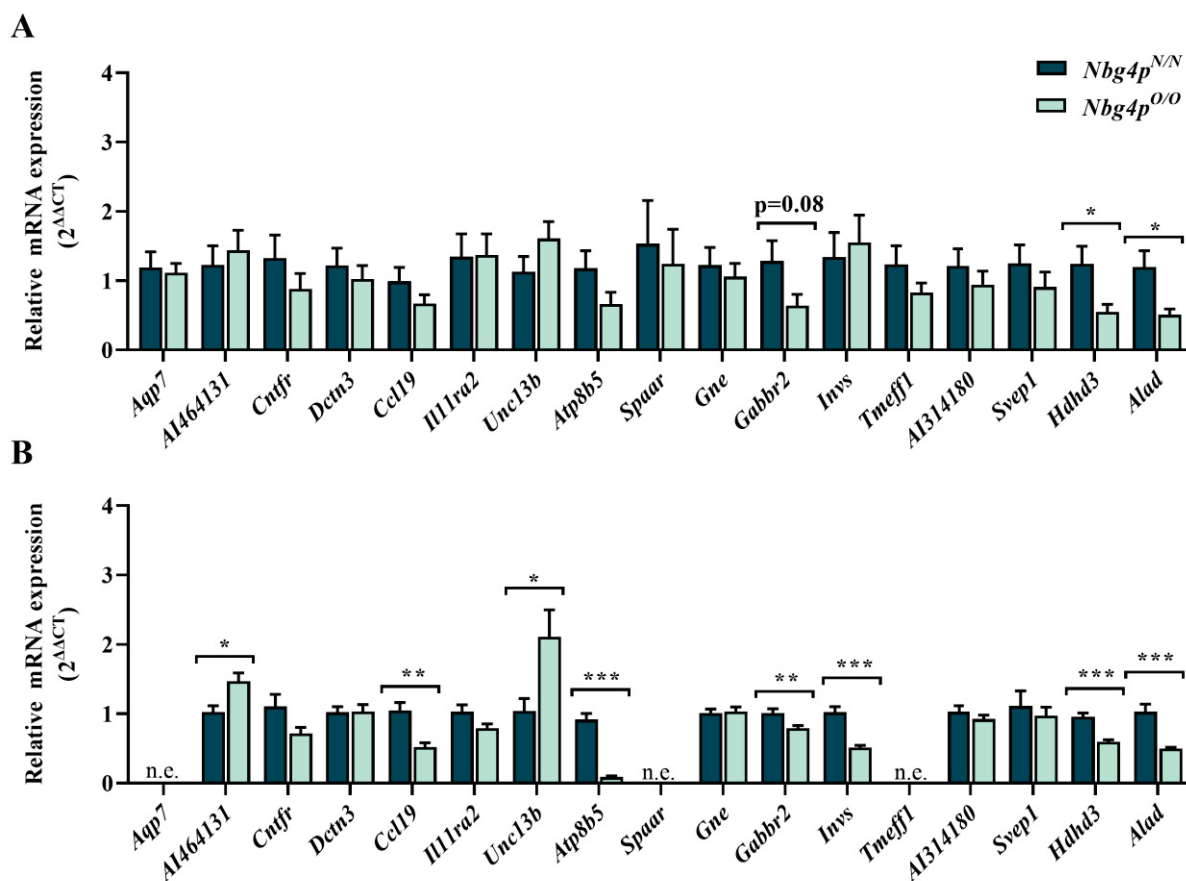
Fig. 24: mRNA expression levels of genes identified in the microarray analysis. Adipose (A) and hepatic (B) gene expression of candidate genes detected in the microarray analysis were determined by qRT-PCR and normalized to 18S (gWAT) or Tbp (liver), respectively. Data are shown as mean ± SEM (n = 3-9) and analysed using unpaired, two-tailed Student's t-test. *p<0.05, **p<0.01 and ***p<0.001.

Since the critical region of *Nbg4p* spanning 37 Mb harbours in total 624 genes, the power of selected candidate genes was enhanced by combining both haplotype and gene expression analyses. Thus, genes that were significantly differentially expressed in the microarray and qPCR analysis, as well as part of the non-IBD region from haplotype mapping, were further designated as most likely candidates for *Nbg4p*. In this context, three liver-specific regulating genes (*Unc13b, Atp8b5* and *Invs*) were identified, as well as two genes (*Alad* and *Al464131),* that were defined as the most likely candidate genes across both tissues (Tab. 24).

Tab. 24: Combined analysis for the identification of genetic modifier of *Nbg4p*. n.s. = not specified, n.e. = no expression detected. Significant differences were marked in bold letters as indicated by the q-(microarray) or p-value (qPCR).

Gene-ID	Mb-Pos.	Microarray (Fold change)		qPCR (p-value)		Haplotype (non-IBD)
		gWAT	liver	gWAT	liver	
Aqp7	41.03	**1.49***	1.05	0.79	n.e.	No
AI464131	41.50	**1.82***	**2.10***	0.61	**0.01***	Yes
Fam219a	41.52	**1.42***	1.04	0.56	0.40	Yes
Cntfr	41.66	**1.48***	1.03	0.29	0.07	Yes
Dctn3	41.71	**1.62***	1.02	0.55	0.93	Yes
Ccl27a	41.77	1.17	**1.38**	n.s.	n.s.	Yes
Fam205a4	41.97	**1.29***	**1.40***	n.s.	n.s.	n.s.
Ccl27b	42.15	1.17	**1.38**	n.s.	n.s.	n.s.
Fam205a3	42.32	**1.27***	1.20	n.s.	n.s.	n.s.
Fam205a2	42.52	**1.27***	**1.20**	n.s.	n.s.	n.s.
Ccl19	42.63	**1.46***	1.30	0.20	**0.002***	n.s.
Il11ra2	42.66	1.03	**1.23***	0.96	0.52	n.s.
Fam205a1	42.85	**1.43***	**1.48***	n.s.	n.s.	Yes
Unc13b	43.06	1.19	**1.37***	0.18	**0.05***	Yes
Atp8b5	43.27	1.03	**1.39***	n.e.	**0.00001***	Yes
Spaar	43.73	**1.63***	1.05	0.73	n.e.	Yes
Gne	44.03	**1.48***	1.13	0.60	0.76	Yes
Gabbr2	46.66	**1.32***	1.38	0.08	**0.006***	No
Invs	48.28	1.21	**2.03***	0.69	**0.0001***	Yes
Tmeff1	48.59	**1.96***	1.08	0.21	n.e.	Yes
Svep1	58.04	**1.56***	1.05	0.24	0.59	Yes
AI314180	58.80	**1.24***	1.08	0.34	0.36	Yes
Hdhd3	62.50	**1.33***	1.19	**0.03***	**0.0001***	No
Alad	62.51	**2.66***	**2.28***	**0.02***	**0.00005***	No

3.2 Functional investigation of candidate genes for T2D

Since T2D is a polygenic disease, the collective diabetes cross project aimed the identification of novel susceptibility genes from different strains to increase the genomic background, and with this the probability to discover crucial regulators of the metabolic disease. Through deep metabolic characterization and the combination of different mouse genetic approaches, novel candidate genes have been identified within this crossbreeding project. The following sections aimed to give new insights of selected candidate genes on two genetically different blood glucose-related QTL. In this context, the potential causal genes *Alad* and *Nudt19* were selected for functional *in vitro* analyses to elucidate a contribution on *Nbg4p* and *Nbg7,* respectively.

3.2.1 *Alad* as a candidate gene for *Nbg4p* linked to adipocyte glucose metabolism

The *δ-aminolevulinate dehydratase* (*Alad*) was selected as novel candidate gene after combined transcriptome and gene expression analysis of the RCS.NZO.129Ola-*Nbg4p* mouse line (3.1.3.2). In 6 weeks old mice, *Alad* was shown to be significantly lower expressed in adipose and liver tissues of homozygous Ola-allele carriers of *Nbg4p* (Fig. 24). Moreover, *Alad* mRNA expression showed significant correlation with fasting blood glucose levels (Suppl. Fig. 7). Additionally, expression QTL (eQTL) analysis from previous studies reveal an eQTL for *Alad* in the gWAT of the N2(NZOxOla) backcross population, which was overlapping with the proximal peak region of *Nbg4* [98]. These results strongly point to a diabetogenic effect of the gene in the gWAT of Ola-allele carriers of *Nbg4p*. Therefore, 3T3-L1 adipocytes (2.1.3) were used to investigate a potential impact of *Alad* gene expression on adipocyte glucose metabolism *in vitro*.

Prior experiments have shown that *Alad* is moderately expressed in 3T3-L1 fibroblasts as well as in differentiated adipocytes. However, overexpression of this gene inhibited differentiation of fibroblasts and therefore hindered the metabolic analysis in these cells (data not shown). As a consequence, a stable *Alad* knockdown (KD) cell line of 3T3-L1 fibroblasts was generated using a retroviral transduction system (2.2.2.6). In these cells, *Alad* mRNA expression was reduced by 80 % when compared to control cells (NC), which were transduced only with an empty vector (Fig. 25A). Following differentiation to mature adipocytes, an *in vitro* glucose uptake assay was performed to investigate possible effects of this gene on the glucose metabolism in adipocytes (2.2.2.2). Briefly, cells were starved for 24 hours and incubated with DMEM supplemented with or without 100 nM insulin or 50 mM cytochalasin B. Uptake of 2-Deoxy-D-glucose was measured by a fluorescent signal that is proportional to the concentration of 2-deoxyglucose-6-phosphate (2DG6P). The results show that knockdown of *Alad* mRNA

expression led to a significant decrease in basal glucose uptake (*Alad* KD: 42.81 ± 12.93 % vs. NC: 100 ± 17.31 %, p=0.03). Insulin supplementation significantly increased the rate of glucose uptake in both *Alad* KD and NC cells, however, no differences were observed between the two conditions (Fig. 25B). To further investigate the differentiation status of *Alad* KD cells, mRNA expression of several genetic marker of the fat cell differentiation process were analysed (2.4.6). Except of a significant increase in *Fasn* mRNA expression in *Alad* KD compared to NC cells, no further differences were detected in the context of adipogenesis (Fig. 25C).
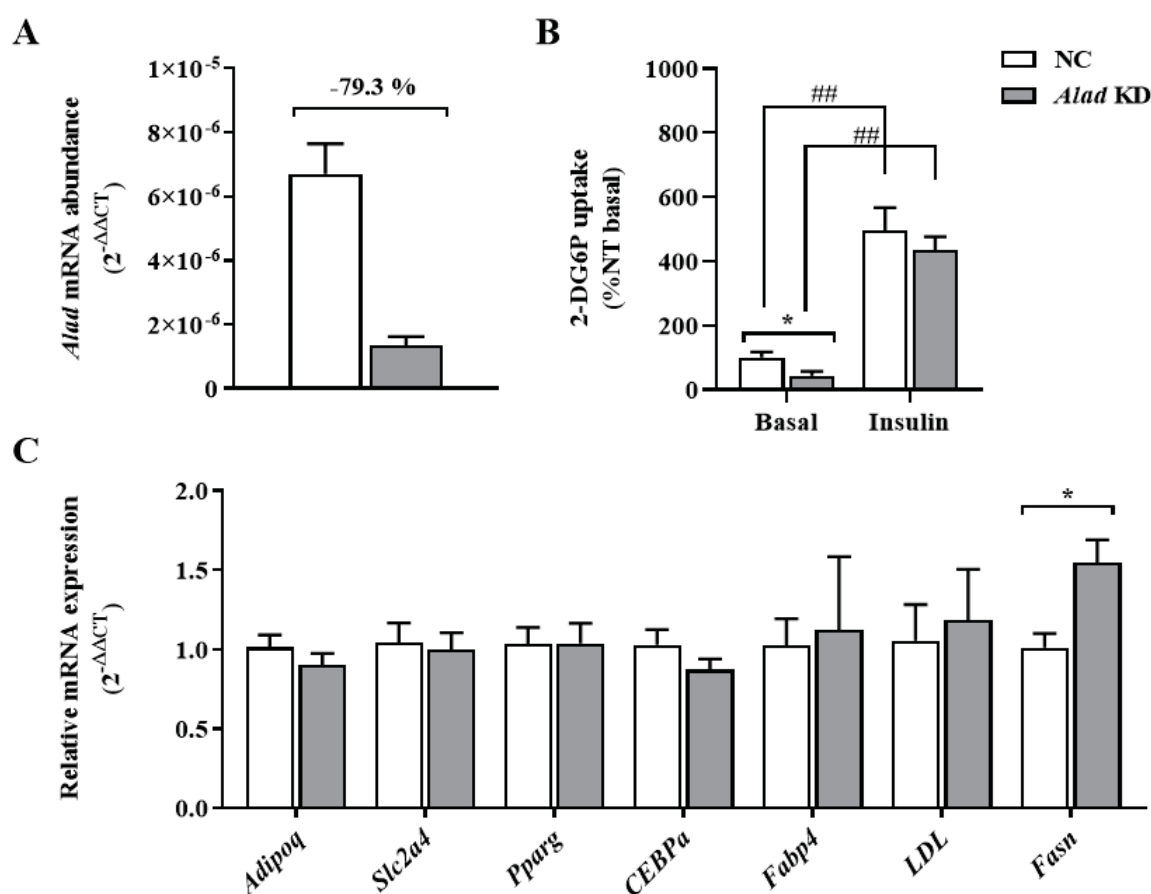
Fig. 25: Differentiation and glucose uptake after *Alad* KD in 3T3-L1 cells. Generation of 3T3-L1 cells with stable *Alad* knockdown was conducted by retroviral transduction. Cells were differentiated into mature adipocytes and mRNA expression of *Alad* (A) and further adipogenic marker (C) were analysed by qPCR. Uptake of 2-deoxyglucose (B) was measured in accordance with the respective fluorescent signals. Data represent mean values ± SEM from 6-7 independent experiments. Student's t-test, two-tailed, unpaired (A+C) and 2- way-ANOVA with Bonferroni's multiple comparisons test (B), *p< 0.05 for NC vs. KD; ##p<0.01 for basal vs. insulin stimulated condition.

Glucose and lipid metabolism strongly depend on intracellular energy supply provided by mitochondrial processes like oxidative phosphorylation and beta-oxidation of fatty acids. To investigate a potential impact of mitochondrial function on the observed differences on endogenous glucose uptake in *Alad* KD cells, extracellular flux analysis was used (2.2.2.4). The real-time cell metabolic analysis showed that knockdown of *Alad* mRNA in mature 3T3-L1 adipocytes led to increased levels of basal mitochondrial respiration (10 %) when compared to NC cells (Fig. 26B). After the injection with oligomycin, *Alad* KD cells displayed an elevated proton leakage that was approx. 18 % higher compared to NC cells, however ATP-production was unchanged. In response to the uncoupling agent FCCP, maximal respiration was unchanged and also non-mitochondrial respiration did not show any differences when comparing *Alad* KD with NC cells (Fig. 26E-F). A possible contribution of the observed changes in mitochondrial function on adipose glucose uptake still need to be discussed.
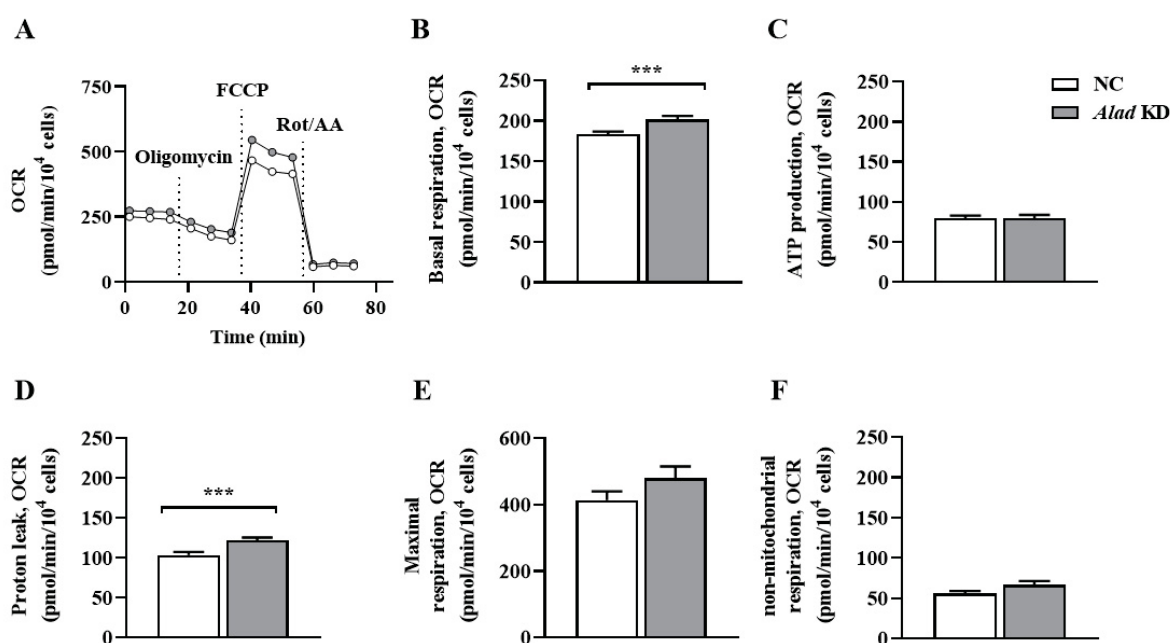
Fig. 26: Effects of *Alad* knockdown on mitochondrial function in 3T3-L1 adipocytes. Quantification of the oxygen consumption rates of basal respiration (B), ATP production (C), proton leak (D), maximal (E) and non-mitochondrial respiration (F) in *Alad* KD versus control (NC) cells. Data represent mean values ± SEM from 3 independent experiments. Student's t-test, two-tailed, unpaired, ***p=0.001.

3.2.2 *Nudt19* as a candidate gene for *Nbg7* regulating hepatic lipid metabolism

The *nucleoside diphosphate linked moiety X-type motif 19* (*Nudt19*) was originally identified within the collective diabetes cross project from a crossbreeding of NZO with lean and T2D-resistant C3H mice. Haplotype and gene expression analysis led to the selection of *Nudt19* as a potential candidate gene that may contribute to the blood glucose-related QTL on chromosome 7 (*Nbg7*) identified in this mouse cross. Gene expression of *Nudt19* was significantly different in the liver tissues, whereby NZO-allele carriers of *Nbg7* showed lower mRNA levels when compared to C3H-allele carriers [111]. Further analysis of fatty acid beta-oxidation led to the hypothesis, that *Nudt19* might regulate hepatic energy metabolism which contributes to the phenotypic effect of *Nbg7*.

To encourage a potential impact of *Nudt19* in hepatic energy metabolism, transcriptome analysis of mouse livers from different NZO mouse crossbreedings was performed. The used data originate from the collective mouse cross project, from mouse backcross populations which carry a highly diverse genetic background differing in their T2D susceptibilities. The results from microarray analysis were used for further investigation of genes within the lipid metabolic pathway. In this context, *Nudt19* was identified as one of the most significantly differentially expressed genes between the strains as annotated in the KEGG lipid metabolism pathway. Thereby, lowest expression rates were observed for NZO-allele carriers which strongly pointed to a NZO-specific regulation of *Nudt19* on hepatic lipid metabolism (Fig. 27A+B). Interestingly, comparison of liver triglyceride contents showed significantly increased amounts of hepatic triglycerides in NZO compared to C3H and Ola livers (Fig. 27B).
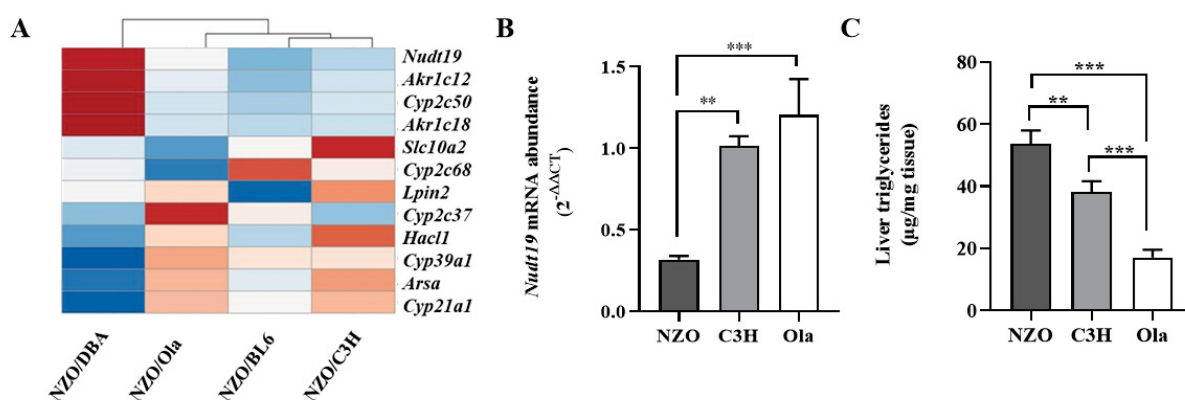
Fig. 27: *Nudt19* gene expression is linked to hepatic lipid metabolism. Heatmap of significantly differentially expressed genes from mouse liver microarray studies that were annotated in the KEGG lipid metabolism database identified *Nudt19* as most likely candidate gene (A). Data are displayed as the ratio of NZO-specific gene expression compared to control strains. Shades of red means a higher expression level compared to other conditions in the same row. *Nudt19* mRNA abundance relative to *Tbp* (B) and hepatic triglyceride contents (C) of NZO, C3H and Ola mice. Data represent mean values ± SEM from 7-8 mice per genotype and analysed by one-way ANOVA, **p < 0.01 and ***p < 0.001. Modified from Görigk *et. al*., 2022.

In order to elucidate whether *Nudt19* influences hepatic lipid metabolism, siRNA-mediated knockdown (KD) was conducted (2.2.2.5) in the murine hepatoma cell line Hepa 1-6. Following the KD, extracellular flux analysis was performed (2.2.2.4) to determine the impact of *Nudt19* KD on mitochondrial function and fatty acid oxidation. The results show that a reduction of already 67 % of the *Nudt19* mRNA expression improved the metabolic profile of the cells when comparing to control cells transfected with non-target (NC) siRNA as indicated by the oxygen consumption rate (OCR) of the respective cells (Fig. 28A+B). Furthermore, it was observed that a detailed analysis of the mitochondrial function resulted in increased mitochondrial respiration rates already at basal states (*Nudt19* KD: 691.09 ± 16.54 OCR vs. NC: 529.66 ± 22.33 OCR, $p<0.001$). Injection of oligomycin showed increased ATP-production rates (*Nudt19* KD: 386.75 ± 29.33 OCR vs. NT: 272.88 ± 31.82 OCR, $p=0.01$), as well as a higher proton leak (*Nudt19* KD: 147.68 ± 5.78 OCR vs. NT: 120.87 ± 3.87 OCR, $p<0.001$) in *Nudt19* KD versus NT cells (Fig. 28C-E).

To elucidated a previously suggested function of *Nudt19* in fatty acid oxidation [111, 112], one aim was to specify these findings by evaluating the oxidation of exogenous palmitate and oleate in *Nudt19* knockdown vs. control cells. Similar to the previous findings, *Nudt19* knockdown in Hepa 1-6 cells enhanced the oxidation of palmitate as indicated by the significant increase of the OCR signal for basal respiration (*Nudt19* KD: 106.18 ± 4.00 OCR vs. NT: 82.90 ± 3.90 OCR, $p<0.001$). Likewise, also increases in the oxidation of exogenous oleate were observed (*Nudt19* KD: 96.27 ± 2.39 OCR vs. NT: 82.79 ± 3.09 OCR, $p=0.001$) (Fig. 28F). By inducing energetic stress due to the injection of FCCP, the maximal capacity of fatty acid utilization was determined. Thereby, respiration rates were observed which were twice as high as at basal states for both, palmitate (*Nudt19* KD: 208.29 ± 9.57 OCR vs. NT: 166.63 ± 8.33 OCR, $p=0.002$) and oleate (*Nudt19* KD: 220.81 ± 12.60 OCR vs. NT: 160.98 ± 10.65 OCR, $p<0.001$) (Fig. 28G). All together, these findings show that knockdown of *Nudt19* mRNA expression in liver cells lead to a more energetic profile by increases in mitochondrial function and fatty acid oxidation.
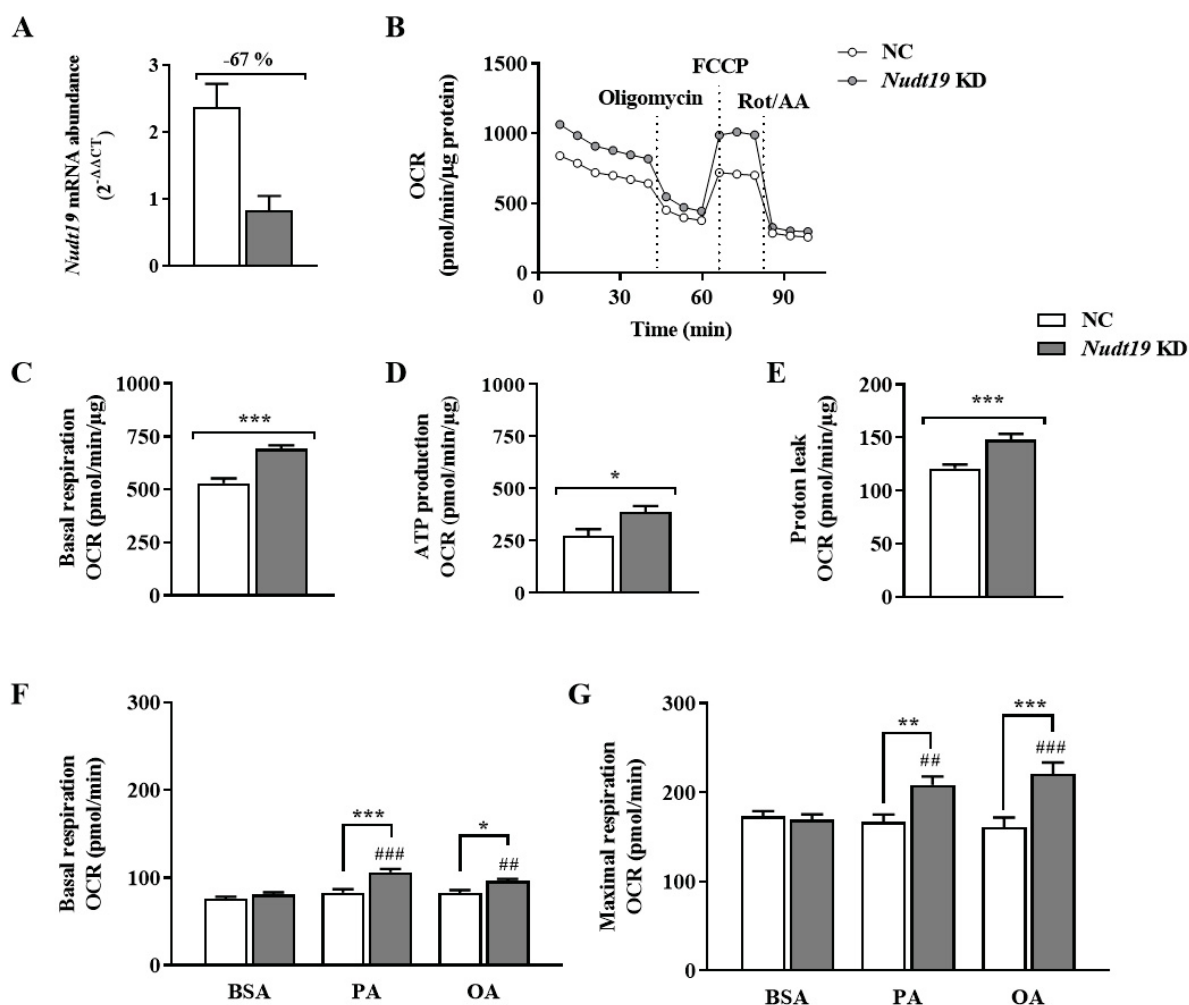
Fig. 28: Mitochondrial function and fatty acid oxidation in *Nudt19* KD cells. siRNA-mediated knockdown of *Nudt19* in Hepa 1-6 cells was confirmed by qPCR analysis and normalisation to *Tbp* (A). Mitochondrial function was analysed by a mitostress test of untreated cells (C-E) or after incubation with either BSA, palmitate (PA) or oleate (OA) (F-G). Data are shown as mean ± SEM of 7 independent experiments. Student's t-test, two-tailed, unpaired (*p=0.05, **p=0.01, ***p=0.001) and one-way ANOVA with Sidak's multiple comparison test (##p=0.01, ###p=0.001). Modified from Görigk *et al.,* 2022.

After the confirmation of a potential impact of *Nudt19* KD cells on mitochondrial function, further investigation was performed to clarify if a reduced *Nudt19* mRNA expression in the hepatoma cells affects the gene and protein abundance of specific lipid metabolism determinants. For this purpose, the mRNA-expression of several markers (2.1.9) of the mitochondrial and peroxisomal fatty acid oxidation pathway were quantified by qPCR analysis (2.4.6). Although, *Nudt19* mRNA expression was reduced by 67 % after siRNA-mediated knockdown (*Nudt19* KD: 0.351 ± 0.033 $2^{-\Delta\Delta CT}$ vs. NT: 1.030 ± 0.091 $2^{-\Delta\Delta CT}$, p=0.003), minor differences were observed in the analysed genes. Thereby, only *Pdk4* mRNA expression was conspicuously differentially expressed with a 1.3-fold increase in *Nudt19* KD versus NT cells (*Nudt19* KD: 1.685 ± 0.117 $2^{-\Delta\Delta CT}$ vs. NT: 1.062 ± 0.135 $2^{-\Delta\Delta CT}$, p=0.03) (Fig. 29A). Further analysis revealed a significant negative correlation between *Nudt19* and *Pdk4* mRNA levels

($r^2=0.628$, $p=0.006$) (Fig. 29B), which was in line with the 26 % increase of PDK4 protein abundance in *Nudt19* KD cells (Fig. 29C).
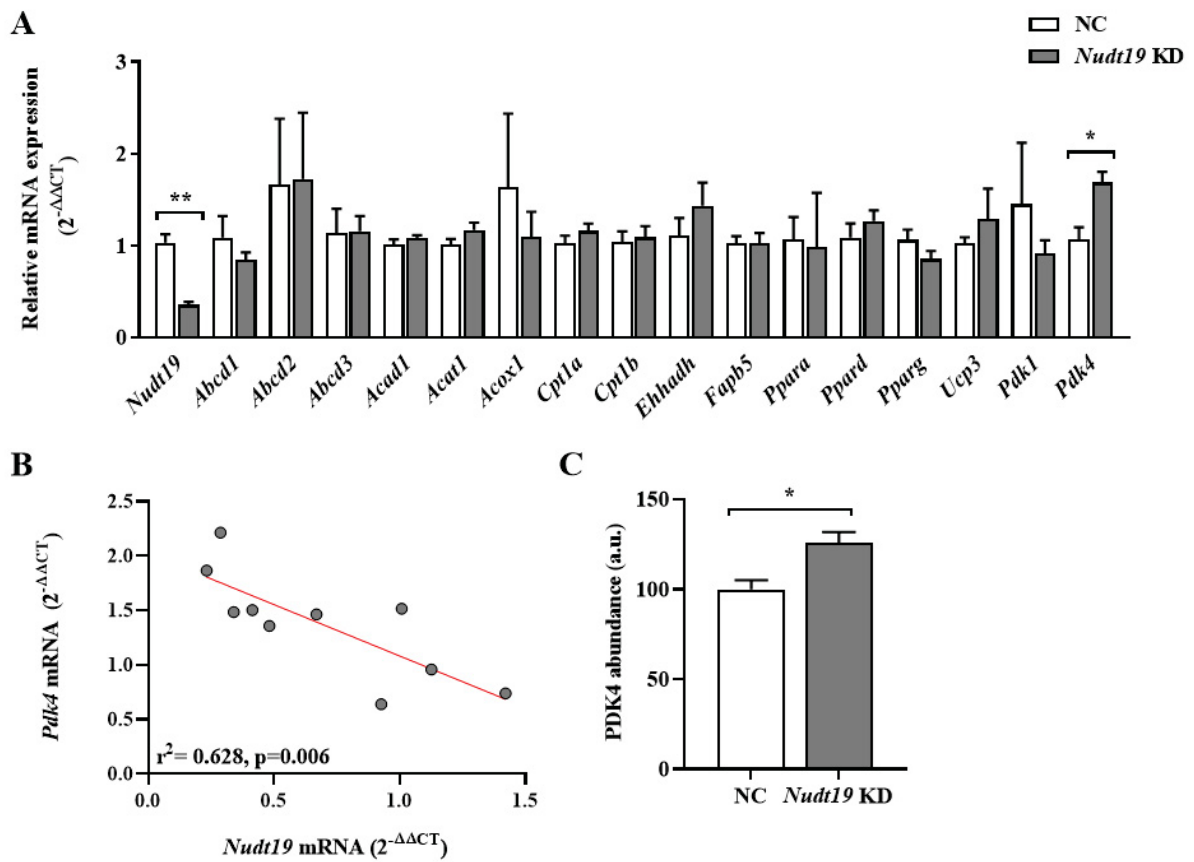
Fig. 29: Effect of *Nudt19* knockdown on the expression of lipid metabolism determinants. Expression levels of several mitochondrial and peroxisomal marker were analysed by qPCR in *Nudt19* KD versus NT cells and normalized for *Tbp* expression levels (A). Correlation analysis revealed significant differences between *Nudt19* and *Pdk4* mRNA expression (B). Quantification of PDK4 protein abundance and representative Western blots with normalization to GAPDH expression levels of respective cells validated the expression differences (C). Data are shown as mean ± SEM of 5-10 independent experiments. Student's t-test, two-tailed, unpaired, *p< 0.05 and **p<0.01. Modified from Görigk *et al*., 2022.

4. Discussion

In the past, research on the genetic landscape of type 2 diabetes (T2D) led to identification of about 190 genomic regions with association to different diabetes-related traits. However, only a minor fraction of causal gene variants have been determined and their heritability is believed to account only for a small proportion (10-30 %) [113, 114]. To further increase the understanding of gene-driven mechanisms of T2D pathogenesis, a novel crossbreeding approach was conducted with mouse strains that vary in their diabetes susceptibilities (1.5). For this purpose, the obese and T2D-prone NZO mouse strain was used as these mice develop characteristics of the human metabolic syndrome and therefore represents a suitable model for the examination of complex traits in humans. Previously, whole-genome linkage analysis from a crossbreeding of the NZO mouse strain with lean and T2D-resistant Ola mice led to the identification of a novel blood glucose-related QTL on chromosome 4 (NZO blood glucose QTL on chromosome 4; *Nbg4*) [95, 98]. In this study, a combination of different approaches was used to further characterize the identified *Nbg4* locus, aiming to identify novel genetic determinants for T2D. For this purpose, the critical region was narrowed down by the generation of different recombinant congenic strains (RCS) and potential disease genes of the critical fragment were filtered using haplotype and gene expression analyses.

4.1 Validation of the diabetogenic *Nbg4* QTL in RCS carrying a proximal sublocus

The *Nbg4* QTL is characterized by two different subloci linked to blood glucose levels, which showed the strongest association in the cross between NZO and Ola mice (LOD 5.8 and 7.1) [95, 98]. Interestingly, metabolic phenotyping of the N2(NZOxOla) population showed, that blood glucose levels were higher in mice carrying NZO/Ola heterozygous alleles for *Nbg4*. These results provided evidence for genetically inherited diabetogenic variants that derived from the lean and T2D-resistant Ola mouse strain, whose phenotypic outcome strongly depends on the genetic background. As already reported in other studies, the genetic background can be of high importance when investigating diabetes-related traits [94, 96]. Similar observations have been made for the *Nidd/SJL* QTL in a mouse cross of NZO with lean SJL mice where it was shown that the introgression of this locus onto the genome of different lean or obese mouse strains resulted into different diabetogenic effects. Although, heterozygous NZO/SJL-allele carriers of the *Nidd/SJL* locus showed a similar hyperglycaemic phenotype as seen in NZO/Ola mice for the *Nbg4* QTL, the disease progression was completely different. While NZO/SJL-allele carriers showed hypoinsulinemic features of manifested T2D that were accompanied by

a reduction in the body weight, NZO/Ola-allele carriers of the *Nbg4* locus showed rather hyperinsulinemic features with unaltered body weight development. Furthermore, it was shown that the *Nidd/SJL* locus harbours a SJL-unique variant of the *Zfp69* gene which was inactive (loss of function) at the obese background of NZO-alleles. This observation was further explained by alternative splicing which occurred only in diabetic mouse strains, highlighting a potential interaction with other genes from the background strain [96]. Therefore, it is very likely that the diabetogenic outcome of *Nbg4* on the obese NZO genetic background can be ascribed to (a) Ola-specific genetic variant(s).

In order to identify such diabetogenic variants within the *Nbg4* locus, the first strategy was to narrow down the *Nbg4* genomic region into a smaller fragment by the generation of congenic strains. Therefore, three different RCS lines were generated by introgressing either the whole *Nbg4* locus (33-134 Mb), the proximal peak region (33-77 Mb, *Nbg4p*) or the distal peak region (91-134 Mb, *Nbg4d*) of the Ola alleles into the NZO genetic background (Fig. 7). In contrast to the N2(NZOxOla) population, which shows a genetic distribution of approx. 75 % of NZO- and 25 % of Ola-alleles, these RCS mice are genetically identical except for the selected region on chromosome 4 and therefore allow to reliably validate the phenotypic effect of the *Nbg4* locus. Subsequent metabolic characterization of these mice on standard diet (SD) showed a similar phenotype as observed in the N2(NZOxOla) population in mice carrying the Ola-alleles of proximal *Nbg4*. These mice reached a difference in blood glucose levels which was the highest at week 17 of life, and was accompanied by significantly elevated fasted plasma insulin levels at week 21 (Fig. 8). These effects were also the strongest when comparing to the other RCS lines with mice carrying the distal or the consomic fragment of *Nbg4* (Suppl. Fig. 2, Suppl. Tab. 2-4). Hence, these findings led to the suggestion that the proximal fragment of *Nbg4* is most likely linked to the diabetogenic effect that was described by the N2(NZOxOla) population. Moreover, the metabolic outcome of the hyperglycaemic phenotype seems to be prevented in mice carrying Ola-alleles of the whole or the distal *Nbg4* locus, although the distal peak of the *Nbg4* QTL showed an even higher probability to be associated with blood glucose levels as indicated by the higher LOD-score. A possible explanation might be a compensatory effect of anti-diabetic genes within the distal region of *Nbg4* that contribute to the lean and T2D-resistant character of the Ola mouse strain. This would lead to the conclusion that only the proximal region of this locus harbours diabetes-related genes that are differentially regulated on an obese genetic background, similar to the effect described for the *Nidd/SJL* QTL mentioned above.

By the generation of an obese background with the introduction of a high-fat diet (HFD), further characterization of the diabetogenic effect in *Nbg4p* mice was performed. Similar to the results of RCS mice on SD (Suppl. Tab. 2), HFD-feeding showed early increases in blood glucose concentrations of mice carrying the Ola-alleles of *Nbg4p*. Thereby, HFD-fed mice reached the diabetic state with blood glucose concentrations over 300 mg/dL and a genotype-specific difference of up to 60.5 mg/dL. In contrast, SD-fed mice were not diabetic at any time point and only reached genotypic differences of 32 mg/dL. Together with the elevated T2D-prevalence in HFD-fed *Nbg4p*$^{O/O}$ mice, it was confirmed that the proximal fragment of *Nbg4* exerts diabetogenic features. Consequently, the critical region of the initial *Nbg4* QTL could be narrowed to a fragment of 37 Mb that most likely consists at least of one underlying diabetes-related gene. Although many QTL studies have identified diabetes-related traits on murine chromosome 4, linkage was mainly described for obesity and pancreatic ß-cell failure, whereby the critical genomic region was mostly located on the distal part of this locus [87, 93, 94, 96, 115]. Therefore, the possibility that already identified candidate genes, like *Zfp69* from the *Nidd/SJL* QTL, may influence the diabetogenic effect of *Nbg4p*, seems rather unlikely.

4.1.1 Increased T2D-prevalence in Ola-allele carriers of *Nbg4p* is independent from the body weight development

Obesity is known to be the main cause of peripheral insulin resistance and T2D and is mainly characterized by a higher body weight and fat mass [116, 117]. To investigate a possible link between the obesity status and T2D-prevalence in *Nbg4p* mice, body weight measurements as well as the analysis of the body composition were performed. The results showed, that mice carrying the Ola-alleles for *Nbg4p* displayed an increased body weight development starting at 7 weeks of life when fed a SD. However, these differences seem to rather occur due to increases in the lean mass which was shown to be significantly different between the genotypes at week 9 of life and persisted at least until week 15 where the last measurement of the body composition was performed. In contrast, fat mass development was not different between the genotypes (Suppl. Tab. 2). These results led to the suggestion that the phenotype observed in Ola-allele carriers of *Nbg4p,* compared to NZO-allele carriers, does not result from obesity, but is rather driven by an increased lean mass that is indicative for the lean phenotype of the Ola mouse strain.

When comparing SD- versus HFD-fed mice, the body weight increased for up to 10 grams in week 15 of life, which accounts for the increases in fat but not in lean mass. Except for a

genotype-specific increased fat accumulation in Ola-allele carriers at week 6 of life, body weight development was not different between the genotypes for any time point, concluding that HFD-feeding induced an obese phenotype in both Ola- and NZO-allele carriers of *Nbg4p* (Fig. 9, Suppl. Tab. 5). In line with the N2(NZOxOla) population also the other RCS strains, carrying either only the distal or the whole *Nbg4* locus of the Ola mouse strain, did not show any association to the body weight or its composition. Therefore, it is not very likely that the observed changes in SD-fed *Nbg4p* mice contribute to the diabetogenic effects of this locus. These results led to the hypothesis that the association of *Nbg4p* to blood glucose levels is more likely driven by at least one genetic modifier that is located on proximal *Nbg4* within the defined genomic region of 40-77 Mb.

4.1.2 Ola-alleles of *Nbg4p* associate with impaired glucose disposal and insulin sensitivity

Since the hyperglycemic phenotype of *Nbg4p* was shown to be independent from the body weight, further investigations of glucose metabolizing steps were assessed. As already shown by the indirect measurement of the Homeostasis Model Assessment for Insulin Resistance (HOMA-IR) in SD-fed *Nbg4p* mice, Ola-allele carriers seem to have a high probability that the increase in blood glucose and plasma insulin levels occur due to insulin resistance. The measure of HOMA-IR is widely used in the clinical indication of peripheral insulin resistance as it serves as good alternative to the much more complicated direct measurement by hyperinsulinemic euglycemic clamp. Although different studies show slightly variable ranges for the HOMA-IR, all agree that the higher the HOMA-IR, the more pronounced is the insulin resistant state. As Ola-allele carriers of the *Nbg4p* locus showed a HOMA-IR that was almost twice as high as shown for NZO allele carriers, indicating that the hyperglycaemic phenotype occurs due to restrictions of the peripheral tissues to properly respond to insulin. To investigate insulin action in whole-body glucose homeostasis, HFD-fed *Nbg4p* mice with different metabolic states of fasting and glucose incorporation were phenotyped at different time points (Fig. 7).

First, a fasting-refeeding experiment was performed at week 11 of life which was based on the natural feeding behaviour. Interestingly, 16 hours of fasting did not show any genotype-specific differences in blood glucose or plasma insulin levels. However, a subsequent period of 2 hours with free access to food *ad libitum* resulted into a significant increase in blood glucose levels of Ola-allele carriers although plasma insulin levels remained unchanged when comparing to NZO-allele carriers of *Nbg4p* (Fig. 11). These differences can be explained either by the feeding

behaviour, characterized by different amounts of food intake, or by decreased insulin secretion from pancreatic islets. Since, plasma insulin levels were at the same level for both genotypes, further investigation is needed to identify the cause of the observed blood glucose differences. Although body weight measurements before and after the feeding period did not show any changes between the genotypes, a possible difference in food intake cannot be excluded. To monitor changes in the feeding behaviour, there are much better methods available like manual or automated weighing of the food before and after a certain time period. A possible impact of insulin-secreting islets on the difference of BG levels will be discussed at a later time point within this work.

As it is most likely that $Nbg4p^{O/O}$ mice develop hyperglycaemia due to an impaired insulin action on peripheral tissues, further responses after the administration of glucose or insulin on glucose homeostasis were monitored. Similar to the effect seen in 13 weeks old mice on SD, 6 weeks old $Nbg4p^{O/O}$ mice fed a HFD showed normal glucose tolerance although plasma insulin levels were significantly increased after glucose injection (Fig. 12, Suppl. Fig.1). In contrast, measurements at a later time point showed decreases in the glucose tolerance of Ola-allele carriers combined with unaltered plasma insulin concentrations, suggesting that young animals, different from adult animals, may still have the capacity to compensate for the high glucose concentrations.

In this study, it has been shown that $Nbg4p^{O/O}$ mice displayed an insulin resistant phenotype around the age of 11 weeks, right after reaching a state of severe diabetes where blood glucose levels stayed above the diabetic threshold of 300 mg/dL. However, long before reaching a diabetic state, young mice showed elevated plasma insulin levels to maintain glucose homeostasis. With these results it becomes evident that the Ola allele of $Nbg4p$ may harbour genetic determinants for insulin sensitivity, whereby the phenotypic effect seem to be essentially influenced by the genetic background. The fact that a different phenotypic outcome of a gene can strongly depend on the genetic background, was already reported by many studies [68, 96, 118, 119]. Regarding diabetes-related genes, the first researchers that recognized such an effect were Coleman and Hummel who described a severe hyperglycaemic phenotype with β-cell failure triggered by a mutation of the leptin gene that appeared in C57BL/KsJ but not in C57BL/6J mice. The high probability of gene interactions across the whole genome shows an increasing importance since also recent studies regularly report the different impacts of the genetic background on diabetogenic genes, such as the above mentioned effect of the $Zfp69$ gene. To detect the underlying mechanisms causing hyperglycaemia and insulin resistance in $Nbg4p$ mice, deep metabolic characterization and functional *ex vivo* examination of the insulin-

responsive cells from pancreatic islets, skeletal muscle, adipose tissue and liver were performed.

4.1.3 *Nbg4p* represents a risk allele causing early-onset insulin resistance in gWAT

Since the maintenance of glucose homeostasis is tightly regulated by insulin-secreting and insulin-responsive tissues, metabolic investigation of pancreatic beta-cells, skeletal muscle, adipose tissue and the liver were performed. Therefore, juvenile *Nbg4p* mice at an age of 6 weeks, showing only a mild hyperglycaemia, were selected to avoid the contribution of potential secondary metabolic changes. Chronic hyperglycemia and the accompanied insulin resistant state that occurs during the manifestation of severe diabetes are well known factors contributing to the dysregulation of insulin synthesis and secretion from pancreatic beta-cells [120, 121]. It has been shown that in the fed state, 6-weeks old *Nbg4p*$^{O/O}$ mice showed a mild hypoinsulinemic response to elevated blood glucose concentrations when comparing to NZO-allele carriers. In contrast, the fasted state was distinguished by elevated plasma insulin concentrations in Ola-allele carriers that were obviously needed to maintain a normoglycemic state. Therefore, the first question addressed the proper regulation of insulin secretion from pancreatic beta-cells at the state of different glucose concentrations. In general, insulin secretion from isolated primary islets of Langerhans was significantly increased after the stimulation with high glucose concentrations for both genotypes. However, since there were no genotype-specific differences, a potential contribution of the insulin secreting beta-cells to the phenotype from *Nbg4p*$^{O/O}$ mice seems rather unlikely. Nevertheless, it has to be taken into account that this experiment cannot reflect the real state *in vivo* as the signals from peripheral insulin-resistant tissues are non-existent in a petri dish. The investigation of isolated islets that are disconnected from the cellular environment of other endocrine cells as well as from the vasculature is not only limited by the absent supply of other hormones, cytokines and oxygen but also by technical issues and the normalization process [122]. A more precisely method to determined insulin secretion is represented by the hyperglycaemic clamp that allows the *in vivo* investigation also of severely diabetic individuals. However, both methods, *in vivo* and *ex vivo* GSIS, cannot determined the maturity of synthetized insulin as well as the overall capacity of insulin secretion over long time periods. Therefore, it might be interesting to look further into proinsulin and C-peptide concentrations since plasmatic insulin has a half-time of only 3-5 minutes and therefore also might not reflect the real state of the actual amount of released insulin [123, 124].

Assuming that the cause of impaired glycaemia in $Nbg4p^{O/O}$ mice does not result from differences in the overall amount of secreted insulin, the next question addressed the insulin sensitivity of peripheral tissues such as skeletal muscle, adipose tissue and the liver. Although, the skeletal muscle represents the main tissue for glucose disposal, insulin-stimulated uptake of radiolabelled glucose was unchanged in isolated EDL and soleus muscles (Fig. 15A+B). Interestingly, isolated primary adipocytes from $Nbg4p^{O/O}$ mice showed a markedly reduced insulin-responsive glucose uptake which lead to the assumption that in $Nbg4p$ mice adipose tissue and not skeletal muscle insulin resistance may lead to whole-body glucose intolerance and hyperinsulinemia. Similar effects have been reported in the past, where HFD-induced insulin resistance was shown to progress time- and tissue-dependent, thereby showing that adipose tissue-specific insulin resistance precedes that in muscle [125, 126]. As the examined animals were at the early-onset of diabetes, it would be interesting to know whether adipose tissue insulin resistance will also affect the skeletal muscle at the progress of the disease.

Since glucose uptake into the adipose tissue is mainly facilitated by the glucose transporter GLUT4, the observed reduction in GLUT4 protein abundance may explain the decreased uptake of glucose in $Nbg4p^{O/O}$ mice (Fig. 16A+B). This hypothesis can be supported by the study of Abel and colleagues, who observed that adipose-specific GLUT4 knockdown resulted into insulin resistance and glucose intolerance in mice. This study further implicates that again other tissues than skeletal muscle and the liver are secondarily affected by adipose insulin resistance, thus indicating that glucose transport in the adipose tissue plays a crucial role in the development of T2D [127]. However, it has been noted that GLUT4 mRNA expression was unaltered in the adipose tissue of $Nbg4p$ mice suggesting that the Ola-allele of $Nbg4p$ might regulate GLUT4 protein abundance rather on a posttranscriptional level as a secondary response to the insulin resistant state. As the detected GLUT4 protein abundance only represents the total amount within the tissue, it would be also interesting to determine if intracellular GLUT4 storage vesicles or the translocation to the plasma membrane is altered in $Nbg4p^{O/O}$ mice. For this purposes, fractioning or surface labelling of isolated adipocytes could help to separate intracellular space and plasma membrane for the detailed analysis of GLUT4 trafficking [128, 129].

To further investigate the potential cause of adipose tissue insulin resistance, adipocyte morphology was examined. Thereby, Ola-allele carriers of $Nbg4p$ showed increased adipocyte hypertrophy in the gWAT as described by a relatively higher amount of large and less small adipocytes (Fig. 17). Several studies have shown that expanding visceral adipose tissue represents a risk factor for obesity and T2D while subcutaneous fat was described to have

beneficial effects on whole-body metabolism [130-133]. In general, it has been reported that especially in the state of overnutrition, adipose depots try to compensate lipid-overloads by first increasing adipocyte size (hypertrophy) and then inducing proliferation (hyperplasia). In this context, not necessarily increased visceral fat mass, but especially adipocyte hypertrophy has been shown to substantially influence insulin sensitivity in adipose tissue [32, 134]. Thus, adipocyte hypertrophy in $Nbg4p^{O/O}$ mice may appear as one of the first signs of the diabetic outcome. The underlying mechanism connecting adipocyte hypertrophy to insulin sensitivity remains to be clarified. However, previous studies have shown that there is a close link of adipocyte size to adipokine expression and the lipolytic capacity, both factors that may influence the onset of T2D [135, 136]. Furthermore, it has been reported that larger adipocytes are linked to impaired GLUT4 trafficking which subsequently results into lower rates of insulin-stimulated glucose uptake. Thereby, researcher hypothesize that a potential alteration of the cytoskeleton development in hypertrophic adipocytes inhibits docking of GLUT4 vesicles to the plasma membrane [137]. To investigate if and which of the previously reported mechanisms may be connected to the observed phenotype from $Nbg4p^{O/O}$ mice still needs to be elucidated. Initial quantification of genetic lipolytic markers and plasma adiponectin concentrations showed no differences between the genotypes. Future studies could include the measurement of lipolytic substrates and further adipokines, like IL-6 or leptin, to evaluate a possible link to adipocyte size and the mechanism of how these factors contribute to adipose tissue insulin resistance. In summary, the observed data suggest that adipose tissue insulin resistance is the leading cause of whole-body glucose intolerance in young Ola-allele carriers of $Nbg4p$ mice, indicating that the causative gene(s) may directly influence metabolic dysfunctions in adipocytes.

4.1.4 Hepatic gluconeogenesis contributes to the hyperglycaemic effect of $Nbg4p$

In addition to skeletal muscle and adipose tissue, also the liver represents an important organ in the regulation of glucose homeostasis. In states of liver-specific insulin resistance, hyperglycemia can be triggered by an insufficient suppression of endogenous glucose production and inadequate transport of glucose [138, 139]. As already mentioned in the previous paragraphs, it is likely that adipose tissue insulin resistance may contribute to the disruption of insulin signalling in other tissues, including the liver, by the secretion of adipokines or the increased release of fatty acids (4.1.3). To investigate a potential impact of

the liver on the hyperglycemic phenotype in *Nbg4p* mice, several metabolic processes were examined in primary isolated hepatocytes.

First, hepatic gluconeogenesis was investigated to evaluate the amount of produced glucose in states of glucose starvation, insulin-mediated suppression or pyruvate and lactate-mediated induction. Thereby, it was shown that hepatocytes from Ola-allele carriers of *Nbg4p* exhibited significantly higher rates of produced glucose compared to those of NZO-allele carriers, even during conditions where this process is inhibited by insulin supplementation (Fig. 18). The process of insulin suppression in hepatocyte glucose production is described by two key mechanisms. Firstly, the regulation of the gluconeogenic genes phosphoenolpyruvate carboxykinase (PEPCK) and glucose-6-phosphatase (G6P) by the downstream activation of the protein kinase B (PKB or AKT) have shown to play a crucial role. In a healthy state when insulin binds to its receptor, autophosphorylation of tyrosine residues enables further protein binding to intracellular receptors by activating a phosphorylation cascade of numerous proteins. As a consequence, transcription factors of the forkhead box, class O (FoxO)-family that regulate the transcription of PEPCK and G6P are inhibited [26, 140]. Apart from the *de novo* synthesis of glucose, insulin can also suppress the conversion of stored glycogen to glucose (glycogenolysis). This second signalling pathway is also targeted by AKT which inactivates glycogen synthesis by the transcriptional inhibition of glycogen synthase kinas-3 (GSK3) [25]. In insulin resistant states, the absence of glucose production inhibition via both pathways lead to a hyperglycemic environment. As the results show an increased rate of glucose production from hepatocytes of *Nbg4p*$^{O/O}$, it is possible that a proper regulation of insulin-mediated inhibition of gluconeogenic genes is altered in these mice. Furthermore, the increased hepatic glycogen content of these mice suggests that endogenous glucose is elevated rather due to the process of gluconeogenesis than by glycogenolysis. To provide evidence for this hypothesis, different phosphorylation states of relevant proteins due to prior incubation of insulin could be determined in hepatocytes by western blotting. Furthermore, hepatic glycogen synthesis could be investigated by incorporated radiolabelled glucose as described elsewhere [141]. However, technical issues and limited tissue availability did not allow a closer look onto the metabolic causes of the altered hepatic glucose metabolism in *Nbg4p* mice.

Another interesting finding that indicates a potential role of the liver in whole-body glucose homeostasis in *Nbg4p* mice, is the increased gene expression of the glucokinase regulator (*Gckr*) in Ola-allele carriers (Fig. 19). At states of high glucose concentrations, the primary glucose phosphorylating enzyme glucokinase (GCK) translocates to the cytoplasm to induce glucose disposal and storage into the liver. In contrary, a fasted state triggers binding of GCK

92

with the glucokinase regulator protein (GKRP) to form an inhibitory complex in the nucleus that further leads to the increased production of endogenous glucose. In the past it has been shown that ablation of the inhibitory effect of GKRP leads to persisting glycolysis that results in a hypoglycaemic state in rodents and human [142]. However, this effect was ablated in individuals with insulin-resistant T2D suggesting that an imbalanced regulation of GCK and its binding to GKRP is a crucial step in glucose maintenance. In this context, it has been shown that reduced hepatic GCK activity led to decreased glucose disposal and insufficient suppression of glucose production already in heterozygous GCK knockout mice [143]. This leads to the hypothesis that increased *Gckr* gene expression in *Nbg4p*$^{O/O}$ mice may lead to decreased cytoplasmic GCK due to the competitive inhibition by GKRP. As a consequence, the lower affinity of GCK to glucose may lead to the ongoing process of endogenous glucose production. The potential role of increased GKRP on increased hepatic glucose production and the underlying mechanism still needs to be elucidated yet. Furthermore, it has to be clarified whether these effects result as a consequence of the insulin-resistant features that derive from the adipose tissue or due to genetic modifier that are located within the risk locus of *Nbg4p*. Nevertheless, it can be summarized that the increased production of endogenous glucose in Ola-allele carriers of the *Nbg4p* locus may, at least partially; contribute to the hyperglycemic phenotype.

4.2 Detection of genetic determinants for *Nbg4p*

Linkage studies of polygenic diseases like T2D often result in large genomic candidate regions and low penetrance for metabolic phenotypes [83]. Therefore combined approaches are very useful to narrow down critical regions to a small number of genes that are most likely associated to the observed traits. By the generation of congenic strains and validation of the phenotype in mice carrying the proximal region of the *Nbg4* locus, the genomic region of potential candidate genes could be reduced to a fragment of 37 Mb. Furthermore, metabolic investigation of insulin-responsive tissues indicated a potential impact of the adipose tissue and the liver on the hyperglycemic phenotype of *Nbg4p*. In order to identify the causal genes within this *Nbg4p* locus, a combination of haplotype, gene expression and prediction analyses were used.

4.2.1 Combined haplotype- and gene expression analysis identified five potential candidate genes for the diabetogenic effect of *Nbg4p*

To investigate the genetic cause of hyperglycemia and insulin resistance in *Nbg4p* mice, firstly a haplotype analysis of the parental strains was performed to generate information about regions that are unique for the Ola genome. Since common inbred mouse strains are genetically highly related to each other, haplotype mapping follows the fact that genetic differences in such strains are clustered in relatively small genomic areas that have not been separated by recombination. This enables the dissection of genomic regions that are either identical by descent (IBD) or polymorphic when comparing two strains (non-IBD). By the use of informative SNP marker from combined databases, *Nbg4p* was separated into 36 % non-IBD and 64 % IBD regions. Thus, haplotype analysis narrowed down the number of potential causal gene variants by the identification of 84 SNPs that were polymorphic for the Ola-mouse strain.

Based on the assumption, that the *Nbg4p* genomic region harbors genetic determinants that regulate adipose and hepatic glucose metabolism, gWAT and liver samples from 6 weeks old *Nbg4p* mice were used for transcriptome analysis. Whole-genome analysis of significantly differentially expressed genes showed most expression changes in the gWAT, which indicate a strong association of genetically-driven metabolic events. Since only a small number of these genes was assigned to the *Nbg4p* genomic region, there is a high probability of inter-chromosomal gene-interaction. However, it has been shown that microarrays are prone to artifacts which may influence candidate gene identification [144]. To increase the evidence of selected genes, an additional analysis of the mRNA expression of genes that were differentially expressed in the array was performed by qPCR. From 24 identified genes that were significantly differentially expressed in the microarray, only 10 were validated in the qPCR analysis. Finally, genes matching a confirmed significant differential expression in both tissues, or at least hitting all three analyses (haplotype, microarray and qPCR), were selected as potential candidates. By this, the *Nbg4p* genomic region could be further narrowed down to a maximum of five candidate genes (*AI464131, Unc13b, Atp8b5, Invs* and *Alad*). Thereof, *Unc13b, Atp8b5* and *Invs* were selected as novel candidate genes exclusively for the liver, while the significant expression changes of *AI464131* and *Alad* in both, liver and gWAT, suggest a predominant role for the phenotypic outcome of *Nbg4p*.

As reported before in different QTL studies, the combination of different approaches using congenic strains, haplotype mapping and gene expression profiling led to the successful identification of causal genes that are associated with diabetes-related traits [87, 88, 145, 146].

Although the here identified candidate genes are most likely involved in the pathophysiology of diabetic $Nbg4p^{O/O}$ mice, it has to be taken into account that the outcome of disease-related genes strongly depend on the applied filtering criteria. In this context, causal genes may be excluded from the analysis by the setting of different significance thresholds, leading to falsified results. Additionally, the high number of pseudo and predicted gene variants that were excluded from the transcriptome analysis of the gWAT of $Nbg4p$ mice do not necessarily exclude a potential role in genomic function. Increasing research on pseudogenes have shown that also non-coding transcripts are able to regulate coding gene variants [147, 148], however the low probability of functional effects makes it rather unlikely that one of these genes might have an impact on the phenotypic outcome of $Nbg4p$. The combination of different approaches, including haplotype and gene expression analysis, gave again high evidence for the identification of candidate genes for $Nbg4p$. This was not only shown by the validation of differential gene expression via qPCR, but also by the correlation of the candidates transcripts with a $Nbg4p$-specific physiological trait, which therefore additionally confirms the principle of the Mendelian Randomization [149]. As a consequence, significant correlation of the mRNA expression with the $Nbg4p$-specific phenotypic traits fasting blood glucose, plasma insulin and liver glycogen content, supported a potential impact of $Alad, AI464131$ and $Invs$ on T2D-prevalence (Suppl. Fig. 7+8).

4.2.2 Candidate genes of $Nbg4p$ show alternative splice events

To explain expression differences of the identified candidate genes, a closer look on possible gene variants (isoforms) and their transcriptional impact might get additional insights. It is known that most gene expression differences occur due to the presence of different variants, regulating important cellular processes (e.g. proliferation or cell differentiation). In this context, tissue-specific variants have shown to emerge for more than 50 % by alternative splice events. However, the complex regulation of alternative splicing is highly susceptible to errors, thus leading to aberrant variants with high impact on protein function which in turn can result to metabolic dysfunction. One example in the context of T2D is represented by the gene that encodes the insulin receptor ($Insr$) in skeletal muscle, liver and adipose tissue. Expression of this gene is essential as insulin-binding to its receptor represents the initial step in the maintenance of blood glucose levels. Alternative splicing of the $Insr$ gene has shown to result in two different isoforms, IR-A and IR-B, that significantly impair tissue-specific insulin sensitivity [150]. Thereby, increases in the IR-A/IR-B ratio were shown to have a proliferative

and migratory advantage in pancreatic beta-cells as well as favoring actions in the regulatory pathway of insulin-like growth factors (IGF). A disruptive expression pattern of both isoforms due to alternative splicing was therefore linked to insulin resistant features and metabolic diseases such as obesity, diabetes or cardiovascular complications [151].

To provide evidence for such genetic modifications regarding the identified candidate genes of *Nbg4p*, a variant effect prediction (VEP) analysis was performed (Suppl. Fig. 4). By using available dbSNP identifier for the SNPs that have been determined within the non-IBD regions of *Nbg4p*, transcript consequences were predicted for amino acids substitutions that were different from the reference genome (*Mus musculus*-C57BL/6J). With this tool (VEP-Ensembl) altered transcripts were classified depending on their predicted impact on protein function. For this purpose, variants were separated into those which might have disruptive or non-disruptive consequences, probably causing a loss of function or decreased protein effectiveness ("High" or "Moderate") and variants that have no evidence of impact or are of a harmless character ("Modifier" or "Low") where a change in protein behavior is very unlikely. The analyzed variants that may derive from strain-specific features of NZO or Ola mice did not show any evidence of a potential impact of the identified candidate genes on protein function (Suppl. Tab. 7). However, it must be taken into account that the inter-chromosomal gene-interaction in generated RCS mice might lead to different gene modifications due to a different genetic background of the Ola-allele of *Nbg4p*. Therefore, a potential impact cannot be entirely excluded by this prediction tool.

Since metabolic phenotyping showed distinct diabetogenic features only in gWAT and livers of *Nbg4p* mice, the possibility of tissue-specific splice events on the identified candidate genes was investigated using an exon array that was included within the transcriptome analysis (Suppl. Tab. 8). Except for *Unc13b*, all other candidate genes that were identified in this study showed significant exon splicing indices. Thereby, only *Atp8b5* showed a higher splicing index in livers of NZO-allele carriers of *Nbg4p*. The other genes (*AI464131*, *Invs* and *Alad*) showed strikingly elevated indices for splice variants in Ola-allele carriers for both tissues. The detailed mechanisms of alternative splicing is a complex field which therefore could not be discovered in this study, however, analysis of the exon architecture from identified splice events within the exon array could already bring new insights on a potential impact of respective transcripts. Nevertheless, the observed information give evidence that the differential expression of *AI464131, Atp8b5, Invs* and *Alad* may result due to alternative splice events, probably triggered by the obese background of the *Nbg4p* locus.

4.2.3 Pathway analysis confirmed a role in fatty acid and hepatic carnitine metabolism

In order to determine the tissue-specific metabolic impact of the identified candidate genes on the phenotype of *Nbg4p* mice, *in silico* pathway analysis was performed using the output of transcriptome analysis. For that, the Consensus PathDB (CPDB) was chosen, which consists of a broad collection of molecular interaction data with different options for computational methods and visualization. In general, the observed predictions for the gWAT of *Nbg4p* mice observed a high impact for alterations in the metabolism of branched chain amino acids (BCAA) as well as for adipocyte differentiation and lipolysis (Fig. 22A+B). In the literature it has been described that insulin resistance and T2D are highly associated with an elevation in circulating BCAAs [152, 153]. Thereby, gene expression of the two main enzymes BCAT2 and BCKDH were shown to be significantly reduced, while serum blood glucose, insulin and HOMA-IR were increased. Furthermore, these features were linked to an increased adipocyte size in the omental adipose tissue of insulin resistant subjects [154, 155]. Since the described phenotypic traits are in line with the observed features of *Nbg4p*$^{O/O}$ mice, it would be interesting to determine a potential association with BCAA metabolism. Although, transcriptome analysis revealed a reduced expression for *Bcat2* and *Bckdh*, validation of the results by qPCR and further determination of plasmatic BCAA concentrations would be needed to elucidate a possible impact of genetic variants from the *Nbg4p* locus. Furthermore, it has to be clarified whether changes in the BCAA metabolism occurs as a result of adipose tissue-specific insulin resistance or primary due to genetic modification within the critical region. Moreover, since key lipogenic genes were unaltered the gWAT of *Nbg4p* mice, a more detailed investigation of a potential linkage of the critical fragment with lipogenic features is needed to validate the predicted impact from CPDB analysis.

Since *Nbg4p* mice showed a strong linkage with the regulation of endogenous glucose production that may be associated with one of the identified gene variants, CPDB analysis was additionally performed for the liver tissue of these mice. With this, the carnitine metabolism was predicted to be one of the most likely affected pathways and further gene expression analysis indeed revealed a significant expression differences of the carnitine acetyltransferase (*Crat*) gene. CRAT is an important enzyme that, similar to the liver-type carnitine palmitoyltransferase I and II (CPT1A and CPT2), regulates intracellular pools of acyl-coenzyme A (CoA) esters [156]. In the past it has been shown that muscle-specific deletion of Crat led to impaired whole-body glucose homeostasis by suppressing pyruvate dehydrogenase activity, thus resembling an insulin resistant state [157]. Moreover, Seiler et al. described a

decreased CRAT activity in response to genetic diabetes and HFD-feeding in rodents that promotes the hypothesis of a possible mechanistic link in *Nbg4p* mice [158].

Taken together, the CPDB pathway analysis revealed a high evidence for a dysregulated fatty acid metabolism in the gWAT of *Nbg4p* mice, whereby the metabolic regulation of BCAA and lipolysis represent the most likely pathways that might be affected by the *Nbg4p* locus. Together with the predicted impact on hepatic carnitine metabolism, one could hypothesize that the causal genes of *Nbg4p* might regulate glucose homeostasis by the modulation of energy metabolism in a tissue-specific manner. To proof this, metabolic investigation of BCAA or carnitine contents in gWAT or liver tissues, respectively, as well as protein expression analysis of the above mentioned key enzymes, are needed. However, in consideration of getting a first view of possible mechanisms that may be responsible for a certain phenotype, this prediction tool represents a good possibility to get quick and reliable insights into the deserved research field.

4.3 Functional investigation of diabetogenic genes

The identification of novel disease genes already represents a big step in the right direction of metabolic research. However, neither haplotype, gene expression analysis nor the combination with pathway-related prediction tools involves the functional evidence of the causality of a candidate gene. Therefore, several cell models have been generated in the past to implement gene modifications and to investigate the metabolic function *in vitro*. To provide functional evidence of candidate genes identified within the collective cross breeding approach, two different genes were investigated for their tissue-specific associations with diabetes-related traits.

4.3.1 *Alad* affects glucose uptake in 3T3-L1 adipocytes

The *δ-aminolevulinate dehydratase* (*Alad*) gene represents a promising candidate gene that was identified within the blood glucose-related QTL of *Nbg4* in a crossbreeding of diabetic NZO and lean Ola mice. Significant gene expression differences in liver and adipose tissue were already detected within a previously conducted transcriptome analysis of the N2(NZOxOla) population and was further confirmed in congenic mice carrying the proximal Ola-fragment of *Nbg4* as described above (4.2) [98]. Briefly, heterozygous NZO/Ola-allele carriers of *Nbg4* as well as homozygous Ola/Ola-allele carrier of the proximal *Nbg4* locus showed a significant reduction in *Alad* gene expression that was associated with increased blood glucose levels when compared to NZO controls. Thereby, it has to be taken into account, that the backcross population carried a completely heterogenous background which consists in theory of 75 %

NZO- and 25 % Ola-alleles, whereas the recombinant congenic strains (RCS) generated within this study, only differed in the *Nbg4p* region which accounts for less than 3 % of the Ola genome. This ensured that the expression differences in the *Alad* gene did not occur due to gene interaction within the whole genome, but rather represents a unique feature of the *Nbg4p* locus. Furthermore, since RCS mice carrying Ola-alleles of the *Nbg4p* locus showed an early-onset insulin resistant phenotype in the adipose tissue, linkage to *Alad* gene expression became more evident. To confirm the causality of potential candidate genes on a specific phenotype, the analysis of expression QTLs (eQTLs) have shown to be a useful tool [159]. This method allows the identification of genetic sequence variation between two genotypes that reside within a physiological QTL. The previous detection of an eQTL for *Alad* in the gWAT of the backcross population therefore encourages the causal relationship between the reduced mRNA expression and increased blood glucose levels in Ola-allele carriers. Moreover, correlation analysis showed significant associations of the mRNA expression in adipose tissue with blood glucose levels in the backcross population as well as in congenic mice [98].

In the literature it has been reported, that blood samples from T2D patients showed a reduction in ALAD enzyme activity, supporting the hypothesis of a possible impact on glucose metabolism [160]. Researcher further suggest that the ALAD enzyme plays a crucial role in aerobic organisms as it participates in the heme biosynthetic pathway. Thereby, it catalyses the condensation of aminolevulinic acid (ALA) to form porphobilinogen (PGB) which is a precursor of the cellular heme pigmentation of haemoglobin. Thus, a deficiency of hepatic ALAD activity results into autosomal recessive porphyria that is further characterized by abdominal pain and neuropsychiatric symptoms [161, 162]. These symptoms have not been recognized neither in the backcross population of NZO and Ola mice, nor in congenic *Nbg4p* mice. However, in mice it is much more difficult to record signs that can be assigned to pain or psychiatric symptoms, therefore the detection of porphyrins in blood samples would be an alternative. Nevertheless, reduction of *Alad* gene expression in several tissues increases the probability that Ola-allele carrier of *Nbg4p* are affected by an impaired heme biosynthesis. This assumption may be supported by the appearance of the liver tissues from *Nbg4p* mice which visibly show a less intense colour in livers from Ola-allele carriers. Since liver weight, triglyceride content as well as hepatic *de novo* lipogenesis was not different when compared to NZO-allele carriers of *Nbg4p*, the faded appearance may occur rather due to a reduced blood pigmentation than due to lipid accumulation. This hypothesis is additionally encouraged by the potential impact of the hepatic pigment biosynthetic pathway as predicted within the CPDB analysis.

As described above, heme biosynthesis mainly takes part in blood vessels and the liver, leading to the question why such a considerably high expression difference of the *Alad* gene was also determined in the gWAT of *Nbg4p* mice. First of all, the generated cDNA of gWAT samples that was used for gene expression analysis in this study derived from whole adipose tissue samples which also contains blood cells, endothelial cells, macrophages and even more [163, 164]. Therefore, it cannot be excluded that the expression differences was affected by embedded blood vessels rather than from adipocytes alone. A repeated analysis of primary isolated adipocytes would help to clarify this aspect. Another explanation can be found in the observation that heme is required in all nucleated cells for the production of respiratory cytochrome proteins. These proteins ensure appropriate adipogenesis and lipogenesis as shown by Dang and Yun in 2021 [165]. Recent studies have performed a detailed research on the close link of *Alad* gene expression to glucose and lipid metabolism of adipocytes [166-168]. In this context, it has been shown that *Alad* knockdown was accompanied with decreases in adipocyte glucose uptake and mitochondrial function. Although, a reduction of the *Alad* gene expression was achieved for almost 80 % after retroviral transduction, the before mentioned effects could not be reproduced in the present study (Fig. 25+26). A possible reason for the inconsistent results may lie in the used cell model as well as in the transfection system. The before mentioned study was performed in immortalized human adipose-derived mesenchymal stem cells that differentiate to mature adipocytes similar to 3T3-L1 adipocytes. However, functional analysis of both cell lines can differ since human adipocytes that originate from the bone marrow are not as genetically diverse as murine cell lines and therefore might show different metabolic features [169]. Moreover, the retroviral transduction system may be a great tool for the generation of stable cell lines, however, the possibility of insertional mutagenesis is higher compared to lentiviral vectors [170]. In conclusion, a diabetogenic effect of *Alad* gene expression on adipose glucose and lipid metabolism could not be validated in this study.

4.3.2 *Nudt19* regulates hepatic lipid metabolism

Another genetic modifier, which has been identified within the collective diabetes cross project is the *nucleoside diphosphate linked moiety X (nudix)-type motif 19* (*Nudt19*). This gene was found within the *Nbg7* QTL of a crossbreeding approach between diabetic NZO with lean and T2D-resistant C3H mice that showed linkage with hyperglycemia and hypoinsulinemia in NZO-allele carriers. Transcriptome analysis in these mice showed a significantly lower *Nudt19* gene expression in livers of NZO compared to lean C3H and Ola mice. In combination with the observed strain-specific differences in hepatic TG content, the data suggest a potential impact on the hepatic lipid metabolism as further annotated by the KEGG database. (Fig. 27).

Previous studies on *Nudt19* function focussed rather on the energy metabolism of murine kidneys, where NUDT19 has been associated with the intracellular degradation of coenzyme A (CoA) [112, 171]. In general, nudix proteins have shown to produce 3′, 5′-ADP and 4′-(acyl)phosphopantetheine by their hydrolytic activity on (acyl-) Coenzyme A (CoA). Since CoA is a major acyl carrier and important cofactor for numerous metabolic processes [172]. The key mechanism that links hepatic energy and lipid metabolism to each other is the mitochondrial fatty acid oxidation. Thereby, abnormal lipid accumulation in the liver increases the amount of fatty acyl-CoA, which represent the main product of mitochondrial fatty acid oxidation [173].

Assuming that NUDT19 exerts a similar function in the degradation of intracellular CoA in the liver, investigation of *Nudt19* gene expression on mitochondrial function and fatty acid oxidation in murine hepatoma cells was conducted in this work. The results showed that a reduction of *Nudt19* mRNA increased overall mitochondrial respiration which was accompanied with an elevated production of energetic ATP and fatty acid oxidation (Fig. 28) [174]. With regard to the metabolic phenotype observed in NZO mice, one could speculate that increased mitochondrial function may occur to compensate hepatic lipid overload, maintaining insulin sensitivity of the tissue. Similar effects were observed in a mouse model for the non-alcoholic fatty liver disease (NAFLD), where an increase of the oxidative capacity of liver mitochondria was determined prior to a mitigation of a fatty liver [175]. However, also contrary findings were reported where obese objects showed rather decreases in mitochondrial function [176]. Although it remains likely that *Nudt19* regulates mitochondrial respiration due to the availability of CoA, a contribution through further unknown mechanisms cannot be excluded. Thus, the observed correlation between *Nudt19* and *Pdk4* gene expression provides evidence that mitochondrial function may be affected secondarily due to PDK4-specific inhibition of the pyruvate dehydrogenase (PDH). A direct impact of liver-specific *Pdk4* overexpression on elevated mitochondrial function and fatty acid oxidation have been demonstrated in recent studies of obese and diabetic mouse models [177, 178]. However, a detailed mechanism of how *Nudt19* affects *Pdk4* expression, directly or secondarily due to indirect regulation of mitochondrial respiration, remains to be elucidated. Additionally, the investigation of liver-specific *Nudt19* knockout animals would provide further evidence of a possible relationship to the pathophysiology of NAFLD in T2D.

4.4 Conclusion and future perspectives

In this study, the collective diabetes cross project again showed the great benefit of combining mouse crossbreedings with bioinformatic and gene expression analyses to nominate novel diabetes-related candidate genes. With this, the previously identified blood glucose-associated QTL on murine chromosome 4 (*Nbg4*) was narrowed down by the generation of recombinant congenic strains (RCS) to a critical fragment of 37 Mb located on the proximal region of *Nbg4*. Subsequent tissue-specific analyses revealed five novel potential candidate genes (*AI464131*, *Unc13b*, *Atp8b5*, *Invs* and *Alad*) that might affect glucose metabolism in the adipose tissue and/or the liver. So far, functional evidence could be provided exclusively for the gene *Alad* that showed a contribution in the regulation of glucose uptake into 3T3-L1 adipocytes. However, since the modification of *Alad* gene expression did not reveal the desired efficiency so far, future studies could replicate *Alad* knockdown using shRNAs as described in the work of Moreno-Navarrete [166]. Furthermore, gene modification of *Alad* and *AI464131* in primary isolated adipocytes is a good alternative to investigate a possible impact on adipose glucose metabolism *ex vivo*.

Future studies will further investigate whether the other four candidate genes may contribute to the phenotype mediated by *Nbg4p*. These could include the analysis of different splice variants that have shown to occur predominantly in Ola-allele carriers of *Nbg4p* to find a metabolic impact on the diabetogenic features of the QTL. Individual base exchanges on protein-coding regions, or mutations within a regulatory sequence can induce substantial changes in gene expression and protein function that might contribute to phenotypic outcome of *Nbg4p*. *In vitro* functional investigation of identified splice variants, that seem to have a potential impact on the protein level, could clarify a possible contribution in glucose and lipid metabolism. Since the analysis of glucose-related pathways in immortalized liver cell lines has shown to be inappropriate due to a marginal expression of respective key regulator (e.g. PEPCK), a conceivable alternative would be the analysis of isolated primary hepatocytes after gene modification. With this, a possible impact of the liver-specific genes *Atp8b5* and *Invs* on glucose production and glycogen metabolism could be examined. Furthermore, generation of transgenic mice, that either lack or overexpress the gene of interest, will be useful to investigate a mechanistic role on whole-body glucose homeostasis.

5. Literature

1. OECD/EU. *Obesity Update* 2017; Available from: http://www.oecd.org/health/obesity-update.htm.
2. Seery, C. *Blood Sugar Level Ranges*. 2019; Available from: https://www.diabetes.co.uk/diabetes_care/blood-sugar-level-ranges.html.
3. Federation, I.D., *IDF Diabetes Atlas*. 2021.
4. WHO. *WHO reveals leading causes of death and disability worldwide: 2000-2019*. 2020; Available from: https://www.who.int/news/item/09-12-2020-who-reveals-leading-causes-of-death-and-disability-worldwide-2000-2019.
5. Froguel, P., et al., *Close linkage of glucokinase locus on chromosome 7p to early-onset non-insulin-dependent diabetes mellitus.* Nature, 1992. **356**(6365): p. 162-4.
6. Shira Eytan, S.W. *What Is Type 1 Diabetes?* 2009.
7. Beulens, J.W.J., et al., *Environmental risk factors of type 2 diabetes-an exposome approach.* Diabetologia, 2022. **65**(2): p. 263-274.
8. Tillil, H. and J. Kobberling, *Age-corrected empirical genetic risk estimates for first-degree relatives of IDDM patients.* Diabetes, 1987. **36**(1): p. 93-9.
9. Poulsen, P., et al., *Heritability of type II (non-insulin-dependent) diabetes mellitus and abnormal glucose tolerance--a population-based twin study.* Diabetologia, 1999. **42**(2): p. 139-45.
10. Meigs, J.B., L.A. Cupples, and P.W. Wilson, *Parental transmission of type 2 diabetes: the Framingham Offspring Study.* Diabetes, 2000. **49**(12): p. 2201-7.
11. Stranger, B.E., E.A. Stahl, and T. Raj, *Progress and promise of genome-wide association studies for human complex trait genetics.* Genetics, 2011. **187**(2): p. 367-83.
12. Herder, C. and M. Roden, *A novel diabetes typology: towards precision diabetology from pathogenesis to treatment.* Diabetologia, 2022. **65**(11): p. 1770-1781.
13. Herder, C., et al., *Differences in Biomarkers of Inflammation Between Novel Subgroups of Recent-Onset Diabetes.* Diabetes, 2021. **70**(5): p. 1198-1208.
14. Zaharia, O.P., et al., *Role of Patatin-Like Phospholipase Domain-Containing 3 Gene for Hepatic Lipid Content and Insulin Resistance in Diabetes.* Diabetes Care, 2020. **43**(9): p. 2161-2168.
15. Zaharia, O.P., et al., *Risk of diabetes-associated diseases in subgroups of patients with recent-onset diabetes: a 5-year follow-up study.* Lancet Diabetes Endocrinol, 2019. **7**(9): p. 684-694.
16. Stephen L. Aronoff, K.B., Barb Schreiner, Laura Want, *Glucose Metabolism and Regulation: Beyond Insulin and Glucagon.* Diabetes Spectrum, 2004. **17**(3).
17. Leslie, R.D., *Metabolic changes in diabetes.* Eye (Lond), 1993. **7 (Pt 2)**: p. 205-8.
18. Washburn, R.L., et al., *C-Peptide as a Therapy for Type 1 Diabetes Mellitus.* Biomedicines, 2021. **9**(3).
19. Kido, Y., J. Nakae, and D. Accili, *Clinical review 125: The insulin receptor and its cellular targets.* J Clin Endocrinol Metab, 2001. **86**(3): p. 972-9.
20. Kim, E.K. and E.J. Choi, *Pathological roles of MAPK signaling pathways in human diseases.* Biochim Biophys Acta, 2010. **1802**(4): p. 396-405.
21. Dresner, A., et al., *Effects of free fatty acids on glucose transport and IRS-1-associated phosphatidylinositol 3-kinase activity.* J Clin Invest, 1999. **103**(2): p. 253-9.
22. Petersen, K.F. and G.I. Shulman, *Etiology of insulin resistance.* Am J Med, 2006. **119**(5 Suppl 1): p. S10-6.
23. Rabol, R., *Mitochondrial function in skeletal muscle in type 2 diabetes.* Dan Med Bull, 2011. **58**(4): p. B4272.

24.   Zierath, J.R., et al., *C-peptide stimulates glucose transport in isolated human skeletal muscle independent of insulin receptor and tyrosine kinase activation.* Diabetologia, 1996. **39**(3): p. 306-13.

25.   Summers, S.A., et al., *The role of glycogen synthase kinase 3beta in insulin-stimulated glucose metabolism.* J Biol Chem, 1999. **274**(25): p. 17934-40.

26.   Schmoll, D., et al., *Regulation of glucose-6-phosphatase gene expression by protein kinase Balpha and the forkhead transcription factor FKHR. Evidence for insulin response unit-dependent and -independent effects of insulin on promoter activity.* J Biol Chem, 2000. **275**(46): p. 36324-33.

27.   Savage, D.B. and R.K. Semple, *Recent insights into fatty liver, metabolic dyslipidaemia and their links to insulin resistance.* Curr Opin Lipidol, 2010. **21**(4): p. 329-36.

28.   Softic, S., et al., *Insulin concentration modulates hepatic lipid accumulation in mice in part via transcriptional regulation of fatty acid transport proteins.* PLoS One, 2012. **7**(6): p. e38952.

29.   Nye, C., et al., *Reassessing triglyceride synthesis in adipose tissue.* Trends Endocrinol Metab, 2008. **19**(10): p. 356-61.

30.   Neeland, I.J., et al., *Dysfunctional adiposity and the risk of prediabetes and type 2 diabetes in obese adults.* JAMA, 2012. **308**(11): p. 1150-9.

31.   Yki-Jarvinen, H., *Fat in the liver and insulin resistance.* Ann Med, 2005. **37**(5): p. 347-56.

32.   Rosen, E.D. and B.M. Spiegelman, *What we talk about when we talk about fat.* Cell, 2014. **156**(1-2): p. 20-44.

33.   Long, Y.C., et al., *Insulin receptor substrates Irs1 and Irs2 coordinate skeletal muscle growth and metabolism via the Akt and AMPK pathways.* Mol Cell Biol, 2011. **31**(3): p. 430-41.

34.   Bruning, J.C., et al., *A muscle-specific insulin receptor knockout exhibits features of the metabolic syndrome of NIDDM without altering glucose tolerance.* Mol Cell, 1998. **2**(5): p. 559-69.

35.   Kelley, D.E., et al., *Skeletal muscle fatty acid metabolism in association with insulin resistance, obesity, and weight loss.* Am J Physiol, 1999. **277**(6): p. E1130-41.

36.   Koves, T.R., et al., *Mitochondrial overload and incomplete fatty acid oxidation contribute to skeletal muscle insulin resistance.* Cell Metab, 2008. **7**(1): p. 45-56.

37.   Itani, S.I., et al., *Lipid-induced insulin resistance in human muscle is associated with changes in diacylglycerol, protein kinase C, and IkappaB-alpha.* Diabetes, 2002. **51**(7): p. 2005-11.

38.   Reitman, M.L. and O. Gavrilova, *A-ZIP/F-1 mice lacking white fat: a model for understanding lipoatrophic diabetes.* Int J Obes Relat Metab Disord, 2000. **24 Suppl 4**: p. S11-4.

39.   Jensen, M.D., *Adipose tissue and fatty acid metabolism in humans.* J R Soc Med, 2002. **95 Suppl 42**: p. 3-7.

40.   Horowitz, J.F., *Fatty acid mobilization from adipose tissue during exercise.* Trends Endocrinol Metab, 2003. **14**(8): p. 386-92.

41.   Girard, J., *[Mechanisms of action of thiazolidinediones].* Diabetes Metab, 2001. **27**(2 Pt 2): p. 271-8.

42.   McQuaid, S.E., et al., *Downregulation of adipose tissue fatty acid trafficking in obesity: a driver for ectopic fat deposition?* Diabetes, 2011. **60**(1): p. 47-55.

43.   Shi, J., et al., *Cytokines and Abnormal Glucose and Lipid Metabolism.* Front Endocrinol (Lausanne), 2019. **10**: p. 703.

44.   Park, S.Y., et al., *C1q tumor necrosis factor alpha-related protein isoform 5 is increased in mitochondrial DNA-depleted myocytes and activates AMP-activated protein kinase.* J Biol Chem, 2009. **284**(41): p. 27780-27789.

45. Carey, A.L., et al., *Interleukin-6 increases insulin-stimulated glucose disposal in humans and glucose uptake and fatty acid oxidation in vitro via AMP-activated protein kinase.* Diabetes, 2006. **55**(10): p. 2688-97.

46. Ellingsgaard, H., et al., *Interleukin-6 enhances insulin secretion by increasing glucagon-like peptide-1 secretion from L cells and alpha cells.* Nat Med, 2011. **17**(11): p. 1481-9.

47. Peppler, W.T., et al., *Acute administration of IL-6 improves indices of hepatic glucose and insulin homeostasis in lean and obese mice.* Am J Physiol Gastrointest Liver Physiol, 2019. **316**(1): p. G166-G178.

48. Unger, R.H., Y.T. Zhou, and L. Orci, *Regulation of fatty acid homeostasis in cells: novel role of leptin.* Proc Natl Acad Sci U S A, 1999. **96**(5): p. 2327-32.

49. Kadowaki, T., et al., *Adiponectin and adiponectin receptors in insulin resistance, diabetes, and the metabolic syndrome.* J Clin Invest, 2006. **116**(7): p. 1784-92.

50. Yoda-Murakami, M., et al., *Change in expression of GBP28/adiponectin in carbon tetrachloride-administrated mouse liver.* Biochem Biophys Res Commun, 2001. **285**(2): p. 372-7.

51. Fon Tacer, K., et al., *Research resource: Comprehensive expression atlas of the fibroblast growth factor system in adult mouse.* Mol Endocrinol, 2010. **24**(10): p. 2050-64.

52. Arner, P., et al., *FGF21 attenuates lipolysis in human adipocytes - a possible link to improved insulin sensitivity.* FEBS Lett, 2008. **582**(12): p. 1725-30.

53. Hotamisligil, G.S., N.S. Shargill, and B.M. Spiegelman, *Adipose expression of tumor necrosis factor-alpha: direct role in obesity-linked insulin resistance.* Science, 1993. **259**(5091): p. 87-91.

54. Rotter, V., I. Nagaev, and U. Smith, *Interleukin-6 (IL-6) induces insulin resistance in 3T3-L1 adipocytes and is, like IL-8 and tumor necrosis factor-alpha, overexpressed in human fat cells from insulin-resistant subjects.* J Biol Chem, 2003. **278**(46): p. 45777-84.

55. Donath, M.Y. and S.E. Shoelson, *Type 2 diabetes as an inflammatory disease.* Nat Rev Immunol, 2011. **11**(2): p. 98-107.

56. Flint, J. and E. Eskin, *Genome-wide association studies in mice.* Nat Rev Genet, 2012. **13**(11): p. 807-17.

57. Bogdanov, P., et al., *The db/db mouse: a useful model for the study of diabetic retinal neurodegeneration.* PLoS One, 2014. **9**(5): p. e97302.

58. Lindstrom, P., *The physiology of obese-hyperglycemic mice [ob/ob mice].* ScientificWorldJournal, 2007. **7**: p. 666-85.

59. Yoshioka, M., et al., *A novel locus, Mody4, distal to D7Mit189 on chromosome 7 determines early-onset NIDDM in nonobese C57BL/6 (Akita) mutant mice.* Diabetes, 1997. **46**(5): p. 887-94.

60. Axton, E. *JAX Diversity Outbred Mice: A Genetically Diverse Mouse for a Diverse Human Population*. 2020; Available from: https://www.jax.org/news-and-insights/jax-blog/2020/august/jax-diversity-outbred-mice-a-genetically-diverse-mouse-for-a-diverse-human.

61. Bielschowsky, M. and C.M. Goodall, *Origin of inbred NZ mouse strains.* Cancer Res, 1970. **30**(3): p. 834-6.

62. Ortlepp, J.R., et al., *A metabolic syndrome of hypertension, hyperinsulinaemia and hypercholesterolaemia in the New Zealand obese mouse.* Eur J Clin Invest, 2000. **30**(3): p. 195-202.

63. Jurgens, H.S., et al., *Hyperphagia, lower body temperature, and reduced running wheel activity precede development of morbid obesity in New Zealand obese mice.* Physiol Genomics, 2006. **25**(2): p. 234-41.

64. Vogel, H., et al., *Estrogen deficiency aggravates insulin resistance and induces beta-cell loss and diabetes in female New Zealand obese mice.* Horm Metab Res, 2013. **45**(6): p. 430-5.

65. Kluge, R., et al., *Quantitative trait loci for obesity and insulin resistance (Nob1, Nob2) and their interaction with the leptin receptor allele (LeprA720T/T1044I) in New Zealand obese mice.* Diabetologia, 2000. **43**(12): p. 1565-72.

66. Igel, M., et al., *Hyperleptinemia, leptin resistance, and polymorphic leptin receptor in the New Zealand obese mouse.* Endocrinology, 1997. **138**(10): p. 4234-9.

67. Almind, K. and C.R. Kahn, *Genetic determinants of energy expenditure and insulin resistance in diet-induced obesity in mice.* Diabetes, 2004. **53**(12): p. 3274-85.

68. Kulkarni, R.N., et al., *Impact of genetic background on development of hyperinsulinemia and diabetes in insulin receptor/insulin receptor substrate-1 double heterozygous mice.* Diabetes, 2003. **52**(6): p. 1528-34.

69. Leiter, E.H., et al., *A new mutation (db3J) at the diabetes locus in strain 129/J mice. I. Physiological and histological characterization.* Diabetologia, 1980. **19**(1): p. 58-65.

70. Brilliant, M.H., et al., *The original pink-eyed dilution mutation (p) arose in Asiatic mice: implications for the H4 minor histocompatibility antigen, Myod1 regulation and the origin of inbred strains.* Genetics, 1994. **138**(1): p. 203-11.

71. Mackay, T.F., E.A. Stone, and J.F. Ayroles, *The genetics of quantitative traits: challenges and prospects.* Nat Rev Genet, 2009. **10**(8): p. 565-77.

72. Chen, C.H., et al., *A genome-wide scan using tree-based association analysis for candidate loci related to fasting plasma glucose levels.* BMC Genet, 2003. **4 Suppl 1**: p. S65.

73. Bush, W.S. and J.H. Moore, *Chapter 11: Genome-wide association studies.* PLoS Comput Biol, 2012. **8**(12): p. e1002822.

74. Schwenk, R.W., H. Vogel, and A. Schurmann, *Genetic and epigenetic control of metabolic health.* Mol Metab, 2013. **2**(4): p. 337-47.

75. Darvasi, A., *Experimental strategies for the genetic dissection of complex traits in animal models.* Nat Genet, 1998. **18**(1): p. 19-24.

76. Manolio, T.A., et al., *Finding the missing heritability of complex diseases.* Nature, 2009. **461**(7265): p. 747-53.

77. Burke, D.T., et al., *Dissection of complex adult traits in a mouse synthetic population.* Genome Res, 2012. **22**(8): p. 1549-57.

78. Cirillo, E., et al., *From SNPs to pathways: Biological interpretation of type 2 diabetes (T2DM) genome wide association study (GWAS) results.* PLoS One, 2018. **13**(4): p. e0193515.

79. Christians, J.K., et al., *Identification and reciprocal introgression of a QTL affecting body mass in mice.* Genet Sel Evol, 2004. **36**(5): p. 577-91.

80. Liu, K.J., et al., *Interspecific introgressive origin of genomic diversity in the house mouse.* Proc Natl Acad Sci U S A, 2015. **112**(1): p. 196-201.

81. Groot, P.C., et al., *The recombinant congenic strains for analysis of multigenic traits: genetic composition.* FASEB J, 1992. **6**(10): p. 2826-35.

82. Markel, P., et al., *Theoretical and empirical issues for marker-assisted breeding of congenic mouse strains.* Nat Genet, 1997. **17**(3): p. 280-4.

83. Brockmann, G.A. and C. Neuschl, *Positional cloning of diabetes genes.* Methods Mol Biol, 2012. **933**: p. 275-89.

84. Darvasi, A., *Interval-specific congenic strains (ISCS): an experimental design for mapping a QTL into a 1-centimorgan interval.* Mamm Genome, 1997. **8**(3): p. 163-7.

85. Frazer, K.A., et al., *Segmental phylogenetic relationships of inbred mouse strains revealed by fine-scale analysis of sequence variation across 4.6 mb of mouse genome.* Genome Res, 2004. **14**(8): p. 1493-500.

86. Browning, S.R. and B.L. Browning, *Haplotype phasing: existing methods and new developments.* Nat Rev Genet, 2011. **12**(10): p. 703-14.

87. Aga, H., et al., *Identification of Novel Potential Type 2 Diabetes Genes Mediating beta-Cell Loss and Hyperglycemia Using Positional Cloning.* Front Genet, 2020. **11**: p. 567191.

88. Altenhofen, D., et al., *E96V Mutation in the Kdelr3 Gene Is Associated with Type 2 Diabetes Susceptibility in Obese NZO Mice.* Int J Mol Sci, 2023. **24**(1).

89. Kuhn, T., et al., *Comparative genomic analyses of multiple backcross mouse populations suggest SGCG as a novel potential obesity-modifier gene.* Hum Mol Genet, 2022.

90. Schwerbel, K., et al., *Immunity-related GTPase induces lipophagy to prevent excess hepatic lipid accumulation.* J Hepatol, 2020. **73**(4): p. 771-782.

91. Shi, L.J., et al., *Genetic Connection between Hyperglycemia and Carotid Atherosclerosis in Hyperlipidemic Mice.* Genes (Basel), 2022. **13**(3).

92. Takeshita, S., et al., *Diabetic modifier QTLs identified in F2 intercrosses between Akita and A/J mice.* Mamm Genome, 2006. **17**(9): p. 927-40.

93. Leiter, E.H., et al., *NIDDM genes in mice: deleterious synergism by both parental genomes contributes to diabetogenic thresholds.* Diabetes, 1998. **47**(8): p. 1287-95.

94. Plum, L., et al., *Characterisation of the mouse diabetes susceptibilty locus Nidd/SJL: islet cell destruction, interaction with the obesity QTL Nob1, and effect of dietary fat.* Diabetologia, 2002. **45**(6): p. 823-30.

95. Schallschmidt, T., et al., *Two Novel Candidate Genes for Insulin Secretion Identified by Comparative Genomics of Multiple Backcross Mouse Populations.* Genetics, 2018. **210**(4): p. 1527-1542.

96. Scherneck, S., et al., *Positional cloning of zinc finger domain transcription factor Zfp69, a candidate gene for obesity-associated diabetes contributed by mouse locus Nidd/SJL.* PLoS Genet, 2009. **5**(7): p. e1000541.

97. Vogel, H., et al., *A collective diabetes cross in combination with a computational framework to dissect the genetics of human obesity and Type 2 diabetes.* Hum Mol Genet, 2018. **27**(17): p. 3099-3112.

98. Lebek, S., *Identifizierung von Suszeptibilitätsloci für Typ-2-Diabetes mellitus in einem Mausmodell für das metabolische Syndrom.* 2018, Heinrich-Heine-Universität Düsseldorf.

99. Darlington, G.J., et al., *Expression of liver phenotypes in cultured mouse hepatoma cells.* J Natl Cancer Inst, 1980. **64**(4): p. 809-19.

100. Mystkowski, P., et al., *Validation of whole-body magnetic resonance spectroscopy as a tool to assess murine body composition.* Int J Obes Relat Metab Disord, 2000. **24**(6): p. 719-24.

101. Mackrell, J.G. and G.D. Cartee, *A novel method to measure glucose uptake and myosin heavy chain isoform expression of single fibers from rat skeletal muscle.* Diabetes, 2012. **61**(5): p. 995-1003.

102. Maguire, A.S., et al., *Whole-slide image analysis outperforms micrograph acquisition for adipocyte size quantification.* Adipocyte, 2020. **9**(1): p. 567-575.

103. Honecker, J., et al., *A distribution-centered approach for analyzing human adipocyte size estimates and their association with obesity-related traits and mitochondrial function.* Int J Obes (Lond), 2021. **45**(9): p. 2108-2117.

104. Muir, L.A., et al., *Adipocyte hypertrophy-hyperplasia balance contributes to weight loss after bariatric surgery.* Adipocyte, 2017. **6**(2): p. 134-140.

105. Akie, T.E. and M.P. Cooper, *Determination of Fatty Acid Oxidation and Lipogenesis in Mouse Primary Hepatocytes.* J Vis Exp, 2015(102): p. e52982.

106. Lund, J., et al., *Increased Glycolysis and Higher Lactate Production in Hyperglycemic Myotubes.* Cells, 2019. **8**(9).

107. Selig, J.I., et al., *Impact of hyperinsulinemia and hyperglycemia on valvular interstitial cells - A link between aortic heart valve degeneration and type 2 diabetes.* Biochim Biophys Acta Mol Basis Dis, 2019. **1865**(9): p. 2526-2537.

108. McLaren, W., et al., *The Ensembl Variant Effect Predictor.* Genome Biol, 2016. **17**(1): p. 122.

109. Knebel, B., et al., *Peroxisomes compensate hepatic lipid overflow in mice with fatty liver.* Biochim Biophys Acta, 2015. **1851**(7): p. 965-76.

110. Matthews, D.R., et al., *Homeostasis model assessment: insulin resistance and beta-cell function from fasting plasma glucose and insulin concentrations in man.* Diabetologia, 1985. **28**(7): p. 412-9.

111. Schallschmidt, T., *Identification of novel susceptibility genes for diabetes-related traits in a backcross of obese NZO with lean C3H mice.* 2018, Heinrich-Heine-University Duesseldorf. p. 152.

112. Shumar, S.A., et al., *Nudt19 is a renal CoA diphosphohydrolase with biochemical and regulatory properties that are distinct from the hepatic Nudt7 isoform.* J Biol Chem, 2018. **293**(11): p. 4134-4148.

113. DeForest, N. and A.R. Majithia, *Genetics of Type 2 Diabetes: Implications from Large-Scale Studies.* Curr Diab Rep, 2022. **22**(5): p. 227-235.

114. Prasad, R.B. and L. Groop, *Genetics of type 2 diabetes-pitfalls and possibilities.* Genes (Basel), 2015. **6**(1): p. 87-123.

115. Takeshita, S., et al., *Diabetic modifier QTL, Dbm4, affecting elevated fasting blood glucose concentrations in congenic mice.* Genes Genet Syst, 2012. **87**(5): p. 341-6.

116. Chadt, A., et al., *Molecular links between Obesity and Diabetes: "Diabesity",* in *Endotext,* K.R. Feingold, et al., Editors. 2000: South Dartmouth (MA).

117. Kahn, S.E., R.L. Hull, and K.M. Utzschneider, *Mechanisms linking obesity to insulin resistance and type 2 diabetes.* Nature, 2006. **444**(7121): p. 840-6.

118. Coleman, D.L. and K.P. Hummel, *The influence of genetic background on the expression of the obese (Ob) gene in the mouse.* Diabetologia, 1973. **9**(4): p. 287-93.

119. Linder, C.C., *Genetic variables that influence phenotype.* ILAR J, 2006. **47**(2): p. 132-40.

120. Hudish, L.I., J.E. Reusch, and L. Sussel, *beta Cell dysfunction during progression of metabolic syndrome to type 2 diabetes.* J Clin Invest, 2019. **129**(10): p. 4001-4008.

121. Fu, Z., E.R. Gilbert, and D. Liu, *Regulation of insulin synthesis and secretion and pancreatic Beta-cell dysfunction in diabetes.* Curr Diabetes Rev, 2013. **9**(1): p. 25-53.

122. Corbin, K.L., et al., *A Practical Guide to Rodent Islet Isolation and Assessment Revisited.* Biol Proced Online, 2021. **23**(1): p. 7.

123. Jones, A.G. and A.T. Hattersley, *The clinical utility of C-peptide measurement in the care of patients with diabetes.* Diabet Med, 2013. **30**(7): p. 803-17.

124. Hudak, S., et al., *Reproducibility and discrimination of different indices of insulin sensitivity and insulin secretion.* PLoS One, 2021. **16**(10): p. e0258476.

125. Burchfield, J.G., et al., *High dietary fat and sucrose results in an extensive and time-dependent deterioration in health of multiple physiological systems in mice.* J Biol Chem, 2018. **293**(15): p. 5731-5745.

126. Turner, N., et al., *Distinct patterns of tissue-specific lipid accumulation during the induction of insulin resistance in mice by high-fat feeding.* Diabetologia, 2013. **56**(7): p. 1638-48.

127. Abel, E.D., et al., *Adipose-selective targeting of the GLUT4 gene impairs insulin action in muscle and liver.* Nature, 2001. **409**(6821): p. 729-33.

128. Chadt, A., et al., *Deletion of both Rab-GTPase-activating proteins TBC14KO and TBC1D4 in mice eliminates insulin- and AICAR-stimulated glucose transport. Diabetes 2015;64:746-759.* Diabetes, 2015. **64**(4): p. 1492.

129. Nishiumi, S. and H. Ashida, *Rapid preparation of a plasma membrane fraction from adipocytes and muscle cells: application to detection of translocated glucose transporter 4 on the plasma membrane.* Biosci Biotechnol Biochem, 2007. **71**(9): p. 2343-6.

130. Lee, M.J., Y. Wu, and S.K. Fried, *Adipose tissue heterogeneity: implication of depot differences in adipose tissue for obesity complications.* Mol Aspects Med, 2013. **34**(1): p. 1-11.

131. Preis, S.R., et al., *Abdominal subcutaneous and visceral adipose tissue and insulin resistance in the Framingham heart study.* Obesity (Silver Spring), 2010. **18**(11): p. 2191-8.

132. Ross, R., et al., *Abdominal adiposity and insulin resistance in obese men.* Am J Physiol Endocrinol Metab, 2002. **282**(3): p. E657-63.

133. Shi, H., et al., *The effect of fat removal on glucose tolerance is depot specific in male and female mice.* Am J Physiol Endocrinol Metab, 2007. **293**(4): p. E1012-20.

134. Veilleux, A., et al., *Visceral adipocyte hypertrophy is associated with dyslipidemia independent of body composition and fat distribution in women.* Diabetes, 2011. **60**(5): p. 1504-11.

135. Laurencikiene, J., et al., *Regulation of lipolysis in small and large fat cells of the same subject.* J Clin Endocrinol Metab, 2011. **96**(12): p. E2045-9.

136. Skurk, T., et al., *Relationship between adipocyte size and adipokine expression and secretion.* J Clin Endocrinol Metab, 2007. **92**(3): p. 1023-33.

137. Kim, J.I., et al., *Lipid-overloaded enlarged adipocytes provoke insulin resistance independent of inflammation.* Mol Cell Biol, 2015. **35**(10): p. 1686-99.

138. Saini, V., *Molecular mechanisms of insulin resistance in type 2 diabetes mellitus.* World J Diabetes, 2010. **1**(3): p. 68-75.

139. Schinner, S., et al., *Molecular mechanisms of insulin resistance.* Diabet Med, 2005. **22**(6): p. 674-82.

140. Hatting, M., et al., *Insulin regulation of gluconeogenesis.* Ann N Y Acad Sci, 2018. **1411**(1): p. 21-35.

141. Horbelt, T., et al., *The novel adipokine WISP1 associates with insulin resistance and impairs insulin action in human myotubes and mouse hepatocytes.* Diabetologia, 2018. **61**(9): p. 2054-2065.

142. Chen, G., et al., *Additive genetic effect of GCKR, G6PC2, and SLC30A8 variants on fasting glucose levels and risk of type 2 diabetes.* PLoS One, 2022. **17**(6): p. e0269378.

143. Rossetti, L., et al., *Abnormal regulation of HGP by hyperglycemia in mice with a disrupted glucokinase allele.* Am J Physiol, 1997. **273**(4): p. E743-50.

144. Draghici, S., et al., *Reliability and reproducibility issues in DNA microarray measurements.* Trends Genet, 2006. **22**(2): p. 101-9.

145. Delpero, M., et al., *QTL-mapping in the obese Berlin Fat Mouse identifies additional candidate genes for obesity and fatty liver disease.* Sci Rep, 2022. **12**(1): p. 10471.

146. Jonas, W., et al., *Identification of Novel Genes Involved in Hyperglycemia in Mice.* Int J Mol Sci, 2022. **23**(6).

147. Balakirev, E.S. and F.J. Ayala, *Pseudogenes: are they "junk" or functional DNA?* Annu Rev Genet, 2003. **37**: p. 123-51.

148. Pink, R.C., et al., *Pseudogenes: pseudo-functional or key regulators in health and disease?* RNA, 2011. **17**(5): p. 792-8.

149. Drake, T.A., et al., *Integrating genetic and gene expression data to study the metabolic syndrome and diabetes in mice.* Am J Ther, 2005. **12**(6): p. 503-11.

150.   Moller, D.E., et al., *Tissue-specific expression of two alternatively spliced insulin receptor mRNAs in man.* Mol Endocrinol, 1989. **3**(8): p. 1263-9.

151.   Escribano, O., et al., *The Role of Insulin Receptor Isoforms in Diabetes and Its Metabolic and Vascular Complications.* J Diabetes Res, 2017. **2017**: p. 1403206.

152.   Shah, S.H., et al., *Branched-chain amino acid levels are associated with improvement in insulin resistance with weight loss.* Diabetologia, 2012. **55**(2): p. 321-30.

153.   Wang, T.J., et al., *Metabolite profiles and the risk of developing diabetes.* Nat Med, 2011. **17**(4): p. 448-53.

154.   Lackey, D.E., et al., *Regulation of adipose branched-chain amino acid catabolism enzyme expression and cross-adipose amino acid flux in human obesity.* Am J Physiol Endocrinol Metab, 2013. **304**(11): p. E1175-87.

155.   Serralde-Zuniga, A.E., et al., *Omental adipose tissue gene expression, gene variants, branched-chain amino acids, and their relationship with metabolic syndrome and insulin resistance in humans.* Genes Nutr, 2014. **9**(6): p. 431.

156.   Ramsay, R.R. and V.A. Zammit, *Carnitine acyltransferases and their influence on CoA pools in health and disease.* Mol Aspects Med, 2004. **25**(5-6): p. 475-93.

157.   Muoio, D.M., et al., *Muscle-specific deletion of carnitine acetyltransferase compromises glucose tolerance and metabolic flexibility.* Cell Metab, 2012. **15**(5): p. 764-77.

158.   Seiler, S.E., et al., *Obesity and lipid stress inhibit carnitine acetyltransferase activity.* J Lipid Res, 2014. **55**(4): p. 635-44.

159.   Ponsuksili, S., et al., *Genetic architecture and regulatory impact on hepatic microRNA expression linked to immune and metabolic traits.* Open Biol, 2017. **7**(11).

160.   Bonfanti, G., et al., *delta-Aminolevulinate dehydratase activity in type 2 diabetic patients and its association with lipid profile and oxidative stress.* Clin Biochem, 2011. **44**(13): p. 1105-1109.

161.   Jaffe, E.K. and L. Stith, *ALAD porphyria is a conformational disease.* Am J Hum Genet, 2007. **80**(2): p. 329-37.

162.   Sassa, S., *ALAD porphyria.* Semin Liver Dis, 1998. **18**(1): p. 95-101.

163.   Hepler, C., L. Vishvanath, and R.K. Gupta, *Sorting out adipocyte precursors and their role in physiology and disease.* Genes Dev, 2017. **31**(2): p. 127-140.

164.   Lim, S., J. Honek, and Y. Cao, *Blood Vessels in White and Brown Adipose Tissues*, in *Angiogenesis in Adipose Tissue*, Y. Cao, Editor. 2013, Springer New York: New York, NY. p. 77-102.

165.   Dang, T.T.H. and J.W. Yun, *Cytochrome P450 2E1 (CYP2E1) positively regulates lipid catabolism and induces browning in 3T3-L1 white adipocytes.* Life Sci, 2021. **278**: p. 119648.

166.   Moreno-Navarrete, J.M., et al., *Heme Biosynthetic Pathway is Functionally Linked to Adipogenesis via Mitochondrial Respiratory Activity.* Obesity (Silver Spring), 2017. **25**(10): p. 1723-1733.

167.   Choudhary, A.K., et al., *Administration of heme arginate ameliorates murine type 2 diabetes independently of heme oxygenase activity.* PLoS One, 2013. **8**(10): p. e78209.

168.   Saliu, J.A., et al., *Dietary supplementation of jute leaf (Corchorus olitorius) modulates hepatic delta-aminolevulinic acid dehydratase (delta-ALAD) activity and oxidative status in high-fat fed/low streptozotocin-induced diabetic rats.* J Food Biochem, 2019. **43**(8): p. e12949.

169.   Ingenious *Mouse Cell Line*. 2018.

170.   Dufait, I., et al., *Retroviral and lentiviral vectors for the induction of immunological tolerance.* Scientifica (Cairo), 2012. **2012**.

171. Ofman, R., et al., *Proteomic analysis of mouse kidney peroxisomes: identification of RP2p as a peroxisomal nudix hydrolase with acyl-CoA diphosphatase activity.* Biochem J, 2006. **393**(Pt 2): p. 537-43.

172. Leonardi, R., et al., *Coenzyme A: back in action.* Prog Lipid Res, 2005. **44**(2-3): p. 125-53.

173. Perry, R.J., et al., *Hepatic acetyl CoA links adipose tissue inflammation to hepatic insulin resistance and type 2 diabetes.* Cell, 2015. **160**(4): p. 745-758.

174. Gorigk, S., et al., *Nudix hydrolase NUDT19 regulates mitochondrial function and ATP production in murine hepatocytes.* Biochim Biophys Acta Mol Cell Biol Lipids, 2022. **1867**(6): p. 159153.

175. Jelenik, T., et al., *Mechanisms of Insulin Resistance in Primary and Secondary Nonalcoholic Fatty Liver.* Diabetes, 2017. **66**(8): p. 2241-2253.

176. Koliaki, C., et al., *Adaptation of hepatic mitochondrial function in humans with non-alcoholic fatty liver is lost in steatohepatitis.* Cell Metab, 2015. **21**(5): p. 739-46.

177. Park, B.Y., et al., *PDK4 Deficiency Suppresses Hepatic Glucagon Signaling by Decreasing cAMP Levels.* Diabetes, 2018. **67**(10): p. 2054-2068.

178. Shannon, C.E., et al., *Insulin resistance is mechanistically linked to hepatic mitochondrial remodeling in non-alcoholic fatty liver disease.* Mol Metab, 2021. **45**: p. 101154.

179. Reifsnyder, P.C., G. Churchill, and E.H. Leiter, *Maternal environment and genotype interact to establish diabesity in mice.* Genome Res, 2000. **10**(10): p. 1568-78.

180. Su, Z., et al., *Genetic linkage of hyperglycemia, body weight and serum amyloid-P in an intercross between C57BL/6 and C3H apolipoprotein E-deficient mice.* Hum Mol Genet, 2006. **15**(10): p. 1650-8.

181. Vogel, H., et al., *Characterization of Nob3, a major quantitative trait locus for obesity and hyperglycemia on mouse chromosome 1.* Physiol Genomics, 2009. **38**(2): p. 226-32.

182. Taylor, B.A., L.M. Tarantino, and S.J. Phillips, *Gender-influenced obesity QTLs identified in a cross involving the KK type II diabetes-prone mouse strain.* Mamm Genome, 1999. **10**(10): p. 963-8.

183. Smith Richards, B.K., et al., *QTL analysis of self-selected macronutrient diet intake: fat, carbohydrate, and total kilocalories.* Physiol Genomics, 2002. **11**(3): p. 205-17.

184. Kayo, T., et al., *Identification of two chromosomal loci determining glucose intolerance in a C57BL/6 mouse strain.* Comp Med, 2000. **50**(3): p. 296-302.

185. Kobayashi, M., et al., *Major quantitative trait locus on chromosome 2 for glucose tolerance in diabetic SMXA-5 mouse established from non-diabetic SM/J and A/J strains.* Diabetologia, 2006. **49**(3): p. 486-95.

186. Delpero, M., et al., *Identification of four novel QTL linked to the metabolic syndrome in the Berlin Fat Mouse.* Int J Obes (Lond), 2022. **46**(2): p. 307-315.

187. Togawa, K., et al., *Multidimensional genome scans identify the combinations of genetic loci linked to diabetes-related phenotypes in mice.* Hum Mol Genet, 2006. **15**(1): p. 113-28.

188. Zhang, Z., et al., *Genetic analysis of atherosclerosis and glucose homeostasis in an intercross between C57BL/6 and BALB/cJ apolipoprotein E-deficient mice.* Circ Cardiovasc Genet, 2012. **5**(2): p. 190-201.

189. Collin, G.B., et al., *Genetic modifiers interact with Cpe(fat) to affect body weight, adiposity, and hyperglycemia.* Physiol Genomics, 2005. **22**(2): p. 182-90.

190. Ueda, H., et al., *Genetic analysis of late-onset type 2 diabetes in a mouse model of human complex trait.* Diabetes, 1999. **48**(5): p. 1168-74.

191. Shike, T., et al., *Susceptibility and negative epistatic loci contributing to type 2 diabetes and related phenotypes in a KK/Ta mouse model.* Diabetes, 2001. **50**(8): p. 1943-8.

192. Suto, J., et al., *Genetic analysis of non-insulin-dependent diabetes mellitus in KK and KK-Ay mice.* Eur J Endocrinol, 1998. **139**(6): p. 654-61.

193. Toye, A.A., et al., *A genetic and physiological study of impaired glucose homeostasis control in C57BL/6J mice.* Diabetologia, 2005. **48**(4): p. 675-86.

194. Hirayama, I., et al., *Genetic analysis of obese diabetes in the TSOD mouse.* Diabetes, 1999. **48**(5): p. 1183-91.

195. Almind, K., et al., *Identification of interactive loci linked to insulin and leptin in mice with genetic insulin resistance.* Diabetes, 2003. **52**(6): p. 1535-43.

196. Su, Z., et al., *Candidate genes for plasma triglyceride, FFA, and glucose revealed from an intercross between inbred mouse strains NZB/B1NJ and NZW/LacJ.* J Lipid Res, 2008. **49**(7): p. 1500-10.

197. Shi, L.J., et al., *Genetic Evidence for a Causal Relationship between Hyperlipidemia and Type 2 Diabetes in Mice.* Int J Mol Sci, 2022. **23**(11).

198. Kim, J.H., et al., *Genetic analysis of a new mouse model for non-insulin-dependent diabetes.* Genomics, 2001. **74**(3): p. 273-86.

199. Metsalu, T. and J. Vilo, *ClustVis: a web tool for visualizing clustering of multivariate data using Principal Component Analysis and heatmap.* Nucleic Acids Res, 2015. **43**(W1): p. W566-70.

6. Supplement

6.1.1 Supplementary tables

Suppl. Tab. 1: Identified blood glucose-related QTL in mouse crossbreeding approaches. Most prominent susceptibility loci with linkage to glucose homeostasis (LOD > 3.0) identified in male mice with indication of the used animal model and chromosomal location. BG=blood glucose, FBG=fasted blood glucose, PI=plasma insulin, PaI=pancreatic insulin, IPGTT=intraperitoneal glucose tolerance test.

QTL/Locus	Chr.	Trait	Max. LOD	Mouse Cross	Reference
D1Mit123	1	BG/PI	4.92	NON/Lt x NZO/HILt	[179]
Bglu3	1	FBG	4.1	C57BL/6J x C3H/He	[180]
Nob3	1	BG/BW	4.0	C57BL/6J x NZO/HI	[181]
D1Mit425	1	FBG	3.6	KK/H1L1 x C57BL/6J	[182]
Kcal3	2	BG	3.2	C57BL/6J x CAST/EiJ	[183]
D2Mit48	2	PI/IPGTT	8.3	C57BL/6J x C3H/He	[184]
T2dm2sa	2	FBG/BG/IPGTT	12.6	SM/J x SMXA/5	[185]
Gatq1	3	BG	4.2	BFMI861	[186]
D4Mit171	4	IPGTT	5.44	C57BL/KsJ x DBA/2	[187]
Nbg4	4	BG/FBG	7.4	NZO/HI x 129P2/OlaHsd	[95]
Nidd1	4	BG/PI	6.5	NZO/HI x NON/Lt	[93]
Nidd/SJL	4	BG	3.6	NZO/HI x SJL/N	[94]
Nbg4	4	BG/PI/PaI	6.6	NZO/HI x C3H/He	[95]
D4Mit42	4	IPGTT	5.08	C57BL/KsJ x DBA/2	[187]
Nidd/DBA	4	BG/PI/PaI	8.0	NZO/HI x DBA/2	[87]
Bglu13	5	FBG	6.72	C57BL/6J x BALB/cJ	[188]
Find2	5	BG	6.99	C57BL/KsJ x HRS/J	[189]
Nidd3nsy	6	PI/IPGTT	4.69	NSY x C3H/He	[190]
Igt-1	6	IPGTT/PI	4.0	KK/Ta x BALB/cJ	[191]
D6Mit266	6	FBG	6.0	KK/Ay x C57BL/6J	[192]
Nbg7	7	BG/PI	13.3	NZO/HI x C3H/He	[95]
D8Mit155	8	BG/IPGTT	4.67	C57BL/KsJ x DBA/2	[187]
Giq1	8	IPGTT	5.6	KK/Ay x C57BL/6J	[192]
Mnif1	8	BG	4.8	C57BL/6J x CAST/EiJ	[183]
D8Mit4	8	IPGTT	4.10	C57BL/KsJ x DBA/2	[187]
Gluchos3	9	PI	6.7	C57BL/6J x C3H/He	[193]
D10Mit136	10	BG	3.8	SM/J x A/J	[185]
Nidd4	11	IPGTT	9.19	TSOD x BALB/cA	[194]
Gluchos2	11	FBG	5.2	C57BL/6J x C3H/He	[193]
Nidd1nsy	11	FBG/PI/IPGTT	9.5	NSY x C3H/He	[190]
Fbg-1	12	FBG/IPGTT	4.5	KK/Ta x BALB/c	[191]
D13Mit48	13	IPGTT	4.2	C57BL/6J x C3H/He	[184]
Gluchos1	13	IPGTT	5.0	C57BL/6J x C3H/He	[193]
Nidd13/NZO	13	BG/PaI	6.2	C57BL/6J x NZO/HI	[146]
D14Mit55	14	BG/PI	5.6	C57BL/6J x 129S6/SvEvTac	[195]

QTL/Locus	Chr.	Trait	Max. LOD	Mouse Cross	Reference
Nidd2nsy	14	PI/IPGTT	4.88	NSY x C3H/He	[190]
D15Mit159	15	BG	3.55	NON/Lt x NZO/HILt	[179]
Dbm4	15	IPGTT	6.17	Akita x A/J	[115]
D15Mit13	15	FBG/PI	3.3	C57BL/6J x 129S6/SvEvTac	[67]
Bglu8	15	BG	4.3	LP/J x BALB/cJ	[196]
Bglu20	15	FBG/BG	7.03	LP/J x BALB/cJ	[197]
Nbg15	15	BG	6.7	NZO/HI x C3H/He	[95]
Fbg-2	15	FBG	3.3	KK/Ta x BALB/cJ	[191]
D16Mit103	16	IPGTT	3.76	C57BL/KsJ x DBA/2	[187]
Gatlgq	17	BG	8.0	BFMI861	[186]
Kcal1	18	BG	4.4	C57BL/6J x CAST/EiJ	[183]
Nidd2	18	BG	5.0	NZO/HI x NON/Lt	[93]
Tanidd1	19	BG	3.1	TallyHo x C57BL/6J	[198]
Mnic3	X	BG	5.7	C57BL/6J x CAST/EiJ	[183]

Suppl. Tab. 2: Summary data from mouse phenotyping of RCS.NZOx129Ola-*Nbg4p* on SD. BG=blood glucose, FBG=fasted blood glucose, FPI=fasted plasma insulin, BW=body weight, SD=standard diet.

Phenotype	Age	*Nbg4p*N/N		*Nbg4p*O/O		N/N vs. O/O
		Mean	±SEM	Mean	±SEM	p-value
BG (mg/dL)	3	193,27	5,06	161,40	9,77	**0,012**
BG (mg/dL)	4	189,91	6,79	212,60	8,46	0,051
BG (mg/dL)	5	190,73	5,88	229,80	6,20	**0,000**
BG (mg/dL)	6	177,73	7,74	197,10	18,57	0,355
BG (mg/dL)	7	159,18	5,13	207,80	15,22	**0,011**
BG (mg/dL)	8	172,27	7,26	179,90	14,97	0,654
BG (mg/dL)	9	157,55	4,78	179,60	9,19	0,052
BG (mg/dL)	10	139,55	5,18	123,10	4,44	**0,026**
BG (mg/dL)	11	151,55	3,35	183,80	13,04	**0,037**
BG (mg/dL)	12	160,82	8,27	155,30	5,57	0,587
BG (mg/dL)	13	167,09	6,19	146,80	5,60	**0,025**
BG (mg/dL)	14	148,45	5,54	162,60	6,64	0,119
BG (mg/dL)	15	170,36	3,17	143,60	6,69	**0,003**
BG (mg/dL)	16	140,27	3,59	145,10	4,05	0,384
BG (mg/dL)	17	116,82	3,74	168,60	11,32	**0,001**
BG (mg/dL)	18	136,18	2,06	210,00	11,74	**0,000**
BG (mg/dL)	19	147,91	5,85	218,20	23,66	**0,016**
BG (mg/dL)	20	168,55	6,34	153,20	13,58	0,325
BG (mg/dL)	21	179,00	5,68	157,90	10,69	0,104
FBG (mg/dL)	21	148,45	5,41	180,50	11,20	**0,023**
FPI (µg/L)	21	1,70	0,34	3,09	0,50	**0,038**
BW (g)	3	16,02	0,93	13,14	0,93	**0,042**
BW (g)	4	22,76	0,87	20,37	0,93	0,075
BW (g)	5	24,75	0,97	27,01	0,63	0,067
BW (g)	6	29,92	0,79	31,28	0,66	0,205
BW (g)	7	31,88	0,73	34,15	0,62	**0,029**
BW (g)	8	33,67	0,73	36,52	0,66	**0,009**
BW (g)	9	35,32	0,83	38,55	0,93	**0,018**

BW (g)	10	37,24	0,91	40,86	0,92	**0,011**
BW (g)	11	38,31	0,89	42,67	0,85	**0,002**
BW (g)	12	39,72	0,87	43,49	0,75	**0,004**
BW (g)	13	40,33	1,07	44,47	0,79	**0,006**
BW (g)	14	41,76	1,04	45,22	0,71	**0,013**
BW (g)	15	42,00	1,12	47,44	0,84	**0,001**
BW (g)	16	42,85	1,13	47,56	0,86	**0,004**
BW (g)	17	44,07	1,11	49,32	0,99	**0,002**
BW (g)	18	44,63	1,20	49,88	0,91	**0,003**
BW (g)	19	45,97	1,25	50,39	0,94	**0,011**
BW (g)	20	46,30	1,31	51,76	0,96	**0,003**
BW (g)	21	47,15	1,33	52,49	0,96	**0,004**
Lean mass (g)	3	13,17	0,66	10,67	0,74	**0,021**
Lean mass (g)	6	23,64	0,59	25,05	0,86	0,195
Lean mass (g)	10	27,61	0,90	30,50	0,50	**0,013**
Lean mass (g)	15	28,88	0,73	31,54	0,42	**0,006**
Fat mass (g)	3	2,37	0,25	2,13	0,25	0,516
Fat mass (g)	6	5,09	0,28	5,75	0,43	0,225
Fat mass (g)	10	9,11	0,56	9,10	0,44	0,981
Fat mass (g)	15	11,78	0,73	13,69	0,55	0,052

1.

Suppl. Tab. 3: Summary data from mouse phenotyping of RCS.NZOx129Ola-*Nbg4d* on SD. BG=blood glucose, FBG=fasted blood glucose, FPI=fasted plasma insulin, BW=body weight, SD=standard diet.

Phenotype	Age	*Nbg4d*^{N/N}		*Nbg4d*^{O/O}		N/N vs. O/O
		Mean	±SEM	Mean	±SEM	p-value
BG (mg/dL)	3	140,73	5,90	159,10	4,57	**0,024**
BG (mg/dL)	4	168,64	2,85	173,90	5,03	0,378
BG (mg/dL)	5	187,18	6,94	187,20	5,50	0,998
BG (mg/dL)	6	167,45	7,86	170,00	12,13	0,863
BG (mg/dL)	7	151,27	7,89	155,00	6,08	0,713
BG (mg/dL)	8	134,91	9,43	150,11	7,32	0,219
BG (mg/dL)	9	144,73	8,75	199,44	11,06	**0,001**
BG (mg/dL)	10	153,09	14,96	197,89	17,33	0,067
BG (mg/dL)	11	161,82	12,86	145,44	10,55	0,338
BG (mg/dL)	12	115,82	11,24	151,33	12,54	**0,050**
BG (mg/dL)	13	122,91	9,27	139,44	8,09	0,196
BG (mg/dL)	14	133,82	8,32	145,00	4,80	0,262
BG (mg/dL)	15	151,36	17,22	164,11	27,06	0,697
BG (mg/dL)	16	110,27	7,76	140,00	5,63	**0,006**
BG (mg/dL)	17	130,00	13,16	142,67	8,06	0,424
BG (mg/dL)	18	121,09	10,45	147,67	8,60	0,065
BG (mg/dL)	19	117,91	9,52	156,89	16,82	0,065
BG (mg/dL)	20	112,00	7,79	178,78	17,67	**0,005**
BG (mg/dL)	21	127,73	8,92	163,22	16,10	0,076
FBG (mg/dL)	21	125,18	10,08	139,33	12,51	0,391
FPI (µg/L)	21	2,61	0,50	1,44	0,30	0,065
BW (g)	3	14,49	0,43	14,32	0,46	0,791
BW (g)	4	20,26	0,47	21,53	0,73	0,163
BW (g)	5	26,33	0,78	26,40	0,40	0,935
BW (g)	6	30,47	0,48	30,33	0,26	0,799
BW (g)	7	33,24	0,45	32,61	0,41	0,321
BW (g)	8	35,80	0,47	35,06	0,49	0,288
BW (g)	9	38,52	0,48	36,49	0,74	**0,036**
BW (g)	10	39,38	0,61	37,37	0,57	**0,026**

BW (g)	11	40,57	0,55	38,92	0,64	0,066
BW (g)	12	41,32	0,65	39,31	0,78	0,063
BW (g)	13	42,86	0,95	40,98	0,91	0,168
BW (g)	14	43,13	0,90	41,22	0,47	0,079
BW (g)	15	44,26	0,88	41,72	0,67	**0,033**
BW (g)	16	46,19	1,01	42,08	1,01	**0,010**
BW (g)	17	46,54	1,13	43,11	1,18	0,051
BW (g)	18	47,32	1,31	44,46	1,03	0,104
BW (g)	19	48,26	1,29	46,52	1,36	0,366
BW (g)	20	49,18	1,28	47,70	1,71	0,499
BW (g)	21	49,78	1,41	48,08	1,73	0,456
Lean mass (g)	3	11,79	0,36	11,74	0,46	0,930
Lean mass (g)	6	24,53	0,31	24,69	0,48	0,783
Lean mass (g)	10	27,98	0,58	28,64	0,69	0,469
Lean mass (g)	15	30,85	0,65	31,57	0,44	0,373
Fat mass (g)	3	2,51	0,15	2,51	0,14	0,971
Fat mass (g)	6	5,10	0,28	4,90	0,21	0,577
Fat mass (g)	10	8,45	0,36	7,26	0,34	**0,027**
Fat mass (g)	15	10,56	0,53	8,46	0,55	**0,013**

Suppl. Tab. 4: Summary data from mouse phenotyping of RCS.NZOx129Ola-*Nbg4c* on SD. BG=blood glucose, FBG=fasted blood glucose, FPI=fasted plasma insulin, BW=body weight, SD=standard diet.

Phenotype	Age	*Nbg4c*[N/N]		*Nbg4c*[O/O]		N/N vs. O/O
		Mean	±SEM	Mean	±SEM	p-value
BG (mg/dL)	3	150,73	8,13	151,70	3,62	0,914
BG (mg/dL)	4	180,36	6,00	178,10	6,91	0,807
BG (mg/dL)	5	165,73	9,41	191,20	8,88	0,064
BG (mg/dL)	6	157,18	6,71	163,30	9,27	0,600
BG (mg/dL)	7	156,73	9,57	179,00	8,72	0,102
BG (mg/dL)	8	145,18	4,27	155,00	11,91	0,454
BG (mg/dL)	9	161,18	11,05	145,50	8,67	0,279
BG (mg/dL)	10	166,36	10,81	145,60	7,95	0,139
BG (mg/dL)	11	164,82	8,05	148,70	3,89	0,093
BG (mg/dL)	12	151,82	4,98	153,10	3,45	0,835
BG (mg/dL)	13	181,45	21,81	189,30	12,79	0,760
BG (mg/dL)	14	164,45	6,15	152,20	17,30	0,518
BG (mg/dL)	15	141,73	10,51	118,70	3,77	0,061
BG (mg/dL)	16	174,27	16,59	140,80	8,83	0,095
BG (mg/dL)	17	186,18	21,85	149,90	12,02	0,166
BG (mg/dL)	18	142,73	5,21	147,60	9,04	0,647
BG (mg/dL)	19	147,00	6,99	156,30	13,52	0,551
BG (mg/dL)	20	132,73	7,22	172,40	10,55	**0,007**
BG (mg/dL)	21	141,00	7,65	152,90	6,19	0,242
FBG (mg/dL)	21	131,91	8,23	116,10	8,20	0,190
FPI (µg/L)	21	1,34	0,19	1,09	0,25	0,447
BW (g)	3	13,67	0,74	12,02	0,53	0,100
BW (g)	4	15,33	1,12	16,28	0,73	0,486
BW (g)	5	23,07	1,19	24,27	0,74	0,405
BW (g)	6	27,71	0,94	28,59	0,78	0,479
BW (g)	7	30,09	1,16	31,26	0,76	0,410
BW (g)	8	32,04	0,98	32,90	0,86	0,517
BW (g)	9	35,21	0,80	34,33	0,76	0,435
BW (g)	10	36,75	0,88	36,18	0,84	0,647
BW (g)	11	37,51	0,90	37,23	0,98	0,836

BW (g)	12	38,03	0,80	37,07	0,99	0,461
BW (g)	13	40,28	0,73	38,11	0,97	0,092
BW (g)	14	40,19	0,83	38,39	1,03	0,189
BW (g)	15	40,83	0,93	38,93	1,05	0,192
BW (g)	16	41,32	0,87	40,63	0,94	0,597
BW (g)	17	42,81	1,10	41,54	1,05	0,414
BW (g)	18	44,17	1,21	42,13	1,20	0,245
BW (g)	19	45,46	1,26	43,04	1,25	0,189
BW (g)	20	46,53	1,30	44,08	1,21	0,184
BW (g)	21	46,59	1,23	45,41	1,47	0,546
Lean mass (g)	3	10,49	0,35	9,43	0,66	0,175
Lean mass (g)	6	20,89	1,35	23,82	0,62	0,069
Lean mass (g)	10	29,41	0,94	28,98	0,65	0,708
Lean mass (g)	15	30,62	0,64	29,30	0,63	0,159
Fat mass (g)	3	2,36	0,29	1,91	0,22	0,234
Fat mass (g)	6	5,49	0,46	4,85	0,26	0,245
Fat mass (g)	10	6,48	0,53	6,93	0,65	0,601
Fat mass (g)	15	6,68	0,43	7,43	0,86	0,449

Suppl. Tab. 3: Summary data from mouse phenotyping of RCS.NZO.129Ola-*Nbg4p* on HFD. BG=blood glucose, FBG=fasted blood glucose, FPI=fasted plasma insulin, BW=body weight, HFD=high-fat diet.

Phenotype	Age	*Nbg4p*^{N/N}		*Nbg4p*^{O/O}		N/N vs. O/O
		Mean	±SEM	Mean	±SEM	p-value
BG (mg/dL)	3	158.58	5.96	146.00	3.28	0.070
BG (mg/dL)	4	183.76	4.58	193.36	9.83	0.380
BG (mg/dL)	5	227.91	9.29	287.00	15.72	**0.002****
BG (mg/dL)	6	244.18	15.98	305.00	20.29	**0.022***
BG (mg/dL)	7	217.69	25.37	258.58	43.66	0.429
BG (mg/dL)	8	268.15	30.52	322.08	38.78	0.287
BG (mg/dL)	9	311.62	34.77	351.42	42.25	0.475
BG (mg/dL)	10	310.54	35.48	361.42	41.66	0.363
BG (mg/dL)	11	322.92	22.71	378.75	41.24	0.252
BG (mg/dL)	12	384.69	36.66	391.33	40.18	0.904
BG (mg/dL)	13	360.85	36.23	403.75	39.40	0.431
BG (mg/dL)	14	291.23	44.06	335.33	51.51	0.522
BG (mg/dL)	15	309.46	49.80	399.75	41.98	0.179
BG (mg/dL)	16	323.38	45.70	389.75	43.43	0.303
BG (mg/dL)	17	268.20	49.29	348.22	50.13	0.271
BG (mg/dL)	18	333.80	41.47	370.88	48.76	0.571
FBG (mg/dL)	6	137.28	5.74	137.53	6.25	0.952
FBG (mg/dL)	18	265.25	46.93	325.73	47.36	0.375
FPI (µg/L)	6	4.65	0.49	7.92	1.07	**0.010****
FPI (µg/L)	18	9.49	3.41	7.34	2.10	0.601
BW (g)	3	13.48	0.63	14.50	0.75	0.309
BW (g)	4	21.23	0.74	23.93	1.07	0.053
BW (g)	5	30.79	0.59	32.66	0.62	**0.039***
BW (g)	6	34.67	0.68	37.00	0.80	**0.037***
BW (g)	7	37.14	0.77	38.78	0.69	0.130
BW (g)	8	41.23	0.86	41.43	0.67	0.856
BW (g)	9	45.71	0.79	45.17	0.63	0.599
BW (g)	10	47.75	0.90	46.95	0.72	0.496
BW (g)	11	50.40	0.86	49.38	0.76	0.385
BW (g)	12	51.58	0.97	50.77	0.94	0.553
BW (g)	13	54.70	0.99	53.48	1.14	0.427
BW (g)	14	55.42	1.22	53.81	1.38	0.392
BW (g)	15	57.25	1.15	56.19	1.58	0.593
BW (g)	16	57.98	1.19	56.47	1.53	0.443

BW (g)	17	60.80	1.85	59.21	2.31	0.599
BW (g)	18	63.19	1.86	62.39	2.76	0.813
Lean mass (g)	3	10.50	0.20	10.89	0.52	0.488
Lean mass (g)	6	25.42	0.35	25.95	0.32	0.273
Lean mass (g)	9	29.27	0.35	29.19	0.39	0.893
Lean mass (g)	15	32.09	0.32	31.12	0.42	0.082
Fat mass (g)	3	2.51	0.24	2.63	0.11	0.667
Fat mass (g)	6	8.64	0.25	10.43	0.38	**0.001***
Fat mass (g)	9	15.45	0.49	14.63	0.40	0.204
Fat mass (g)	15	21.10	0.91	21.31	1.41	0.900

Suppl. Tab. 5: Genes from non-IBD regions identified within *Nbg4p* by haplotype mapping. All genes were predicted to harbour at least one polymorphic SNP for the 129P2/OlaHsd mouse strain when compared to NZO/HILtJ and C56BL/6J as a reference strain.

SNP-position	Gene	SNP-position	Gene
41317187	Dcaf12	46118124	7SK
41345163	Ubap1	46138721	Ncbp1
41393731	Kif24	46150456	Xpa
41480364	Nudt2	47242533	Col15a1
41490744	AI464131	47349768	Tgfbr1
41500136	Cbe1	48040221	Nr4a3
41517844	Fam219	48120132	Stx17
41637136	Dnaic1	48188385	Erp44
41638189	Enho	48208204	Mir1958
41652646	Cntfr	48279821	Invs
41707167	Rpp25l	48437441	Tex10
41713332	Dctn3	48539512	Msantd3
41719706	Arid3c	48580408	Tmeff1
41737060	Sigmar1	48658623	Murc
41755254	Galt	49387451	Acnat2
41758966	Il11ra1	49529510	Zfp189
41772113	Ccl27a	49532394	Aldob
42856595	Fam205a1	49579852	Tmem246
42865197	Fam205c	49632446	Rnf20
42911665	Phf24	49658444	Grin3a
42944832	Dnajb5	57190887	Ptpn3
42965587	1700022I11Rik	57359882	1700042G15Rik
43007872	Fancg	57370908	Gm12537
43018839	Pigo	57429910	Palm2
43029991	Stoml2	57883115	Akap2
43034250	Atosb	57905139	D630039A03Rik
43054378	Unc13b	57939913	Txn1
43262292	Atp8b5	58008475	Txndc8
43735420	Spaar	58042909	Svep1
43762290	A630077J23Rik	58281054	Musk
43774689	Olfr159	58780659	Olfr267
43838208	Olfr157	58794035	AI314180
43846650	Olfr155	63541488	Atp6v1g1
43873243	Reck	63553995	Tmem268
43990284	Ccin	67513335	Hmgb1-rs18

44002883	Clta	70212495	Cdk5rap2
44029171	Gne	70422225	Megf9
44528484	Pax5	72112509	Tle1
44758289	Zcchc7	72845663	Aldoart1
44986228	Grhpr	73935082	2310002L09Rik
46061005	Tmod1	74008528	Frmd3
46116144	Tstd2	75944802	Ptprd

Suppl. Tab. 6: non-IBD SNPs with predicted functional impact identified by VEP-analysis. SNPs that were polymorph for the 129P2/OlaHsd mouse strain as detected by haplotype analysis of the *Nbg4p* region were analysed for variations in DNA coding and non-coding regions and their predicted impact on transcripts and protein level.

Location	SNP	Gene	Consequence	Impact
4:40174579-40174579	rs27783501	*Aco1*	intron variant	MODIFIER
4:40217887-40217887	rs213114239	*Ddx58*	intron variant	MODIFIER
4:40468381-40468381	rs33008141	*Tmem215*	upstream gene variant	MODIFIER
4:40677587-40677587	rs230225108	*Aptx*	downstream gene variant	MODIFIER
4:40729974-40729974	rs262444100	*Dnaja1*	intron variant	MODIFIER
4:40805010-40805010	rs46850777	*B4galt1*	3-prime UTR variant	MODIFIER
4:40853224-40853224	rs32792552	*Mir5123*	upstream gene variant	MODIFIER
4:41025574-41025574	rs6232550	*Nfx1*	3-prime UTR variant	MODIFIER
4:41035641-41035641	rs32441413	*Aqp7*	intron variant	MODIFIER
4:41088236-41088236	rs226474289	*Aqp3*	downstream gene variant	MODIFIER
4:41128768-41128768	rs237876532	*Nol6*	upstream gene variant	MODIFIER
4:41176874-41176874	rs31921137	*Ube2r2*	intron variant	MODIFIER
4:41193652-41193652	rs28316603	*Ubap2*	downstream gene variant	MODIFIER
4:41345163-41345163	rs32368541	*Ubap1*	upstream gene variant	MODIFIER
4:41393731-41393731	rs28285052	*Kif24*	synonymous variant	LOW
4:41480364-41480364	rs13475615	*Nudt2*	synonymous variant	LOW
4:41490744-41490744	rs246964400	*AI464131*	downstream gene variant	MODIFIER
4:41500136-41500136	rs216568982	*1110017D15Rik*	downstream gene variant	MODIFIER
4:41517546-41517546	rs32507740	*Fam219a*	downstream gene variant	MODIFIER
4:41637136-41637136	rs261746152	*Enho*	downstream gene variant	MODIFIER
4:41637136-41637136	rs261746152	*Dnaic1*	intron variant	MODIFIER
4:41652646-41652646	rs3725452	*Cntfr*	downstream gene variant	MODIFIER
4:41707167-41707167	rs27813831	*Rpp25l*	downstream gene variant	MODIFIER
4:41707167-41707167	rs27813831	*Il11ra1*	intron variant	MODIFIER
4:41713332-41713332	rs27813806	*Dctn3*	downstream gene variant	MODIFIER
4:41719706-41719706	rs247941838	*Arid3c*	downstream gene variant	MODIFIER
4:41737060-41737060	rs27813770	*Sigmar1*	downstream gene variant	MODIFIER
4:41755254-41755254	rs219360050	*Galt*	5-prime UTR variant	MODIFIER
4:42856595-42856595	rs233125149	*Fam205a1*	upstream gene variant	MODIFIER
4:42865197-42865197	rs231727390	*Fam205c*	downstream gene variant	MODIFIER
4:42911665-42911665	rs32586427	*Phf24*	upstream gene variant	MODIFIER
4:42944832-42944832	rs27851433	*Dnajb5*	upstream gene variant	MODIFIER
4:43007872-43007872	rs257040578	*Fancg*	intron variant	MODIFIER
4:43054378-43054378	rs257148934	*Unc13b*	upstream gene variant	MODIFIER
4:43262292-43262292	rs32136560	*Atp8b5*	upstream gene variant	MODIFIER
4:43376980-43376980	rs256441920	*Rusc2*	upstream gene variant	MODIFIER
4:43431952-43431952	rs27849878	*Fam166b*	upstream gene variant	MODIFIER
4:43441396-43441396	rs46189450	*Tesk1*	upstream gene variant	MODIFIER
4:43556478-43556478	rs28327699	*Tln1*	intron variant	MODIFIER
4:43563117-43563117	rs13459506	*Gba2*	downstream gene variant	MODIFIER
4:43563117-43563117	rs13459506	*Creb3*	missense variant	MODERATE
4:43578921-43578921	rs28320762	*Msmp*	downstream gene variant	MODIFIER
4:43578921-43578921	rs28320762	*Rgp1*	upstream gene variant	MODIFIER
4:43631980-43631980	rs225863295	*Npr2*	5-prime UTR variant	MODIFIER

4:43685752-43685752	rs240858872	*Tmem8b*	synonymous variant	LOW
4:43694678-43694678	rs252542587	*Olfr70*	downstream gene variant	MODIFIER
4:43722642-43722642	rs225303082	*Hrct1*	upstream gene variant	MODIFIER
4:43735420-43735420	rs28311506	*Spaar*	downstream gene variant	MODIFIER
4:43767780-43767780	rs230190171	*Olfr159*	downstream gene variant	MODIFIER
4:43846650-43846650	rs31962273	*Olfr155*	upstream gene variant	MODIFIER
4:43873243-43873243	rs219519767	*Reck*	upstream gene variant	MODIFIER
4:43990284-43990284	rs31874930	*Ccin*	downstream gene variant	MODIFIER
4:44029171-44029171	rs27826129	*Gne*	downstream gene variant	MODIFIER
4:44029171-44029171	rs27826129	*Clta*	intron variant	MODIFIER
4:44126902-44126902	rs265609367	*Rnf38*	3-prime UTR variant	MODIFIER
4:44351045-44351045	rs260235244	*Melk*	missense variant	MODERATE
4:44528484-44528484	rs27845952	*Pax5*	3-prime UTR variant	MODIFIER
4:44758289-44758289	rs245416495	*Zcchc7*	upstream gene variant	MODIFIER
4:44986228-44986228	rs27846298	*Grhpr*	intron variant	MODIFIER
4:45021421-45021421	rs214832949	*Polr1e*	intron variant	MODIFIER
4:45047120-45047120	rs243649038	*Fbxo10*	intron variant	MODIFIER
4:45104212-45104212	rs220507399	*Tomm5*	downstream gene variant	MODIFIER
4:45180298-45180298	rs240501639	*Frmpd1*	upstream gene variant	MODIFIER
4:45299098-45299098	rs27877440	*Trmt10b*	intron variant	MODIFIER
4:45318730-45318730	rs27862313	*Exosc3*	intron variant	MODIFIER
4:45349776-45349776	rs32688362	*Dcaf10*	intron variant, non-coding	MODIFIER
4:45399471-45399471	rs48851109	*Slc25a51*	missense variant	MODERATE
4:45419014-45419014	rs246852090	*Shb*	downstream gene variant	MODIFIER
4:45972893-45972893	rs3694836	*Tdrd7*	intron variant	MODIFIER
4:46061005-46061005	rs47151461	*Tmod1*	5-prime UTR variant	MODIFIER
4:46116144-46116144	rs32948652	*Tstd2*	3-prime UTR variant	MODIFIER
4:46138721-46138721	rs52357748	*Ncbp1*	5-prime UTR variant	MODIFIER
4:46150456-46150456	rs27856115	*Xpa*	downstream gene variant	MODIFIER
4:46343684-46343684	rs231326942	*Foxe1*	5-prime UTR variant	MODIFIER
4:46393673-46393673	rs31920708	*Hemgn*	downstream gene variant	MODIFIER
4:46393673-46393673	rs31920708	*Trmo*	upstream gene variant	MODIFIER
4:46446106-46446106	rs240415832	*Anp32b*	upstream gene variant	MODIFIER
4:46500916-46500916	rs32310968	*Trim14*	intron variant, non-coding	MODIFIER
4:46500916-46500916	rs32310968	*Nans*	synonymous variant	LOW
4:46553484-46553484	rs262333118	*Coro2a*	intron variant	MODIFIER
4:46604672-46604672	rs32598224	*Tbc1d2*	3-prime UTR variant	MODIFIER
4:46657457-46657457	rs218810430	*Gabbr2*	downstream gene variant	MODIFIER
4:47012712-47012712	rs32121969	*Anks6*	downstream gene variant	MODIFIER
4:47097328-47097328	rs31813165	*Galnt12*	intron variant	MODIFIER
4:47242533-47242533	rs32539583	*Col15a1*	intron variant	MODIFIER
4:47349768-47349768	rs4139984	*Tgfbr1*	upstream gene variant	MODIFIER
4:47460074-47460074	rs232664787	*Alg2*	downstream gene variant	MODIFIER
4:48040221-48040221	rs260006469	*Nr4a3*	upstream gene variant	MODIFIER
4:48120132-48120132	rs256229579	*Stx17*	upstream gene variant	MODIFIER
4:48188385-48188385	rs27871427	*Erp44*	downstream gene variant	MODIFIER
4:48208204-48208204	rs27871368	*Mir1958*	downstream gene variant	MODIFIER
4:48279821-48279821	rs27856550	*Invs*	5-prime UTR variant	MODIFIER
4:48437441-48437441	rs32881494	*Tex10*	intron variant	MODIFIER
4:48539512-48539512	rs32948124	*Msantd3*	upstream gene variant	MODIFIER
4:48580408-48580408	rs32265065	*Tmeff1*	upstream gene variant	MODIFIER
4:48658623-48658623	rs48932789	*Cavin4*	upstream gene variant	MODIFIER
4:49076477-49076477	rs27812563	*Plppr1*	intron variant	MODIFIER
4:49387451-49387451	rs31809871	*Acnat2*	intron variant	MODIFIER
4:49529510-49529510	rs31866648	*Zfp189*	synonymous variant	LOW
4:49532394-49532394	rs27860603	*Aldob*	downstream gene variant	MODIFIER
4:49579852-49579852	rs27845727	*Tmem246*	downstream gene variant	MODIFIER
4:49658444-49658444	rs27822939	*Grin3a*	downstream gene variant	MODIFIER
4:49658444-49658444	rs27822939	*Rnf20*	downstream gene variant	MODIFIER
4:51212705-51212705	rs240052066	*Cylc2*	upstream gene variant	MODIFIER
4:53029716-53029716	rs255970813	*Abca1*	downstream gene variant	MODIFIER
4:53437730-53437730	rs32967863	*Slc44a1*	upstream gene variant	MODIFIER

4:54940193-54940193	rs32216692	*Zfp462*	upstream gene variant	MODIFIER
4:55345104-55345104	rs51652933	*Rad23b*	upstream gene variant	MODIFIER
4:55522197-55522197	rs27805820	*Klf4*	downstream gene variant	MODIFIER
4:56735510-56735510	rs244149313	*Actl7b*	downstream gene variant	MODIFIER
4:56742004-56742004	rs27835157	*Actl7a*	upstream gene variant	MODIFIER
4:56749785-56749785	rs32194301	*Elp1*	3-prime UTR variant	MODIFIER
4:56798280-56798280	rs3679212	*Fam206a*	upstream gene variant	MODIFIER
4:56813147-56813147	rs27869754	*Ctnnal1*	intron variant	MODIFIER
4:56952553-56952553	rs32863629	*Frrs1l*	downstream gene variant	MODIFIER
4:56992622-56992622	rs45988536	*Epb41l4b*	downstream gene variant	MODIFIER
4:57217962-57217962	rs27890048	*Ptpn3*	intron variant	MODIFIER
4:57429910-57429910	rs13477724	*Palm2*	upstream gene variant	MODIFIER
4:57566765-57566765	rs27838396	*Pakap*	upstream gene variant	MODIFIER
4:57883115-57883115	rs108735561	*Akap2*	synonymous variant	LOW
4:57905139-57905139	rs32702300	*D630039A03Rik*	downstream gene variant	MODIFIER
4:57939913-57939913	rs32831936	*Txn1*	downstream gene variant	MODIFIER
4:58008475-58008475	rs27834784	*Txndc8*	intron variant	MODIFIER
4:58068349-58068349	rs27868133	*Svep1*	intron variant	LOW
4:58281054-58281054	rs50403685	*Musk*	upstream gene variant	MODIFIER
4:58431447-58431447	rs32189893	*Lpar1*	downstream gene variant	MODIFIER
4:58444040-58444040	rs51742792	*Mir3095*	upstream gene variant	MODIFIER
4:58780659-58780659	rs32670820	*Olfr267*	downstream gene variant	MODIFIER
4:58794035-58794035	rs32428588	*Ecpas*	downstream gene variant	MODIFIER
4:58938638-58938638	rs32171392	*Zkscan16*	upstream gene variant	MODIFIER
4:58960485-58960485	rs217312101	*Ptgr1*	downstream gene variant	MODIFIER
4:58990985-58990985	rs108106489	*Dnajc25*	upstream gene variant	MODIFIER
4:59033339-59033339	rs32162782	*Gng10*	upstream gene variant	MODIFIER
4:59041259-59041259	rs13464414	*AI481877*	downstream gene variant	MODIFIER
4:59184910-59184910	rs51541251	*Ugcg*	upstream gene variant	MODIFIER
4:59312818-59312818	rs52375862	*Susd1*	downstream gene variant	MODIFIER
4:59477813-59477813	rs45676388	*Ptbp3*	intron variant	MODIFIER
4:59700598-59700598	rs13477733	*E130308A19Rik*	intron variant	MODIFIER
4:59807247-59807247	rs27829267	*Snx30*	intron variant	MODIFIER
4:59904945-59904945	rs27864071	*Slc46a2*	downstream gene variant	MODIFIER
4:59959947-59959947	rs27849133	*Mup4*	intron variant	MODIFIER
4:59959947-59959947	rs27849133	*Mup6*	upstream gene variant	MODIFIER
4:60139696-60139696	rs243846870	*Mup2*	missense variant	MODERATE
4:60419710-60419710	rs108108047	*Mup9*	intron variant	MODIFIER
4:60657821-60657821	rs245873609	*Mup11*	downstream gene variant	MODIFIER
4:61587364-61587364	rs49092473	*Mup17*	downstream gene variant	MODIFIER
4:61665786-61665786	rs108712947	*Mup18*	downstream gene variant	MODIFIER
4:61783612-61783612	rs248125990	*Mup19*	upstream gene variant	MODIFIER
4:61828968-61828968	rs217495411	*Mup5*	downstream gene variant	MODIFIER
4:62054497-62054497	rs242233082	*Mup20*	upstream gene variant	MODIFIER
4:62082363-62082363	rs31772522	*Mup3*	downstream gene variant	MODIFIER
4:62143000-62143000	rs27893052	*Mup21*	downstream gene variant	MODIFIER
4:62184648-62184648	rs32268442	*Zfp37*	downstream gene variant	MODIFIER
4:62287342-62287342	rs235713830	*Slc31a2*	intron variant	MODIFIER
4:62341678-62341678	rs32753658	*Fkbp15*	intron variant	MODIFIER
4:62427515-62427515	rs46560490	*Prpf4*	downstream gene variant	MODIFIER
4:62427515-62427515	rs46560490	*Rnf183*	downstream gene variant	MODIFIER
4:62455748-62455748	rs31833269	*Wdr31*	intron variant	MODIFIER
4:62608710-62608710	rs3683845	*Rgs3*	intron variant	MODIFIER
4:62960610-62960610	rs27920936	*Zfp618*	upstream gene variant	MODIFIER
4:63144254-63144254	rs27935282	*Ambp*	synonymous variant	LOW
4:63164918-63164918	rs27920776	*Kif12*	downstream gene variant	MODIFIER
4:63213388-63213388	rs31969344	*Col27a1*	upstream gene variant	MODIFIER
4:63340621-63340621	rs228536992	*Orm1*	upstream gene variant	MODIFIER
4:63353875-63353875	rs249995738	*Orm3*	upstream gene variant	MODIFIER
4:63357917-63357917	rs247599962	*Orm2*	upstream gene variant	MODIFIER
4:63362746-63362746	rs254755391	*Akna*	downstream gene variant	MODIFIER
4:63410004-63410004	rs27920428	*Whrn*	downstream gene variant	MODIFIER

4:63541488-63541488	rs215684082	*Atp6v1g1*	upstream gene variant	MODIFIER
4:63553995-63553995	rs220237119	*Tmem268*	upstream gene variant	MODIFIER
4:63607324-63607324	rs246629318	*Tex48*	synonymous variant	LOW
4:63722663-63722663	rs27919783	*Tnfsf15*	downstream gene variant	MODIFIER
4:63865082-63865082	rs218906693	*Tnfsf8*	upstream gene variant	MODIFIER
4:63992905-63992905	rs261270782	*Tnc*	intron variant	MODIFIER
4:63992905-63992905	rs261270782	*8030451A03Rik*	intron variant, non-coding	MODIFIER
4:68756812-68756812	rs240458772	*Brinp1*	downstream gene variant	MODIFIER
4:70422225-70422225	rs50579868	*Megf9*	downstream gene variant	MODIFIER
4:72112509-72112509	rs226550150	*Tle1*	downstream gene variant	MODIFIER
4:72201316-72201316	rs218632637	*C630043F03Rik*	upstream gene variant	MODIFIER
4:72845663-72845663	rs32177339	*Aldoart1*	downstream gene variant	MODIFIER
4:73786310-73786310	rs215613019	*Rasef*	intron variant	MODIFIER
4:74008528-74008528	rs107906452	*Frmd3*	upstream gene variant	MODIFIER
4:74238679-74238679	rs28098627	*Kdm4c*	upstream gene variant	MODIFIER
4:75272779-75272779	rs32242838	*Dmac1*	downstream gene variant	MODIFIER
4:75944802-75944802	rs31956554	*Ptprd*	downstream gene variant	MODIFIER

Suppl. Tab. 5: Exon splicing index of significantly differentially spliced genes from the microarray. Negative values show splicing events in Ola- and positive values in NZO-allele carriers of *Nbg4p* mice. Statistical significance is expressed by the given q-value. *q<0.05, **q<0.01 and ***q<0.001.

Gene-ID	Mb-Pos.	Exon Splicing Index	
		gWAT	liver
AI464131	41.50	-8,1***	-9,82***
Dnaic1	41.57		6,86***
Cntfr	41.66	2,77***	2,45**
Sigmar1	41.74		-3,34***
Il11ra1	41.76	-3,78***	
Fam205a4	41.97	8,32***	12,25***
Ccl27b	42.15		15,57***
Ccl21b	42.17	-4,29**	
Fam205a3	42.32	8,94***	11,91***
Fam205a2	42.52	29,62***	42,59***
Il11ra2	42.66		3,35***
4930578G10Rik	42.67		-2,58*
Ccl21a	42.77	-5,76*	
Fam205a1	42.85	8,56***	11,52***
Atp8b5	43.27		8,59***
Gne	44.03	-20,8***	-143,78***
Rnf38	44.13	-2,41***	
Gabbr2	46.66	3,09***	
Col15a1	47.21	19,37***	6,23***
Stx17	48.12	-2,73***	
Invs	48.28	-3,45***	-4,63***
Tmeff1	48.59	7,45***	
Svep1	58.04	2,16*	
AI314180	58.80	-70,1***	-104,27***
Alad	62.51	-3,08***	-2,5***
Tle1	72.03	-2,3**	
Ptprd	75.86	7,96***	7,18***

6.1.2 Supplementary figures
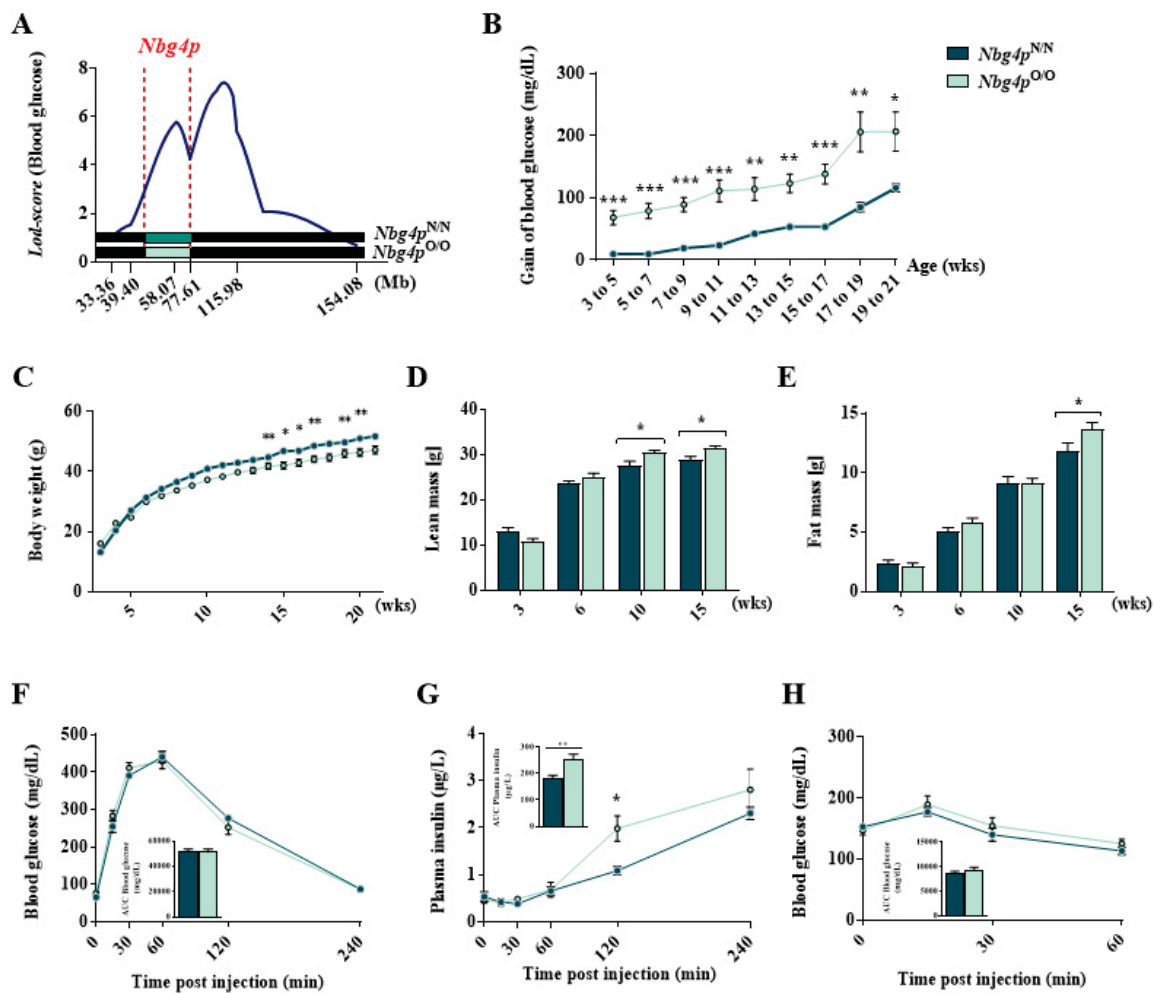
Suppl. Fig. 1: Detailed metabolic characteristics of RCS.NZO.129Ola-*Nbg4p* mice on SD. Congenic mice carrying the proximal *Nbg4* locus (A) showed significantly higher increases in blood glucose (B) and body weight development (C). Ola-allele carrier of *Nbg4p* exhibited higher lean (D) and fat mass (E) starting at week 10 and 15 of life, respectively. Glucose and insulin tolerance tests were ordinary and differed only in the plasma insulin concentration after glucose injection (F-H).
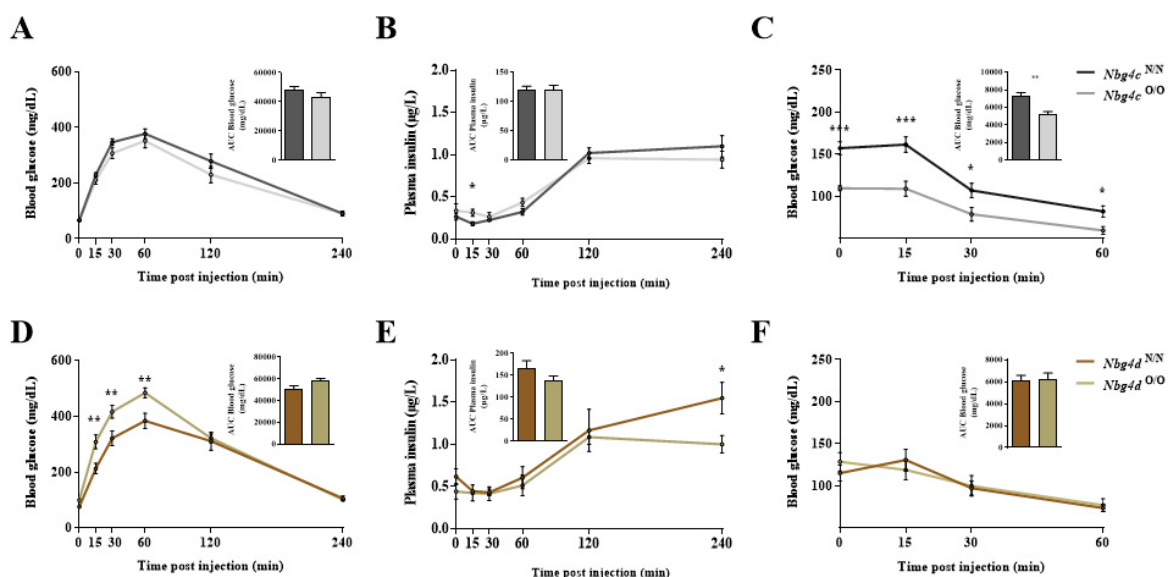
Suppl. Fig. 2: Glucose and insulin tolerance tests of *Nbg4c* and *Nbg4d* mice on SD. Whole-body glucose tolerance was investigated by measuring blood glucose (A+D) and plasma insulin concentrations (B+E) for several time points after the injection of 2 g/kg glucose. Insulin sensitivity was examined by measuring blood glucose levels after intraperitoneal injection of 1 U/kg insulin (C+F). AUC was determined for quantification of each experiment. Data are shown as mean ± SEM of 6-11 mice per genotype and differences were analysed using two-way ANOVA with Bonferroni's multiple comparisons test. * p= 0.05; ** p=0.01.
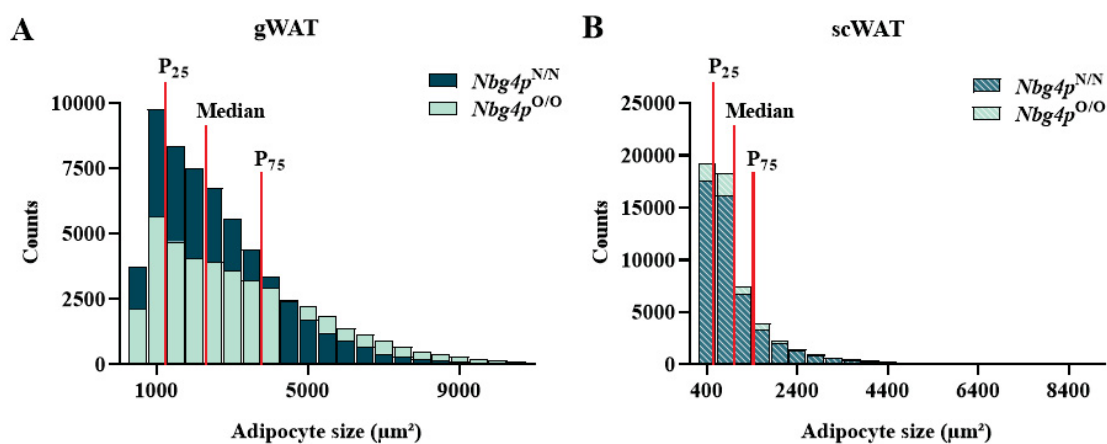
Suppl. Fig. 3: Histology-derived adipocyte size distributions. Histograms showing the total counts of adipocyte size from gonadal (A) and subcutaneous (B) white adipose tissues of 6 weeks old RCS.NZO.129Ola-*Nbg4p* mice fed a HFD (n=4 per genotype). Red vertical lines show the location of the Median, as well as the percentiles P_{25} and P75 which were determined separately for each tissue. In the study, adipocytes that were counted within P_{25} were defined as small, whereas adipocytes counted between P_{25} and P_{75} were defined as medium and over P_{75} as large regarding their size.
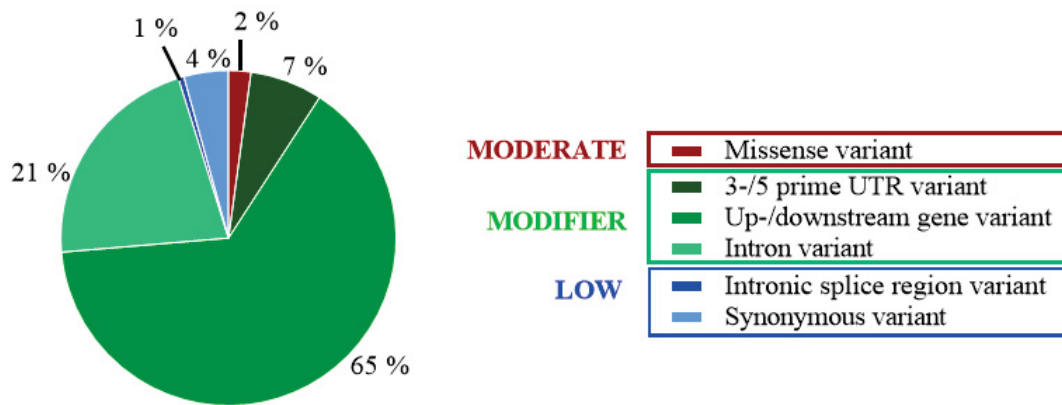
Suppl.

Fig. 4: Variant effect prediction (VEP) of non-IBD SNPs on *Nbg4p*. Frequency of consequences of Ola-polymorphic (non-IBD) SNPs that were identified by haplotype analysis according to Sequence Ontology terms. Moderate = a non-disruptive variant that might change protein effectiveness, Modifier = non-coding variants or variants affecting non-coding genes without precise prediction of impact, Low = variants that are assumed to be harmless or unlikely to change protein behaviour.
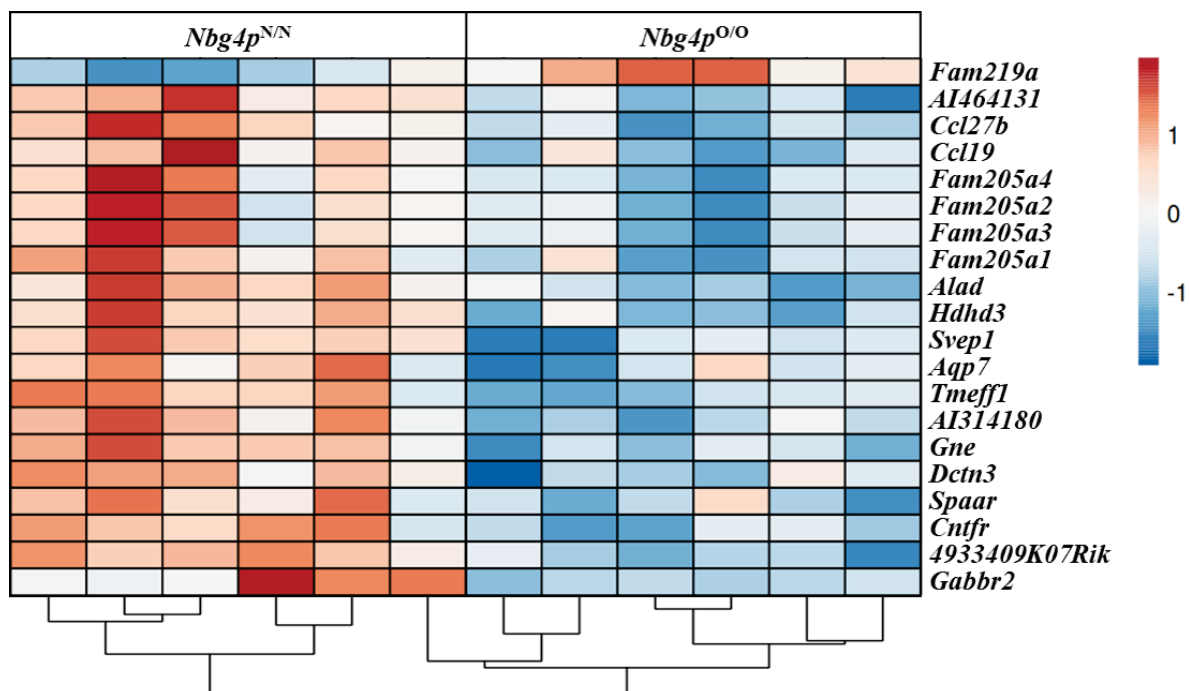
Suppl. Fig. 5: Heatmap of significantly differentially regulated genes in the gWAT located at the *Nbg4p* locus. Fold change of significantly differentially regulated genes from microarray studies of the gWAT from 6 weeks old RCS.NZO.129Ola-*Nbg4p* mice fed a high-fat diet (HFD). The heatmap was generated using ClustVis [199]. Both rows and columns are clustered using correlation distance and average linkage. Shades of red means a higher expression compared to other conditions in the same row.
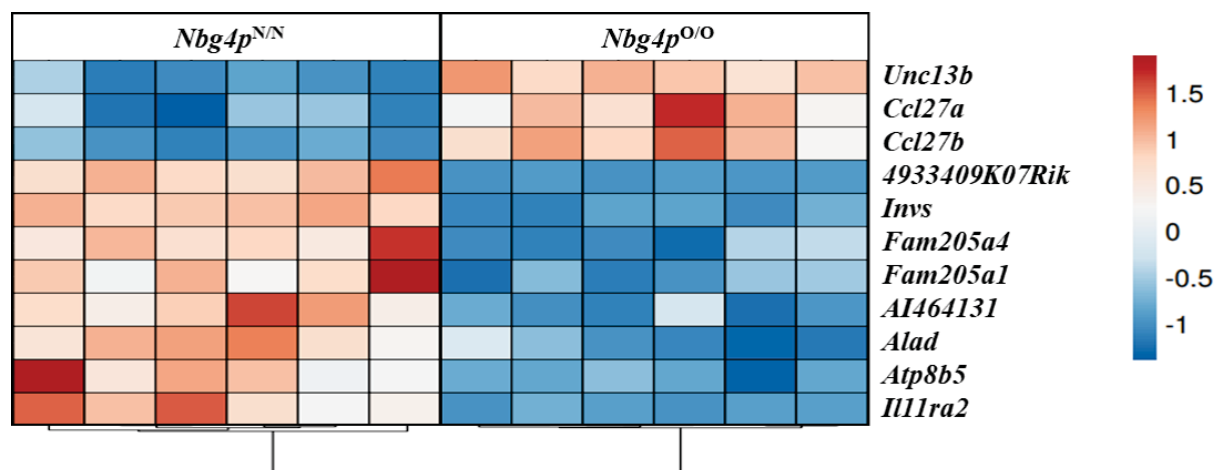
Suppl. Fig. 6: Heatmap of significantly differentially regulated genes in the liver located at the *Nbg4p* locus. Fold change of significantly differentially regulated genes from microarray studies of the liver from 6 weeks old RCS.NZO.129Ola-*Nbg4p* mice fed a high-fat diet (HFD). The heatmap was generated using ClustVis [199]. Both rows and columns are clustered using correlation distance and average linkage. Shades of red means a higher expression compared to other conditions in the same row.
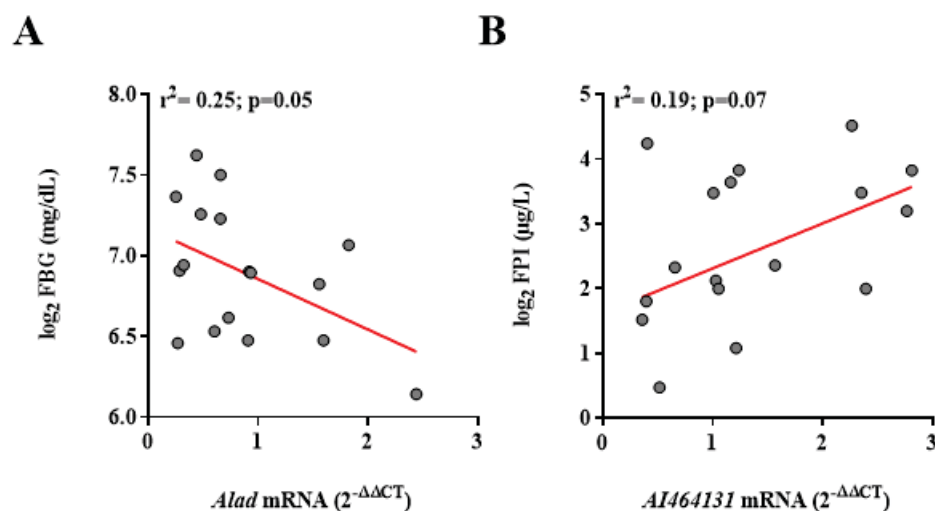
Suppl. Fig. 7: Significant correlations between mRNA levels of the most likely candidate genes from the gWAT with *Nbg4p*-specific diabetogenic traits. *Alad* mRNA expression significantly correlated with fasted blood glucose levels (FBG) (A) while the expression of *AI464131* correlated with fasted plasma insulin (FPI) concentration (B). Dots represent single animals and the correlation was calculated by linear regression: coefficient of determination; $r^2 = 1$: 100 % correlation; $r^2 = 0$: no correlation.
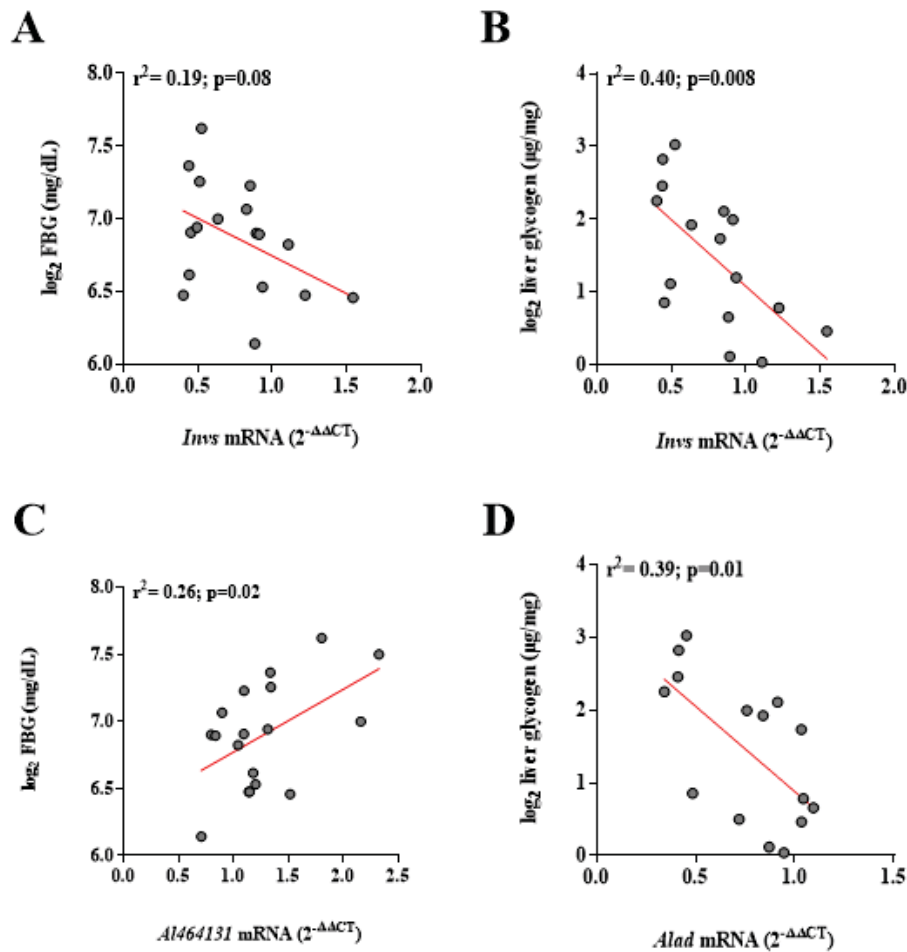
Suppl. Fig. 8: Significant correlations between mRNA levels of the identified candidate genes from the liver with *Nbg4p*-specific diabetogenic traits. *Invs* (A) and *AI464131* (C) mRNA expression significantly correlated with fasted blood glucose levels (FBG). Furthermore, *Invs* (B) and *Alad* (D) mRNA expression showed additional correlation with liver glycogen content. Dots represent single animals and the correlation was calculated by linear regression: coefficient of determination; $r^2 = 1$: 100% correlation; $r^2 = 0$: no correlation.

6.1.3 List of tables

6.1.4 List of figures

6.1.5 Abbreviations

2-DOG	2-deoxyglucose
AA	Amino acids
AI464131	*Myogenesis regulating glycosidase*
Alad	δ-A*minolevulinate dehydratase*
ANOVA	Analysis of variance
approx.	Approximately
AT	Adipose tissue
ATP	Adenosine triphosphate
Atp8b5	*ATPase, class I, type 8B, member 5*
AUC	Area under the curve
BAT	Brown Adipose Tissue
BCA	Bicinchonic acid
BMI	Body mass index
BSA	Bovine serum albumin
BCA	Bicinchoninic acid
CD36	Cluster of differentiation 36
cDNA	Complementary Desoxyribo nucleis acid
Chr4	Chromosome 4
CO_2	Carbon dioxide
CoA	Coenzyme A
cpm	counts per minutes
CT	Cycle threshold
ddH_2O	Aqua bidestillata
DDZ	Deutsches Diabetes Zentrum Düsseldorf (German diabetes center)
DMEM	Dulbecco's Modified Eagles Medium
DNA	Deoxyribonucleic acid
DNL	*De novo* lipogenesis
dNTP	Desoxyribo nucleotide triphosphate
e.g.	Latin: exempli aratia – for example
EDL	*Extensor digitorum longus*
EDTA	Ethylene diamine tetra acetate
EGTA	Ethylene glycol-bis(aminoethylether)-N,N,N',N'-tetra acetate
ELISA	Enzyme-linked immuno sorbent assay
ETC	Electron transport chain
EtOH	Ethanol
F1	First filial generation

F2	Second filial generation (Intercross)
FAO	Fatty acid β-oxidation
FBG	Fasting blood glucose
FBS	Fetal bovine serum
FCCP	Carbonyl cyanide-4-(trifluoromethoxy)phenylhydrazone
FFA	Free fatty acids
Fig.	Figure
FPI	Fasting plasma insulin
Fwd	Forward
G6Pc	Glucose-6-phosphate, catalytic
Gckr	Glucokinase regulatory protein
GLUT4	Glucose Transporter 4
GSIS	Glucose-stimulated insulin secretion
GWAS	Genome wide association studies
gWAT	Gonadal white adipose tissue
HE	Hematoxylin and eosin
HFD	High-fat diet
Invs	*Inversin*
i.p.GTT	Intraperitoneal glucose tolerance test
i.p.ITT	Intraperitoneal insulin tolerance test
KASP	Kompetitive Allele Specific PCR
KD	Knockdown of a gene
kDa	Kilodalton
KRH	Krebs-Ringer-HEPES
LOD	Logarithm of the odd
Mb	Mega base
MODY	Maturity-onset diabetes of the young
mRNA	Messenger RNA
n	Number
N2	Backcross population
NaCl	Sodium chloride
Nbg4	NZO blood glucose QTL on chromosome 4
Nbg4c	Consomic region of the *Nbg4* locus
Nbg4d	Distal region of the *Nbg4* locus
Nbg4p	Proximal region of the *Nbg4* locus
Nbg7	NZO blood glucose QTL on chromosome 7
NEFA	Non-esterified fatty acids
NMR	Nuclear magnetic resonance

NT	Non-target
Nudt19	*Nudix (nucleoside diphosphate linked moiety X)-type motif 19*
NZO	New Zealand Obese
OCR	Oxygen consumption rate
OECD	Organisation for Economic Co-operation and Development
PAGE	Polyacrylamide gel electrophoresis
PBS	Phosphate-buffered saline
PFA	Paraformaldehyde
qPCR	Quantitative polymerase chain reaction
QTL	Quantitative trait locus
g	Relative centrifugal force
RCS	Recombinant congenic strain
RNA	Ribonucleic acid
RT	Room temperature
scWAT	Subcutaneaous white adipose tissue
SEM	Standard error of the mean
shRNA	Short hairpin RNA
siRNA	Small interfering RNA
SD	Standard diet
SNP	Single nucleotide polymorphism
T1D	Type 1 Diabetes Mellitus
T2D	Type 2 Diabetes Mellitus
Tab.	Table
TCA	Tricarboxylic acid cycle
TEMED	Tetramethylethylendiamin
TG	Triglyceride
Unc13b	*Unc-13 homolog B*
UPR	Unfolded protein responses
VEP	Variant effect predictor
WHO	World health organization
WHR	Waist-to-hip ratio

6.1.6 Contributions

1) Altenhofen D, Khuong JM, Kuhn T, Lebek S, **Görigk S**, Kaiser K, Binsch C, Griess K, Knebel B, Belgardt BF, Cames S, Eickelschulte S, Stermann T, Rasche A, Herwig R, Weiss J, Vogel H, Schürmann A, Chadt A, Al-Hasani H. (2023): "E96V Mutation in the *Kdelr3* Gene Is Associated with Type 2 Diabetes Susceptibility in Obese NZO Mice". *Int J Mol Sci*. Jan 3;24(1):845. PMID: 36614300; PMCID: PMC9820861.

   Contribution: In this paper, I assisted with mouse experiments and helped with reviewing and editing the manuscript.

2) Kuhn T, Kaiser K, Lebek S, Altenhofen D, Knebel B, Herwig R, Rasche A, Pelligra A, **Görigk S,** Khuong JM, Vogel H, Schürmann A, Blüher M, Chadt A, Al-Hasani H. (2022) "Comparative genomic analyses of multiple backcross mouse populations suggest SGCG as a novel potential obesity-modifier gene". *Hum Mol Genet*. Nov 28;31(23):4019-4033. PMID: 35796564; PMCID: PMC9703946.

   Contribution: In this paper, I was concerned in the investigation and methodology of cell culture experiments and participated in the correction of the manuscript.

3) **Sarah Görigk,** D. Margriet Ouwens, Tanja Kuhn, Delsi Altenhofen, Christian Binsch, Mareike Damen, Jenny Minh-An Khuong, Katharina Kaiser, Birgit Knebel, Heike Vogel, Annette Schürmann, Alexandra Chadt, Hadi Al-Hasani (2022): "Nudix hydrolase NUDT19 regulates mitochondrial function and ATP production in murine hepatocytes". *Biochimica et Biophysica Acta (BBA) - Molecular and Cell Biology of Lipids*. Volume 1867, Issue 6, 2022, 159153, ISSN 1388-1981.

   Contribution: This manuscript was in most parts written by myself together with D. Margriet Ouwens. The data used for Fig. 1 from the manuscript was generated by Tanja Kuhn and Sandra Lebek. The heatmap in Fig. 1B of the manuscript was generated with the help of Christian Binsch. All other Figures were prepared by myself or with the help of D. Margriet Ouwens and are based on experimental data collected by myself. The results generated for Fig. 25-27 of my dissertation mainly originate from this paper and were only partially modified.

6.1.7 Acknowledgements

Eidesstaatliche Erklärung

Hiermit versichere ich, dass ich die vorliegende Dissertation selbständig und ohne unzulässige fremde Hilfe unter Beachtung der „Grundsätze zur Sicherung guter wissenschaftlicher Praxis an der Heinrich-Heine-Universität Düsseldorf" verfasst habe.

Ich erkläre weiterhin, dass ich bisher noch kein Promotionsversuch unternommen habe und dass die vorliegende Arbeit in dieser oder ähnlicher Form an keiner anderen Hochschule eingereicht wurde.

<u> Düsseldorf, 10.07.2023 </u>   _____

         Ort, Datum   (Sarah Görigk)